The Dissertation Committee for Derek Clyde Thomas
certifies that this is the approved version of the following dissertation:

Stability and Dynamics of Systems of Interacting Bubbles with Time-Delay and Self-Action Due to Liquid Compressibility

Committee:

Mark F. Hamilton, Supervisor

Eric P. Fahrenthold

Yurii A. Ilinskii

Loukas F. Kallivokas

Preston S. Wilson

Stability and Dynamics of Systems of Interacting Bubbles with Time-Delay and Self-Action Due to Liquid Compressibility

by

Derek Clyde Thomas, B.S., M.S.

DISSERTATION

Presented to the Faculty of the Graduate School of

The University of Texas at Austin

in Partial Fulfillment

of the Requirements

for the Degree of

DOCTOR OF PHILOSOPHY

THE UNIVERSITY OF TEXAS AT AUSTIN

August 2012

To my wife, Wendy.

Acknowledgments

The person most deserving of recognition at this time is my Wendy, who has been by my side throughout the last 6 years. Wendy supported me as I finished my undergraduate and master's degrees and subsequently decided to pursue a doctorate. She has almost single-handedly cared for the needs of our family over the last year and a half as I have worked to complete my dissertation, and without her efforts this work would have been impossible. She has believed in me, even when I doubted myself, and I love and thank her for that. I also want to thank my two oldest children, Norah and Ben, for their patience as I have worked to complete my dissertation. I am grateful to my parents for their support and patience, and for their encouragement of my curiosity and fascination with the natural world.

Throughout my life, I have been assisted by family, friends, teachers, and others; without their help, support, and advice I could not have arrived at this point. I am thankful for the instruction, patience, and support I have received from my adviser, Dr. Mark Hamilton. Dr. Hamilton has truly taught me to be a scientist, and to be a better person. I want to thank Dr. Yurii Ilinskii for his assistance, his advice, and his penetrating physical insight, and Dr. Evgenia Zabolotskaya for her kind words and support. I am grateful for the input and advice of the members of my committee, Dr. Eric Fahrenthold, Dr. Loukas Kallivokas, and Dr. Preston Wilson.

Dr. Todd Hay has patiently answered many of my computer and programming questions and introduced me to many useful new tools. I am grateful to Dr. Mark Wochner and Dr. Michael Haberman for their friendship and advice. I also want to thank Daniel and Katie Tengelsen for allowing me to stay with them in order to continue work on my dissertation after moving my family from Austin. I owe thanks to Sumedh Joshi and Kyle Spratt for the time we have spent discussing many fascinating mathematical and physical problems.

Finally, I am grateful to Applied Research Laboratories at the University of Texas at Austin for the generous support provided by ARL:UT McKinney Fellowship in Acoustics, which enabled me to conduct this research and to attend many professional meetings. The support provided by the Cockrell School of Engineering Thrust 2000 Fellowship at UT Austin is also greatly appreciated. This work was connected with research supported by grant number DK070618 from the National Institutes of Health.

Abstract

Stability and Dynamics of Systems of Interacting Bubbles with Time-Delay and Self-Action Due to Liquid Compressibility

Publication No. ____________________

Derek Clyde Thomas, Ph.D.
The University of Texas at Austin, 2012

Supervisor: Mark F. Hamilton

A Hamiltonian model for the radial and translational dynamics of clusters of coupled bubbles in an incompressible liquid developed by Ilinskii, Hamilton, and Zabolotskaya [*J. Acoust. Soc. Am.* **121**, 786-795 (2007)] is extended to included the effects of compressibility in the host liquid. The bubbles are assumed to remain spherical and translation is allowed. The two principal effects of liquid compressibility are time delay in bubble interaction due to the finite sound speed and radiation damping due to energy lost to acoustic radiation. The incorporation of time delays produces a system of delay differential equations of motion instead of the system of ordinary differential equations in models of bubble interaction in an incompressible medium. The form of the Hamiltonian equations of motion is significantly different from the commonly used models based on Rayleigh-Plesset equations for coupled bubble dynamics, and it provides certain advantages in numerical integration of the time-delayed equations of motion. Corrections for radiation damping in clusters of interacting bubbles are developed in the form of a time-delayed expression for bubble self-action following the method of Ilinskii and Zabolotskaya [*J. Acoust. Soc. Am.* **92**, 2837-2841 (1992)]. A set of approximate series expansions of this delayed expression is calculated to first order in the ratio of bubble radius to the characteristic wavelength of acoustic radiation from the bubble, and to varying orders in the ratio of bubble radius to characteristic bubble separation distance. Stability of the delay differential equations of motion is analyzed with four successive levels of approximation for the effects of radiation damping and time delay. The stability is analyzed with and without the effects of viscous and thermal damping. The effect of time delay and radiation damping on the pressure radiated by small systems of bubbles is considered. An approximate method to account for the delays in bubble interaction in a weakly compressible liquid is presented. This method converts the system of delay differential equations into an approximate system of ordinary differential equations, which may simplify numerical integration. Several sets of model equations incorporating propagation time delay in bubble interactions are solved numerically with existing algorithms specialized for delay differential equations. Numerical simulations of the dynamics of single bubbles, pairs of bubbles, and clusters of bubbles are used to compare the different levels of approximation for compressibility effects for low- and high-amplitude radial motion in systems of bubbles under free response and pulsed excitation by an external pressure source.

Table of Contents

List of Tables

List of Figures

Chapter 1

Introduction

This dissertation is focused on developing a more accurate model for the dynamics of clusters of interacting bubbles in high-amplitude motion produced by acoustic excitation in a compressible liquid. The two primary effects of liquid compressibility considered here are radiation damping due to bubble self-action, and time delays in bubble interactions due to acoustic propagation. The original focus of this research effort was to develop a model for the large bubble clusters in high-amplitude motion observed in laboratory shock-wave lithotripsy experiments. Because of the large cluster sizes and high-amplitude bubble motion observed in lithotripsy experiments, a model which incorporated the effects of compressibility in the host medium was sought. Unanticipated numerical difficulties encountered when attempting to model large numbers of interacting bubbles motivated closer examination of compressibility effects, especially associated with the finite acoustic propagation time for the motion of one bubble to be affected by the motion of another bubble some distance away. The dearth of work on time-domain simulation of the dynamics of coupled-bubble systems containing more than two bubbles while including the time delays in bubble interactions and the effect of radiation damping prompted the research presented in this dissertation. An extensive analysis of the stability of multi-bubble systems and the combined effects of time delay in bubble interactions and radiation damping due to bubble self-action has been undertaken. The results of this analysis were used to develop and evaluate corrections for time delay and radiation damping that provide a consistent and stable model for the motion of systems of multiple interacting bubbles in a compressible medium.

1.1 Motivation

The primary motivation for this work was a desire to model and investigate the effects that large clusters of acoustically driven bubbles have on kidney stone comminution in extracorporeal shock-wave lithotripsy,[1] with particular emphasis on the role of bubble interaction within the clusters. We therefore begin with a brief discussion of shock-wave lithotripsy, followed by comments on several other applications in which bubble cluster dynamics are of interest.

1.1.1 Extracorporeal shock-wave lithotripsy

Extracorporeal shock-wave lithotripsy (ESWL) is a procedure for the treatment of kidney stones. In ESWL a single-cycle, shock-wave pulse of very high amplitude (30-100 MPa) is focused on the region in which the kidney stone lies. The rarefaction phase of a lithotripsy pulse produces acoustic cavitation, which results in bubble clusters consisting of thousands of interacting bubbles. It has been found that whereas the shock waves induce fracturing of larger stones, bubble collapse erodes the smaller stone fragments down to sizes that permit them to pass through the urinary tract.[1] Cavitation bubble activity has also been correlated with tissue damage.[2,3] Thus bubble activity is connected to both the positive effect of stone comminution and with undesirable renal damage. It is hoped that a more accurate model for collective bubble dynamics in clusters will guide improvements to lithotripsy treatment.

1.1.2 Other applications

Bubbles clusters have a significant impact on other biomedical treatments such as high-intensity focused ultrasound (HIFU) and histotripsy. In HIFU,[4] a high-intensity ultrasonic pulse is focused in a small region of tissue. This produces heating which results in hyperthermia and tissue necrosis in a precise location. HIFU can also stimulate acoustic cavitation[5] which shields the target region and increases acoustic scattering, and which in turn alters the size of the lesion and reduces the precision of the treatment.[6] Histotripsy[7–9] employs ultrasonic pulses which are comparable in amplitude to the shock waves used in ESWL, but consist of 3–50 acoustic cycles instead of just one.[7] The activity of clusters of cavitation micro-bubbles created by the acoustic pulses drives the tissue erosion in the focal region.[8,9]

The action of clusters of coupled bubbles is also important in ultrasonic cleaning,[10] sonochemistry,[11] and SONAR scattering from bubbly regions generated by breaking waves, ship wakes, and other marine activity.[12] Additionally, gas bubbles coated with a lipid or polymer shell are called ultrasound contrast agents (UCA) and are used to improve ultrasound images and for targeted drug delivery. For high UCA concentrations, bubble interaction effects may be significant. UCA microbubbles in nonlinear motion have been used in the construction of acoustic meta-materials, with applications including an acoustic diode;[13] these applications rely on the highly nonlinear response of bubbles and UCAs, but it is not known if bubble interaction effects are significant. Thus an accurate model for the coupled dynamics of gas bubbles in a compressible liquid has myriad applications.

1.2 Overview of previous research on coupled bubble dynamics

The dynamics of bubbles in liquids has been actively researched since the late nineteenth century.[14] The first theoretical model for the dynamics of a bubble was due to Lord Rayleigh.[15] Since the time of Lord Rayleigh a large body of work focused on the modeling of bubbles in a liquid has developed.

1.2.1 Coupled bubbles

In all of the applications mentioned in the previous section, the collective behavior of clusters of interacting bubbles is important. These diverse applications have driven research on the dynamics of coupled bubbles. Three distinct approaches have been used to model bubbly media and bubble systems: effective medium models, direct numerical simulation, and discrete bubble models.

In an effective medium model, a liquid containing bubbles is modeled as a medium possessing the same average properties (density, etc.) as the bubbly medium, typically through the use of volume-averaged equations.[16] Because effective medium models are usually based on volume-averaged equations and a linearized bubble model they do not capture local features of the field or the effects of nonlinear bubble motion. Recently, several models which combine discrete bubble models with volume-averaged model equations have been proposed. A model based on volume-averaged equations modified to include the nonlinear motion of coupled bubbles in a compressible medium was developed by Fuster and Colonius.[17] A continuum model for bubbly media with a cluster substructure was developed by Grandjean et al.[18]

In direct numerical simulations, a region containing gas inside the bubbles and the surrounding liquid is discretized and the governing partial differential equations are solved numerically. Direct numerical simulation of bubbles in a liquid has been undertaken with impressive results,[19] but the computational requirements severely limit the number of bubbles that may be simulated. Boundary element methods have also been applied to simulations of multiple bubbles.[20] Boundary element methods are limited to simulations of bubbles in incompressible media, suffer from instabilities in the presence of high-amplitude motion and surface tension, and are limited in the number of bubbles that can be simulated.

An alternate approach is to treat the bubbles as discrete entities and use a multipole expansion or similar method to model the bubbles as coupled oscillating spheres or higher-order shapes.[21] This method is attractive because, unlike most effective medium models, it models the behavior of individual bubbles. Unlike direct numerical simulation, it does not require discretization of large regions and surfaces with high resolution. By modeling bubbles as oscillating spheres, Doinikov[22] and Ilinskii et al.[23] developed Lagrangian formulations to obtain the equations of motion for coupled bubble systems. Ilinskii et al.[23] also developed a related Hamiltonian formulation for the equations of motion. The Lagrangian and Hamiltonian formulations treat the bubbles as a system of coupled nonlinear oscillators. The majority of the work on discrete bubble models has focused on bubbles in an incompressible liquid.

1.2.2 Bubble dynamics in a compressible medium

Liquid compressibility produces two distinct effects that must be incorporated in a bubble model: damping due to acoustic radiation and time delays between the motion of bubbles and their effects on other bubbles. It has been shown[24] that radiation damping can be connected to the time delay due to acoustic propagation.

Radiation damping

Early efforts to include the effects of liquid compressibility in models of bubble dynamics were motivated by a need to model underwater explosions.[25,26] Various approximate models for the motion of a single bubble in a compressible liquid were proposed by Gilmore[27] and Akulichev[28] (Gilmore-Akulichev model), Keller and Kolodner,[26] and Keller and Miksis[29] (Keller-Miksis model). Both the Gilmore-Akulichev model and the Keller-Miksis model rely on expansions to first order in the Mach number of the bubble wall motion. Tomita and Shima[30] developed an approximate model valid to second order in the Mach number.[31] These models for bubble motion were compared and unified by the work of Prosperetti and Lezzi[32] and Lezzi and Prosperetti.[33] A comparison of the Gilmore-Akulichev, Keller-Miksis, and Tomita-Shima models with the results of numerical integration of the Navier-Stokes equations[31] showed reasonable agreement of the three approximate models with the direct numerical simulation. All these models rely on a series expansion of the damping terms in powers of the acoustic Mach number.

A significant departure from the series expansions used previously was introduced by Ilinskii and Zabolotskaya,[24] who showed that expressions for the radiation damping of a bubble could be obtained by delaying the pressure radiated by the bubble by the time required for the signal to propagate from the center of the bubble to the bubble wall. This approach is key to the work presented in this dissertation. In their work, Ilinskii and Zabolotskaya showed that the results of a series expansion could be obtained from the delayed self-action term. Rather than considering radiation damping only by a series expansion, here it is considered as a result of time delay in the self-action of a bubble, and as a related series expansion.

1.2.3 Coupled bubble dynamics in a compressible medium

Compared to the work on coupled bubbles in an incompressible liquid, there is a much smaller body of work concerning the dynamics of interacting bubbles in a compressible liquid.

Frequency-domain analyses

Much of the previous work has been focused on acoustic scattering by bubble systems.[34–43] The scattering problem is typically posed in the frequency domain and considers steady-state behavior of linearized bubble systems and therefore necessarily very small pulsation amplitudes. Mettin et al.[44] considered the effect of time delays on the Bjerknes force between two bubbles by analysis in the frequency domain. Feuillade[38,40] analyzed the radiation damping due to bubble interaction in two- and three-bubbles systems over a range of separation distances and determined that bubble interaction effects in a compressible liquid tend to increase damping for closely spaced bubbles oscillating in phase, and reduce damping for anti-phase oscillations. Using the method of images, Cui et al.[45] employed an analytical solution for an infinite line array of equally spaced bubbles in a compressible fluid to model the dynamics of an acoustically driven bubble between infinite rigid parallel plates. Doinikov et al.[46] and Ooi et al.[47] considered the time delays in a line array of bubbles through an eigenvalue analysis of the linearized equations of motion for a system of coupled bubbles, but no time-domain results were presented. Atkisson[48] developed models of planar arrays of bubbles in a compressible fluid for several geometries relevant to analysis of single-bubble dynamics in rigid tubes (rectangular, triangular, and hexagonal) by the method of images. The analyses were conducted primarily in the frequency domain, although Fourier transforms were used to obtain time-domain results.

Time-domain analyses

The high-amplitude, transient response of bubbles in biomedical systems requires that simulations be conducted in the time domain. The earliest explicit inclusion of time delays due to acoustic propagation in bubble-interaction dynamics was by Fujikawa and Takahira,[49] who considered time delay effects on the interaction of a pair of coupled bubbles. Ilinskii and Zabolotskaya[24] modeled a system of coupled bubbles with by converting the delay differential equations of motion to an approximate set of ordinary differential equations by means of a series expansion for small time delays. Ilinskii et al.[50] and Hamilton et al.[51] considered the effect of liquid compressibility by including single-bubble radiation damping and delayed interactions. However, their results were obtained with a numerical integrator that was not specialized for the integration of delay differential equations. Heckman et al.[52] considered the dynamics and stability of bubble pairs with time delay in the interaction. However, the coupling used was non-physical, consisting of a "coupling strength" parameter multiplying the first-order time derivative of the bubble radius. Sinden et al.[53] also considered the dynamics and stability of a pair of bubbles oscillating in phase. Heckman et al. and Sinden et al. both reported instability in the system for certain parameter values, but no further investigation was undertaken to determine if the instability was due to a shortcoming of the model or a physical property of the system.

The previous work on time-domain simulation of coupled bubbles in a compressible medium with time delay in bubble interaction is extremely limited. In all previous work, the effects of radiation damping were considered through damping terms obtained by an asymptotic series expansion for a single bubble.

1.3 Summary and preview

Previous work on bubbles in a compressible medium has not adequately considered the effects of time delays and radiation damping due to liquid compressibility. The inclusion of compressibility effects transforms the ordinary differential equations of motion for a bubble system into a system of delay differential equations.[50,51] The work of Hamilton et al.[51] and Ilinskii et al.[50] explicitly considered time delays in bubble interactions without an integrator specialized for the numerical integration of delay differential equations. In all previous time-domain models and all frequency-domain models except those of Ilinskii and Zabolotskaya[24] and Atkisson,[48] the single-bubble radiation damping expression has been used.

To date there has been no complete model for the behavior of coupled bubbles in a compressible liquid which includes the effect of bubble translation, integrated with methods specialized for the treatment of the delay differential equations of motion. The goal of this work is to incorporate the effects of liquid compressibility into a model for the dynamics of coupled translating bubbles that may be used to predict bubble motion in response to the high-amplitude acoustic excitation typical of biomedical treatments such as shock-wave lithotripsy. This dissertation presents modifications to the model of Ilinskii et al.[23] to include time delay and radiation damping due to liquid compressibility and analyzes the impact of these modifications on the stability of the model and the predicted dynamics of a bubble system.

Chapter 2 presents the model for the dynamics of systems of coupled bubbles in an incompressible liquid developed by Ilinskii et al.[23] using a Hamiltonian formalism. Modifications to the model to incorporate the effects of liquid compressibility are discussed.

In Chapter 3, various metrics for assessing the behavior of bubble systems are presented. The equations of motion obtained in Chapter 2 are linearized and four different approximations for the effects of self-action and time delay due to liquid compressibility are presented. The linearized equations of motion are used to analyze the response of a two-bubble system and determine the effect of the different approximations for liquid compressibility by comparing the natural frequencies and damping coefficients of natural modes of the bubble system. The nonlinear delay differential equations of motion from Chapter 2 are integrated numerically to simulate high-amplitude free response of a two-bubble system and for a two-bubble system subjected to a short acoustic pulse, and the results are analyzed.

Chapter 4 contains stability analyses of the linearized equations of motion for systems of multiple bubbles in a random cluster and in a line array. The stability is analyzed with and without viscous and thermal damping. The results are compared to previous work on modeling line arrays of interacting bubbles.[46,47,54] The response of systems containing multiple bubbles to transient acoustic excitation is considered.

Because the numerical integration of delay differential equations is computationally intensive, the delayed equations of motion cannot be integrated directly for systems containing more than 30–50 bubbles. In Chapter 5, two approximations are developed to facilitate numerical integration of the equations of motion. Similar methods are used to convert the implicitly defined interaction delays given in Chapter 2 to explicit expressions for the delay, and to convert the delay differential equations of motion into an approximate system of ordinary differential equations. A comparison of the results of numerical integration of the delayed equations and the approximate versions is used to assess the accuracy and utility of the approximations.

Chapter 2

Model Equations for Coupled Bubbles in a Compressible Medium

This chapter describes the model equations that will be used to study the dynamics of bubble clusters. First, the Hamiltonian formalism used to obtain the equations of motion for translating, coupled bubbles in an incompressible liquid is presented. Second, several methods by which the effects of liquid compressibility are included in the model for coupled bubble dynamics are described. The two primary effects of liquid compressibility are time delay in bubble interaction and damping of bubble motion due to acoustic radiation of energy. Following the work of Ilinskii and Zabolotskaya,[24] the radiation damping is considered as a consequence of time delay due to acoustic propagation. Several different approximations for the inclusion of radiation damping in systems of interacting bubbles in a compressible medium are presented in this chapter and will be compared in Chapters 3 and 4. It should be noted that although the expressions for bubble translation are included in the model equations developed in this chapter for completeness, the analysis of the stability and dynamics of the model equations in subsequent chapters will neglect translation.

2.1 Description of the coupled-bubble model

The bubble interaction model used in this work was developed by Ilinskii et al.[23] Because a detailed derivation is presented in their paper, only an overview and relevant considerations are presented here.

2.1.1 Modeling bubbles with systems of coupled nonlinear oscillators

The approach that has been chosen for this work models the bubbles as a collection of coupled nonlinear oscillators. Fluid motion is often analyzed by discretizing all fluid in the volume of interest and then integrating the governing partial differential equations. Modeling the motion of multiple bubbles by this method is computationally prohibitive. It is possible to model bubbles by approximating them as a system of discrete, coupled, nonlinear oscillators, one for each oscillatory mode (i.e., spherical harmonic describing the shape of the bubble wall).[21] The resulting ordinary differential equations in time can significantly reduce the computational resources required to simulate bubble motion and thereby increase the number of bubbles that can be simulated. However, one must take care to determine appropriate differential equations of motion for the nonlinear oscillators that accurately capture the relevant physics of the simulated bubble system.

The model employed here uses the approximation that all bubbles in the system are spherical, and undergo spherically symmetric radial motion. The effects of translation are also included. The model allows for large amplitude, nonlinear, radial oscillations of the bubbles. The model does not account for nonspherical bubble shapes, bubble fission, or bubble coalescence, although a method to incorporate effects due to bubble coalescence will be discussed in Appendix D. In summary, the model accounts for interactions between the spherical pulsation mode of the bubbles, and allows for translation of bubbles in the system. Nonlinearity in bubble motion is also included.

Energy-based formalisms such as Lagrangian or Hamiltonian dynamics offer robust methods to obtain governing equations of motion of complicated systems. These methods require analytical expressions for the total kinetic and potential energy in the system. Initially, to obtain expressions for the energy quantities, it is necessary to assume that the liquid occupied by the bubble system is incompressible, inviscid, and irrotational. New techniques to correct for the assumption of an inviscid, incompressible fluid will be introduced in Section 2.2 and compared with existing methods in Chapters 3 and 4.

2.1.2 Potential energy

It is assumed that all potential energy in the system is stored by the compressed state of the gas inside the bubbles and by surface tension at the gas-liquid interface. Because the surrounding fluid is assumed to be incompressible, no energy is stored in compression of the liquid. Furthermore, it is assumed that the gas within the bubble is all equally compressed, that is, there are no spatial variations of the pressure within the gas. In other words, the bubble diameter is small compared with the wavelength of sound in the gas contained inside the bubble.

The assumption of uniform compression is justified by the fact that the radius of the bubble is much smaller than the acoustic wavelength both inside and outside the bubble. It follows that the pressure within the bubble can be completely determined by the bubble radius, and that the gas within the bubble can be modeled as a gas undergoing a polytropic thermodynamic process such that the equation of state is

$$P_g = P_0 \left(\frac{\rho_g}{\rho_{g0}} \right)^{\gamma}. \tag{2.1}$$

Therefore the gas is characterized by the pressure and density of the gas inside the bubble, P_g and ρ_g, respectively, the equilibrium gas density ρ_{g0}, the atmospheric pressure P_0, and the polytropic index γ.

For bubbles with radii much smaller than the thermal diffusion length, the thermodynamic process inside the bubbles is nearly isothermal and the polytropic index is near unity. For bubbles that are large in comparison to the thermal diffusion length, the process is approximately adiabatic and the polytropic index tends to the ratio of specific heats.[55] Effects of gas diffusion and vaporization are not considered in this dissertation. The effects of thermal damping are not considered in the nonlinear model presented in this chapter. Thermal damping of bubble motion is considered with a linearized model in Section 4.2.

The energy stored in the gas inside a bubble (labeled i) is found by integrating the internal, or potential, energy differential

$$d\mathcal{V}_i = (P_0 + p_{ei} - P_i)\, dV_i, \tag{2.2}$$

where P_i is the pressure on the exterior surface of the bubble without the effect of the external source, dV_i is the differential volume element, and p_{ei} is the external pressure due to the acoustic source evaluated at the center of the bubble. The pressure P_i is a function only of the bubble radius and can be written as[55]

$$P_i = \left(P_0 + \frac{2\sigma}{R_{0i}}\right)\left(\frac{R_{0i}}{R_i}\right)^{3\gamma} - \frac{2\sigma}{R_i}, \tag{2.3}$$

where σ is the surface tension, R_i is the bubble radius, and R_{0i} is the equilibrium bubble radius in the presence of surface tension.

Equation (2.3) may be used to evaluate the potential energy differential to obtain

$$\mathcal{V}_i = \frac{4\pi R_i^3}{3}\left[\frac{1}{\gamma - 1}\left(P_0 + \frac{2\sigma}{R_{0i}}\right)\left(\frac{R_{0i}}{R_i}\right)^{3\gamma}\right] + \frac{4\pi R_i^3}{3}(P_0 + p_e) + 4\pi\sigma R_i^2 \tag{2.4}$$

(with the assumption that $\gamma > 1$). The first term in Eq. (2.4) is the internal energy of the gas inside the bubble, the second term is equal to the work done to create a cavity of volume $\frac{4}{3}\pi R_i^3$, and the third term is the potential energy stored in surface tension. The total potential energy is found by summing over all the bubbles in the system:

$$\mathcal{V} = \sum_i \mathcal{V}_i. \tag{2.5}$$

2.1.3 Kinetic energy

An expression for the kinetic energy of the bubble system in terms of the generalized coordinates is derived in Ref. 23 by considering the motion of an inviscid incompressible liquid with density ρ_0. The irrotational motion of such a liquid may be described by a scalar velocity potential ϕ that satisfies Laplace's equation,

$$\nabla^2\phi = 0. \tag{2.6}$$

The kinetic energy in the fluid is given by the integral

$$\mathcal{K} = \frac{\rho_0}{2} \int_V |\nabla\phi|^2 \, dV \tag{2.7}$$

over the entire liquid volume, excluding the volume occupied by bubbles (and thus ignoring the negligible kinetic energy of the gas). With the assumption that the liquid is at rest at infinity, Eq. (2.7) can be rewritten as[56]

$$\mathcal{K} = -\frac{\rho_0}{2} \sum_i \int_{S_i} \phi \, (\nabla\phi) \cdot \mathbf{n}_i \, dS_i, \tag{2.8}$$

where S_i represents the surface of the ith bubble, $\mathbf{n}_i$ is the outward unit normal of this surface, and the sum is carried out over all bubbles in the cluster. This reformulation is obtained by combining Green's theorem with the requirement that the potential function satisfy Laplace's equation.

Evaluation of the kinetic energy integral (Eq. (2.8)) requires knowledge of both the velocity potential and its normal derivative on surface of each bubble. Hereafter, overdots will be used to denote derivatives with respect to the time t. Hence the translational velocity of the bubble, the time derivative of the position vector $\mathbf{X}$, is $\dot{\mathbf{X}}$. A translating sphere with a dynamic radius R and velocity $\dot{\mathbf{X}}$ has a surface velocity given by the sum of two velocity vectors, one for the radial motion and the other for the translation,

$$\mathbf{u}_s = \dot{R}\mathbf{n} + \dot{\mathbf{X}}, \tag{2.9}$$

where $\mathbf{n}$ is again the outward surface normal. By definition $\nabla\phi$ is the fluid velocity. Thus the condition that the fluid velocity at the bubble surface match the velocity of the surface requires that

$$\mathbf{u}|_{S_i} = \boldsymbol{\nabla}\phi|_{S_i} = \dot{R}_i\mathbf{n}_i + \dot{\mathbf{X}}_i \tag{2.10}$$

on the surface of the ith bubble. Substitution of this expression into Eq. (2.8) yields

$$\mathcal{K} = -\frac{\rho_0}{2}\sum_i \int_{S_i} (\dot{R}_i + \dot{\mathbf{X}}_i \cdot \mathbf{n}_i)\phi \, dS_i. \tag{2.11}$$

Further progress requires an expression for the velocity potential, which is obtained by means of an expansion of the potential as a system of monopole and dipole sources. The interaction between the bubbles is included by using a series expansion to approximate the potential and requiring that the potential field satisfy the velocity boundary condition on the surface of the bubbles to order $(R/D)^4$, where R is a characteristic bubble radius and D is a characteristic bubble separation distance. It is necessary to retain fourth-order terms in the expansion in order to accurately represent the effect of an external acoustic source. Once this effect has been determined it is sufficient to retain terms only to second order. This process will not be covered here, and the reader is referred to Ref. 23 for a detailed description of the derivation. Here the boundaries are the moving surfaces of the bubbles in the system, and the velocity potential can be expressed in terms of the natural coordinates of the bubbles, R_i and $\mathbf{X}_i$, and their time derivatives.

One physical interpretation of the multipole expansion is that the system of bubbles has been replaced by a system of point sources with multipole moments that reproduce the imposed conditions on all boundaries. This interpretation of the multipole expansion will be useful later when considering the effects of liquid compressibility on bubble interaction.

With expressions for the kinetic and potential energy of the system expressed in terms of the chosen coordinates, the dynamical equations may be obtained through either a Lagrangian or Hamiltonian formalism. The Hamiltonian formalism has been chosen for this work. This choice is motivated by several advantages provided by the Hamiltonian equations of motion when integrating the equations numerically and considering the effect of liquid compressibility on the system dynamics. The advantages of the Hamiltonian formulation will be discussed in Sections 2.1.7 and 2.2.

2.1.4 Lagrangian and Hamiltonian mechanics

Both Lagrangian and Hamiltonian mechanics are reformulations of classical Newtonian mechanics. The two are closely related and will be discussed briefly.

Lagrangian mechanics begin with a function, known as the Lagrangian $\mathcal{L}$, defined as the difference between the kinetic and potential energy of the system:

$$\mathcal{L}(q_i, \dot{q}_i, t) = \mathcal{K}(q_i, \dot{q}_i, t) - \mathcal{V}(q_i), \tag{2.12}$$

where q_i and $\dot{q}_i$ represent the generalized coordinates of the system and their time derivatives (velocities), respectively. The Lagrangian can be shown[57,58] to completely characterize the dynamics of the system. The dynamical equations can be calculated from a suitable Lagrangian by means of the Euler-Lagrange equations,

$$\frac{d}{dt}\left(\frac{\partial \mathcal{L}}{\partial \dot{q}_i}\right) = \frac{\partial \mathcal{L}}{\partial q_i}. \tag{2.13}$$

For a system with N generalized coordinates, the Euler-Lagrange equations yield N second-order differential equations that describe the evolution of the system in time.

Hamiltonian mechanics reformulate Lagrangian mechanics through a Legendre transform of the Lagrangian to obtain a new function, the Hamiltonian,

$$\mathcal{H}(q_i, p_i, t) = \sum_j p_j \dot{q}_j - \mathcal{L}(q_i, \dot{q}_i, t). \tag{2.14}$$

The new variables p_i are known as the generalized or conjugate momenta of the coordinates q_i and are defined by

$$p_i = \frac{\partial \mathcal{L}}{\partial \dot{q}_i}. \tag{2.15}$$

This equation must ultimately be used to replace all instances of $\dot{q}$ with functions of p_i on the right-hand side of Eq. (2.14). If the relationship between the generalized coordinates and their conjugate momenta are independent of the time (i.e., if $\mathcal{L}$ does not depend explicitly on the time t), which pertains to the case at hand, then it can be shown that the Hamiltonian is simply the total energy in the system,[57]

$$\mathcal{H} = \mathcal{K} + \mathcal{V}. \tag{2.16}$$

The equations of motion for the system are obtained from Hamilton's canonical equations,

$$\dot{q}_i = \frac{\partial \mathcal{H}}{\partial p_i}, \quad \dot{p}_i = -\frac{\partial \mathcal{H}}{\partial q_i}. \tag{2.17}$$

For a system with N generalized coordinates, Hamilton's equations yield $2N$ first-order differential equations that describe the evolution of the system. An important feature of the Hamiltonian equations of motion is that no time derivatives of the generalized coordinates or their momenta appear on the right-hand side of any equation. The Hamiltonian formalism can be used to obtain the first-order equations of motion for the bubble system.

2.1.5 Equations of motion for the bubble model

In order to obtain the equations of motion for the system it is necessary to choose an appropriate coordinate system. The generalized coordinates are chosen as the bubble radius R and the position vector $\mathbf{X}$. The momenta conjugate to these coordinates are the radial momentum G and the linear, or translational momentum vector $\mathbf{M}$, respectively. The coordinates and momenta of different bubbles are distinguished by subscripts. This coordinate system is illustrated in Fig. 2.1. The

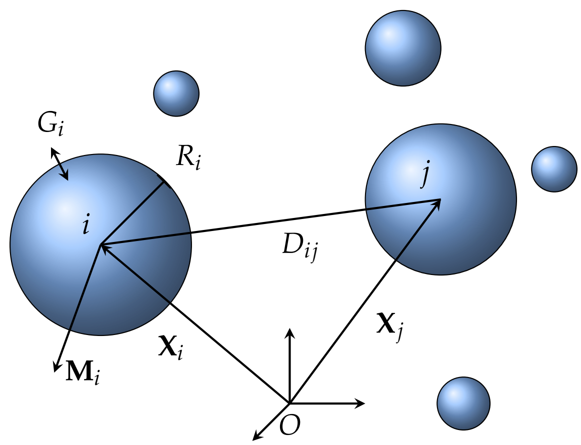

Figure 2.1: Coordinate system and generalized coordinates for Hamiltonian bubble model. R is the bubble radius, G is the radial momentum, the position vector of the bubble is $\mathbf{X}$, and the linear, or translational momentum vector is $\mathbf{M}$. Subscripts are used to distinguish between bubbles, and D_{ij} is the separation distance between bubbles i and j.

generalized momenta obtained from Eq. (2.15),

$$G_i = \frac{\partial \mathcal{L}}{\partial \dot{R}_i}, \quad \mathbf{M}_i = \frac{\partial \mathcal{L}}{\partial \dot{\mathbf{X}}_i}, \tag{2.18}$$

are given by[23]

$$G_i = 4\pi\rho_0 \left[R_i^3 \dot{R}_i + \sum_{j \neq i} \frac{R_i^2 R_j^2}{D_{ij}} \dot{R}_j - \frac{1}{2} \sum_{j \neq i} \frac{R_i^2 R_j^3}{D_{ij}^2} (\dot{\mathbf{X}}_j - \mathbf{u}_{ej}) \cdot \mathbf{n}_{ij} \right] \tag{2.19}$$

and

$$\mathbf{M}_i = \frac{1}{2}\rho_0 V_i (\dot{\mathbf{X}}_i - \mathbf{u}_{ei}) + \frac{3}{2}\rho_0 V_i \sum_{j \neq i} \frac{R_j^2}{D_{ij}} \dot{R}_j \mathbf{n}_{ij}, \tag{2.20}$$

where V_i is the volume of the ith bubble, $D_{ij} = |\mathbf{X}_j - \mathbf{X}_i|$ is the separation distance between the ith and jth bubbles, $\mathbf{n}_{ij} = (\mathbf{X}_j - \mathbf{X}_i)/D_{ij}$ is the normal vector pointing from the ith bubble to the jth bubble, and $\mathbf{u}_{ei}$ is the liquid velocity due to an external source evaluated at the center of the ith bubble. Although they may appear complicated, these expressions for the momenta may be recognized as the product of the liquid mass entrained by the bubble moving radially (Eq. (2.19)) or in translation (Eq. (2.20)) with the radial and translational velocity of the bubble relative to the surrounding fluid, respectively. While the bubble radius and position are natural coordinate choices, their conjugate momenta are not commonly used quantities in studies of bubble dynamics.

When expressed in terms of the generalized coordinates and momenta, the expression for the kinetic energy obtained by the method described in Section 2.1.3 is

$$\begin{aligned}\mathcal{K} = \frac{1}{4\pi\rho_0} \Bigg[& \frac{1}{2} \sum_i \frac{G_i^2}{R_i^3} + 3 \sum_i \frac{M_i^2}{R_i^3} - \frac{1}{2} \sum_{\substack{i,j \\ i \neq j}} \frac{G_i G_j}{R_i R_j D_{ij}} \\ & + 3 \sum_{\substack{i,j \\ i \neq j}} \frac{G_i \left(\mathbf{M}_j \cdot \mathbf{n}_{ij} \right)}{R_i D_{ij}^2} + \frac{1}{2} \sum_{\substack{i,j,k \\ k \neq i,j}} \frac{R_j G_i G_k}{R_i R_k D_{ij} D_{jk}} \Bigg] + \sum_i \mathbf{M}_i \cdot \mathbf{u}_{ei}. \end{aligned} \tag{2.21}$$

The kinetic energy is combined with the potential energy derived in Section 2.1.2 to obtain the Hamiltonian for the bubble system,

$$\begin{aligned}
\mathcal{H} &= \mathcal{K} + \mathcal{V} \\
&= \frac{1}{4\pi\rho_0}\left[\frac{1}{2}\sum_i \frac{G_i^2}{R_i^3} + 3\sum_i \frac{M_i^2}{R_i^3} - \frac{1}{2}\sum_{\substack{i,j\\ i\neq j}} \frac{G_iG_j}{R_iR_kD_{ij}}\right. \\
&\qquad\left. + 3\sum_{\substack{i,j\\ i\neq j}} \frac{G_i\mathbf{M}_j\cdot\mathbf{n}_{ij}}{R_iD_{ij}^2} + \frac{1}{2}\sum_{\substack{i,j,k\\ k\neq i,j}} \frac{R_jG_iG_k}{R_iR_kD_{ij}D_{jk}}\right] \\
&\quad + \sum_i \mathbf{M}_i\cdot\mathbf{u}_{ei} + \sum_i \mathcal{V}_i,
\end{aligned} \tag{2.22}$$

where $\mathcal{V}_i$ is defined in Eq. (2.2). When written in terms of the chosen coordinates, Hamilton's equations are

$$\dot{R}_i = \frac{\partial\mathcal{H}}{\partial G_i}, \quad \dot{\mathbf{X}}_i = \frac{\partial\mathcal{H}}{\partial\mathbf{M}_i}, \quad \dot{G}_i = -\frac{\partial\mathcal{H}}{\partial R_i}, \quad \dot{\mathbf{M}}_i = -\frac{\partial\mathcal{H}}{\partial\mathbf{X}_i}. \tag{2.23}$$

After carrying out the necessary differentiation and simplifying, one obtains the equations of motion for a system of gas bubbles in an incompressible, inviscid, and irrotational liquid with excitation due to an external source written in terms of the generalized coordinates and momenta:

$$\dot{R}_i = \frac{1}{4\pi\rho_0}\left[\frac{G_i}{R_i^3} - \sum_{j\neq i}\frac{G_j}{R_iR_jD_{ij}} + 3\sum_{j\neq i}\frac{\mathbf{M}_j\cdot\mathbf{n}_{ij}}{R_iD_{ij}^2} + \sum_{k\neq i,j}\frac{R_kG_j}{R_iR_jD_{ik}D_{jk}}\right], \tag{2.24a}$$

$$\begin{aligned}\dot{G}_i = \frac{1}{4\pi\rho_0}&\left[\frac{3}{2}\frac{G_i^2}{R_i^4} + 9\frac{M_i^2}{R_i^4} - \sum_{j\neq i}\frac{G_iG_j}{R_i^2R_jD_{ij}} + \sum_{k\neq i,j}\frac{R_kG_iG_j}{R_i^2R_jD_{ik}D_{jk}}\right.\\ &\left.\quad - \frac{1}{2}\sum_{i\neq j,k}\frac{G_iG_k}{R_jR_kD_{ij}D_{ik}} + 3\sum_{j\neq i}\frac{G_i(\mathbf{M}_j\cdot\mathbf{n}_{ij})}{R_i^2D_{ij}^2}\right]\\ &+ 4\pi R_i^2\left(P_i - P_0 - p_{ei}\right),\end{aligned} \tag{2.24b}$$

$$\dot{\mathbf{X}}_i = \frac{3}{2\pi\rho_0}\frac{\mathbf{M}_i}{R_i^3} - \frac{3}{4\pi\rho_0}\sum_{j\neq i}\frac{G_j\mathbf{n}_{ij}}{R_jD_{ij}^2} + \mathbf{u}_{ei}, \tag{2.24c}$$

$$\dot{\mathbf{M}}_i = \frac{1}{4\pi\rho_0}\sum_{j\neq i}\frac{G_iG_j\mathbf{n}_{ij}}{R_iR_jD_{ij}^2} - \frac{4\pi}{3}R_i^3\nabla p_{ei} - (\nabla\mathbf{u}_{ei})^T\mathbf{M}_i. \tag{2.24d}$$

Here the expression $\nabla\mathbf{u}_{ei}$ is interpreted as the spatial gradient of the vector field $\mathbf{u}_{ei}$ evaluated at the bubble center. $\nabla\mathbf{u}_{ei}$ is a second-order tensor field. A modified summation convention is used to express the equations of motion. Unless otherwise indicated, the subscript i represents the index of the current bubble and is not summed. A single summation symbol is used to indicate sums over all other indices, subject to the stated conditions. It should be noted that the corresponding equations presented in Ref. 23 contain an error in the indices of the fifth term on the right-hand of the radial momentum equation. The restrictions on the ranges of the indices are given there as $k \neq i, j$, whereas they should be $i \neq j, k$. In order to integrate the equations of motion presented here, a suitable nondimensional form is required. The nondimensionalization scheme chosen for this work is presented in Section A.1.

2.1.6 Viscosity

The same method used by Ilinskii et al.[23] to include the effects of liquid velocity in the radial and translational equations of motion is used here. The effect of viscosity on the radial motion is included by adding the term

$$-4\eta\frac{\dot{R}_i}{R_i}, \tag{2.25}$$

where η is the coefficient of shear viscosity, to the right-hand side of Eq. (2.3). This term can be interpreted as an effective pressure on the bubble surface due to viscosity of the medium. In the Hamiltonian formalism, the analytical expression for $\dot{R}_i$ (Eq. (2.24a)) must be substituted into the damping term. The result of this substitution in Eq. (2.24b) is the augmented radial momentum equation for a bubble in a viscous incompressible fluid,

$$\begin{aligned}\dot{G}_i = \frac{1}{4\pi\rho_0}\Bigg[&\frac{3}{2}\frac{G_i^2}{R_i^4} + 9\frac{M_i^2}{R_i^4} - \sum_{j\neq i}\frac{G_iG_j}{R_i^2R_jD_{ij}} + \sum_{k\neq i,j}\frac{R_kG_iG_j}{R_i^2R_jD_{ik}D_{jk}}\\ &- \frac{1}{2}\sum_{i\neq j,k}\frac{G_iG_k}{R_jR_kD_{ij}D_{ik}} + 3\sum_{j\neq i}\frac{G_i(\mathbf{M}_j\cdot\mathbf{n}_{ij})}{R_i^2D_{ij}^2}\Bigg]\\ &+ 4\pi R_i^2\left(P_i - P_0 - p_{ei}\right)\\ &+ 4\eta\left[-\frac{G_i}{R_i^2\rho_0} + \sum_{i\neq j}\frac{G_j}{D_{ij}R_j\rho_0} - \sum_{j\neq i,k}\frac{R_jG_k}{D_{ij}D_{jk}R_k\rho_0}\right].\end{aligned} \tag{2.26}$$

The effect of viscosity on the bubble translation is included by adding a drag force to the right-hand side of the translational momentum equation (Eq. (2.24d)) to obtain

$$\dot{\mathbf{M}}_i = \frac{1}{4\pi\rho_0}\sum_{j\neq i}\frac{G_iG_j\mathbf{n}_{ij}}{R_iR_jD_{ij}^2} - \frac{4\pi}{3}R_i^3\nabla p_{ei} - (\nabla\mathbf{u}_{ei})^T\mathbf{M}_i + \mathbf{F}_i^{\text{vis}}. \tag{2.27}$$

While there are many models for the viscous drag force $\mathbf{F}_i^{\text{vis}}$, the simplest is a modified form of Stokes' formula for the drag force on a sphere[23,59,60] given by

$$\mathbf{F}_i^{\text{vis}} = -4\pi\chi\eta R_i\mathbf{u}_{ri}, \tag{2.28}$$

where $\mathbf{u}_{ri}$ is the velocity of the bubble relative to the fluid, and the parameter χ is 1 for flows with a low Reynolds number and 3 for flows with a high Reynolds number. This is the model for viscous drag employed here. When Eq. (2.28) is written in terms of the Hamiltonian coordinates it takes the form

$$\mathbf{F}_i^{\text{vis}} = -2\chi\frac{\eta}{\rho_0R_i^2}\mathbf{M}_i. \tag{2.29}$$

The augmented translational momentum equation with viscosity is then

$$\dot{\mathbf{M}}_i = \frac{1}{4\pi\rho_0}\sum_{j\neq i}\frac{G_iG_j\mathbf{n}_{ij}}{R_iR_jD_{ij}^2} - \frac{4\pi}{3}R_i^3\nabla p_{ei} - (\nabla\mathbf{u}_{ei})^T\mathbf{M}_i - 2\chi\frac{\eta}{\rho_0R_i^2}\mathbf{M}_i. \tag{2.30}$$

2.1.7 Comparison of Hamiltonian and Lagrangian equations of motion

The Lagrangian equations of motion for a system of interacting bubbles without the effect of an external source, bubble translation, or viscosity are

$$R_i\ddot{R}_i + \frac{3}{2}\dot{R}_i^2 = \frac{P_i - P_0}{\rho_0} - \sum_{j\neq i}\frac{R_j}{D_{ij}}\left(R_j\ddot{R}_j + 2\dot{R}_j^2\right). \tag{2.31}$$

Without the summation, this is a general form of the Rayleigh-Plesset equation, the most widely used model of single bubble pulsation in an incompressible fluid. With the summation retained, and with bubble volume given by $V_j = \frac{4}{3}\pi R_j^3$, Eq. (2.31) can be rewritten as

$$\rho_0 \left(R_i \ddot{R}_i + \frac{3}{2} \dot{R}_i^2 \right) = P_i - P_0 - \sum_{i \neq j} \frac{\rho_0 \ddot{V}_j}{4\pi D_{ij}}. \tag{2.32}$$

From this formulation it is seen that the summation is over pressure terms given by the solution for a simple source with volume velocity $\dot{V}_j$ (see Pierce,[61] p. 155). That is, the summation accounts for the acoustic pressure on bubble i radiated by the pulsation of bubble j. Thus, the interaction between the bubbles is transmitted by the acoustic pressure in the medium. Because the host medium is assumed to be incompressible the sound speed is infinite and the interaction occurs instantaneously. Driven by the pressures on the right-hand side, the terms on the left-hand side of Eq. (2.32) represent the inertia of the liquid associated with the motion of bubble i. Equation (2.32) is thus a statement of Newton's law for the radial motion of a bubble.

As is discussed by Hamilton et al.,[51] it is generally necessary to invert a matrix at each time step in order to integrate Eq. (2.31) numerically. This can introduce numerical error into the integration and increase the computational complexity, especially for large systems of bubbles. In contrast, the equations obtained through the Hamiltonian formalism are naturally in the form required for direct numerical integration. They do not require any numerical inversion because no time derivatives appear on the right-hand side of the equations of motion. This is one advantage of the Hamiltonian formulation.

2.2 Time delay due to liquid compressibility

This section describes the effects that the compressibility of the medium surrounding the bubbles has on the dynamics of the system. Methods to extend the model derived in Section 2.1 for an incompressible medium are presented so that the model may be used to study the dynamics of bubbles in compressible media.

2.2.1 Limitations of incompressible theory

The model equations in Section 2.1.5 are derived under the assumption that the compressibility of the liquid surrounding the bubbles is negligible. However, in most bubble systems the effects of liquid compressibility cannot be neglected. The effects of compressibility are typically expected to be important when bubbles are separated by large distances and the acoustic propagation times (delays) are not necessarily short. Also, during large amplitude oscillations, the bubble wall velocities may have Mach numbers near unity in the host medium, and hence compressibility effects are expected to be important. In Chapters 3 and 4 it will be shown that time delay and radiation damping due to liquid compressibility can also have a significant impact on the motion of bubbles in relatively small amplitude oscillations and in close proximity to one another. The present section discusses various effects of liquid compressibility and offers methods by which these effects may be included in the bubble model.

2.2.2 Effects of liquid compressibility

In an incompressible medium, any disturbance immediately influences the entire body; in this sense, an incompressible medium can be considered to have an infinite sound speed. Contrast this with a compressible medium where disturbances travel with a finite propagation speed, which is an intrinsic property of the medium. Small disturbances propagate at the constant acoustic small-signal propagation speed c_0, which can be calculated from the physical properties of the medium.[62] In liquids, the sound speed is

$$c_0 = \sqrt{\frac{K}{\rho_0}}, \tag{2.33}$$

where K is the bulk modulus of the liquid.

2.2.3 Time delays in bubble-bubble interaction

The method for including the effects of acoustic radiation from the bubbles is most transparent in the Lagrangian formulation of the equations of motion. The results may then be extended to the Hamiltonian equations. The Lagrangian equations of motion for a system of interacting bubbles without the effect of an external source or bubble translation is given in Eq. (2.32), repeated here for convenience:

$$\rho_0\left(R_i\ddot{R}_i + \frac{3}{2}\dot{R}_i^2\right) = P_i - P_0 - \sum_{i\neq j}\frac{\rho_0\ddot{V}_j}{4\pi D_{ij}}. \tag{2.34}$$

As stated previously, the sum on the right-hand side of this equation represents the pressure on bubble i produced by the other bubbles in the system. In a compressible medium, a pressure signal requires a finite time to propagate from one bubble to another. This suggests that for a compressible medium the bubble interaction terms on the right-hand side of Eq. (2.34) should be delayed by some time τ_{ij}:

$$\rho_0\left(R_i\ddot{R}_i + \frac{3}{2}\dot{R}_i^2\right) = P_i - P_0 - \sum_{j\neq i}\frac{\rho_0\ddot{V}_j(t-\tau_{ij})}{4\pi D_{ij}}. \tag{2.35}$$

This delayed-interaction method has been used by others to include the effects of time delay due to liquid compressibility,[49–52,63] but there is some variation in the choice of the delay between bubbles. The time required for a signal to propagate between two points in space is determined by the distance D between the two points and the propagation speed c_0 by the equation $\tau = D/c_0$. When considering bubble interaction, it is necessary to choose the appropriate distance across which the signal propagates in order to accurately calculate the delay. Some choices for the delay τ_{ij} used previously are

$$\tau_{ij} = \frac{1}{c_0}\left(|[\mathbf{X}_j]_{\tau_{ij}} - \mathbf{X}_i| - [R_j]_{\tau_{ij}}\right), \tag{2.36}$$

used by Fujikawa and Takahira,[49]

$$\tau_{ij} = \frac{1}{c_0}\left(|[\mathbf{X}_j]_{\tau_{ij}} - \mathbf{X}_i| - R_i - [R_j]_{\tau_{ij}}\right), \tag{2.37}$$

used by Sinden et al.,[53]

$$\tau_{ij} = \frac{1}{c_0}|\mathbf{X}_j - \mathbf{X}_i|, \tag{2.38}$$

used by Doinikov et al.,[46] Ilinskii et al.,[50] Hamilton et al.,[51] Ooi et al.,[47] and Heckman et al.[52], and

$$\tau_{ij} = \frac{1}{c_0}|[\mathbf{X}_j]_{\tau_{ij}} - \mathbf{X}_i|, \tag{2.39}$$

which is very similar to Eq. (2.39), but the position of bubble j is delayed by the distance between the current position of bubble i and the position occupied by bubble j at the time $t - \tau_{ij}$. If translation is neglected, then Eqs. (2.38) and (2.39) are identical. Note that the position and radius of the jth bubble are delayed by the time delay τ_{ij} in Eqs. (2.36)–(2.38). The solutions for R_j and $\mathbf{X}_j$ are not known *a priori*, therefore the presence of delayed instances of these variables on the right-hand sides of these equations represents an implicit definition of the delay τ_{ij} because the equations cannot be solved algebraically. A method by which these equations can be solved by suitable numerical integrators is given in Section B.2.1, and an approximate method to generate explicit definitions for the implicitly defined delays in appropriate cases will be discussed in Section 5.1. Because the physical reasoning for choice of time delay is rarely presented and will be necessary in the coming discussion of the damping of bubble motion due to acoustic radiation, the physical interpretation of each of these delays will be discussed here.

All of the delays except Eq. (2.37) evaluate the effect of other bubbles at the center of the receiving bubble. To justify the choice to evaluate the effect at the bubble center, recall that the bubble is assumed to be much smaller than the acoustic wavelengths of interest. The external pressure field exerts a force on the bubble wall. Given the small size of the bubble in relation to the characteristic acoustic wavelength, it is reasonable to assume that the product of the bubble surface area with the average pressure on the surface of the bubble best approximates this force. Even in transient cases, the average pressure at the center of the bubble provides the best estimate of the pressure experienced by the bubble.

In the bubble model employed here, the pressure produced by a bubble is equivalent to that produced by an ideal point source at the center of the bubble with the same volume velocity as the motion of the bubble wall. Therefore, in order to consider the appropriate form for the delayed pressure produced by one bubble on another, it is helpful to consider the pressure on a sphere produced by an ideal point source placed near the sphere.

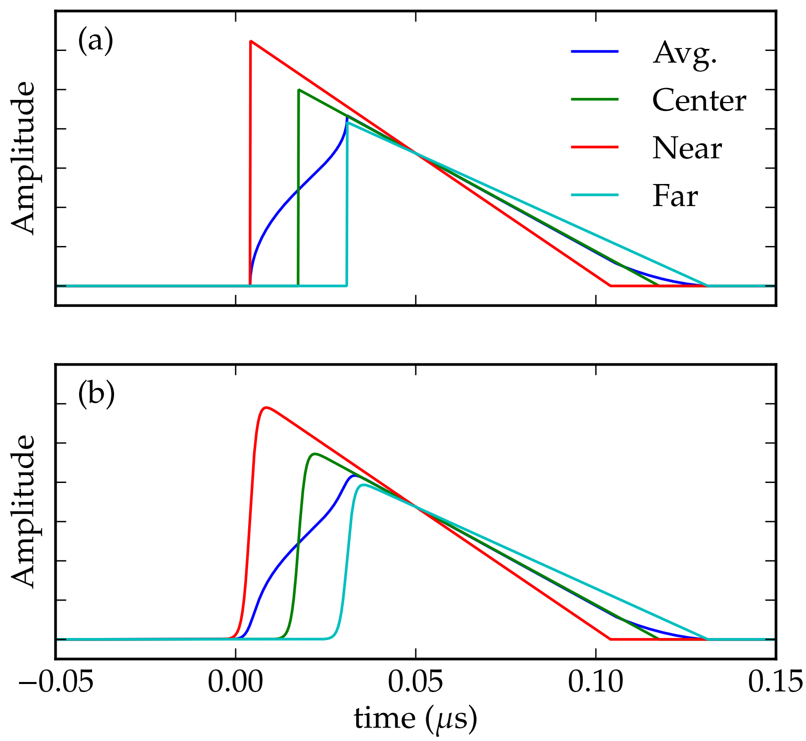

Figure 2.2: The pressure produced by a point source radiating a triangular pulse (a), and a smoothed pulse (b), placed 50 μm from a 20 μm radius sphere: averaged over the surface of the sphere (blue), and evaluated at the center (green), at the near wall (red), and at the far wall (light blue).

The average pressure on the surface of a sphere of radius a due to a point pressure source with a waveform f, placed a distance D from the center of the sphere, is given by the integral

$$p_{\mathrm{avg}} = \frac{1}{2}\int_0^{\pi} \frac{f\left(t - \frac{D}{c_0}\sqrt{1 + 2\frac{a}{D}\cos\theta + \frac{a^2}{D^2}}\right)}{D\sqrt{1 + 2\frac{a}{D}\cos\theta + \frac{a^2}{D^2}}}\sin\theta\, d\theta. \tag{2.40}$$

The result of numerical evaluation of this integral for two different pulse shapes produced by a point source is shown in Fig. 2.2. The sphere has radius $a = 20\,\mu$m and is placed $D = 50\,\mu$m from the source, thus $a/D = 0.4$. The sphere is close enough to the source that the pressure varies significantly over the surface of the sphere, which can be seen in the difference in Fig. 2.2 between the pressure at the near and far sides of the sphere. The pulse is 10 μs in duration or 148 μm long in water, thus the product of wavenumber ($k = 2\pi/\lambda$, where λ is the acoustic wavelength in the liquid) and radius is $ka \approx 0.85$. Note that even though the model is based on the assumption that $ka \ll 1$ and that this is not the case here, the pressure at the center of the sphere provides a reasonable approximation of the amplitude and arrival of the average pressure on the surface of the sphere.

From Fig. 2.2 it is apparent that the pressure evaluated at the center of the sphere provides the best approximation to both the amplitude and the arrival time of an external pressure wave. By the same reasoning, because Eq. (2.37) evaluates the effect of one bubble at the wall of the receiving bubble instead of at the center, it does not provide the most appropriate delay.

In order to compare the other delays in Eqs. (2.36)–(2.39), the positions of the centers and walls of two bubbles are shown in Fig. 2.3 along with the propagation paths, or characteristics, corresponding to each delay. The times and coordinates

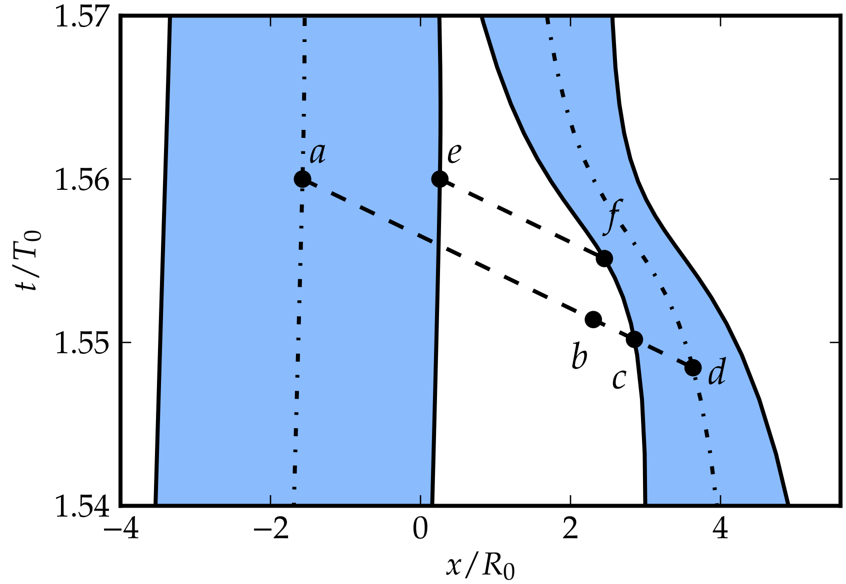

Figure 2.3: Streak plot showing the time evolution of the bubble walls and displacements for two bubbles, along with possible characteristics for propagation of the acoustic signal that couples the bubbles.

of the points shown in the figure will be indicated with subscripts, so that the time at point a is t_a. In order to determine the effect of bubble 2 (the bubble on the right) on bubble 1 at $t = t_a$ it is necessary to determine τ_{12}, the time it takes the motion of bubble 2 to affect bubble 1. The characteristic along which the signal from bubble 2 propagates to bubble 1 is marked by the dashed line. Figure 2.3 illustrates the reasoning for each delay type. Equation (2.37) is the minimal time delay for propagation between the bubbles. The corresponding characteristic is the segment $\overline{ef}$. The results presented in the previous paragraph demonstrate that this is not the appropriate delay. Fujikawa and Takahira[49] chose Eq. (2.36) by reasoning that because the pressure is generated by the motion of the bubble wall, the interaction should be delayed by the distance from the bubble wall at the time the interaction signal was generated to the center of the receiving bubble. This characteristic is represented by the segment $\overline{ac}$ in the figure. The two delays given by Eq. (2.39) and Eq. (2.38) are equal if the bubbles do not translate. If the bubbles are translating, as is the case in Fig. 2.3, then Eq. (2.38) represents radiation (characteristic segment $\overline{ab}$) from a location that does not correspond to any portion of the radiating bubble. The propagation from the past center of one bubble to the current center of another is represented by the characteristic segment $\overline{ad}$

Figure 2.3 seems to suggest that because the propagation characteristic segment $\overline{ac}$ is closest to the path traveled by the physical pressure signal that couples the bubbles, Eq. (2.36) is the best choice for the delay, but this is not the case. In order to determine which of these delays is most appropriate, it is necessary to consider the analytical model for the field produced by the motion of a single bubble. With the assumptions given in Section 2.2.2, the velocity potential in the medium must satisfy the linear wave equation,

$$\nabla^2\phi = \frac{1}{c_0^2}\frac{\partial^2\phi}{\partial t^2}. \tag{2.41}$$

The solution for a spherically symmetric, outward propagating field may be expanded as

$$\phi(r,t) = -\frac{f(t - r/c_0)}{r}. \tag{2.42}$$

The pressure field p and velocity field $\mathbf{u}$ in the liquid may be calculated from the velocity potential:

$$p = -\rho_0 \frac{\partial \phi}{\partial t}, \tag{2.43}$$

$$\begin{aligned} \mathbf{u} &= \boldsymbol{\nabla}\phi \\ &= \frac{\partial \phi}{\partial r}\hat{\mathbf{r}}, \end{aligned} \tag{2.44}$$

where $\hat{\mathbf{r}}$ is the unit vector in the outward radial direction. For a single bubble undergoing spherically-symmetric radial pulsation, the function f is determined by requiring that the bubble wall velocity and fluid velocity match at the bubble wall,

$$\left.\frac{\partial \phi}{\partial r}\right|_{r=R} = \dot{R}, \tag{2.45}$$

or

$$\frac{f(t - R/c_0)}{R^2} + \frac{f'(t - R/c_0)}{Rc_0} = \dot{R}, \tag{2.46}$$

where the prime indicates the total derivative with respect to the argument. The left-hand side of this equation can be expanded in a Taylor series in powers of R/c_0 to obtain:

$$\begin{aligned} \dot{R} &= \frac{f(t - R/c_0)}{R^2} + \frac{f'(t - R/c_0)}{Rc_0} \\ &= \left[\frac{f(t)}{R^2} - \frac{f'(t)}{Rc_0} + \frac{f''(t)}{2c_0^2} + \cdots\right] + \left[\frac{f'(t)}{Rc_0} - \frac{f''(t)}{c_0^2} + \cdots\right] \\ &= \frac{f(t)}{R^2} - \frac{f''(t)}{2c_0^2} + \cdots \\ &= \frac{f(t)}{R^2}\left[1 + O\left(\frac{R^2}{c_0^2 T_0^2}\right)\right]. \end{aligned} \tag{2.47}$$

The last expression can be rearranged to obtain

$$f(t) = R^2\dot{R} \\ = \frac{\dot{V}}{4\pi}, \tag{2.48}$$

where $V = \frac{4}{3}\pi R^3$. The acoustic pressure field valid to $O(1/c_0)$ produced by the bubble is thus given by Eq. (2.43) as

$$p(r,t) = \frac{\rho_0}{4\pi r}\ddot{V}(t - r/c_0). \tag{2.49}$$

This equation indicates that, at $O(1/c_0)$, the pressure produced by the bubble is not delayed by the distance between the receiving point and the bubble wall generating the pressure, but rather by the distance between the receiving point and the bubble center. Thus, the best approximation for the time delay in bubble interactions is proportional to the distance from the center of the radiating bubble at the time the signal was produced to the center of the receiving bubble at the time the signal is received. Therefore, the most appropriate delay is given by Eq. (2.39).

2.2.4 Inclusion of time delays in the Hamiltonian model

In the Lagrangian formulation, the interaction terms are easily identified with the acoustic pressure produced by the motion of the bubble wall, and the relevant delay can easily be determined. The Hamiltonian formulation is more complicated and will be considered in detail here.

The Hamiltonian equations of motion in Section 2.1 are given for the ith bubble in the cluster. All interactions with other bubbles are expressed through functions of the state variables of the other bubbles in the system. As an example, consider the first interaction term in Eq. (2.24a),

$$-\sum_{j\neq i} \frac{G_j}{R_i R_j D_{ij}}. \tag{2.50}$$

This term represents part of the effect that bubble j has on bubble i. The propagation delay due to liquid compressibility is included by delaying this effect by the time required for a pressure signal to propagate between the two bubbles. Hence, all occurrences of variables subscripted with j in Eq. (2.50) must be replaced by the value of that variable at some past time $t-\tau_{ij}$, where the propagation time between the bubbles labeled i and j is represented by τ_{ij}. To distinguish between delayed and non-delayed quantities, delayed quantities will be enclosed by brackets with the delay shown in subscripts, e.g., the value of R_j delayed by τ_{ij} is

$$R_j(t-\tau_{ij}) = [R_j]_{\tau_{ij}}. \tag{2.51}$$

It is also convenient to employ the convention

$$[D_{ij}]_{\tau_{ij}} = \left|[\mathbf{X}_j]_{\tau_{ij}} - \mathbf{X}_i\right|. \tag{2.52}$$

With this notation, expression (2.50) becomes

$$-\sum_{j\neq i} \frac{[G_j]_{\tau_{ij}}}{R_i [R_j D_{ij}]_{\tau_{ij}}}. \tag{2.53}$$

The delay needed to evaluate the terms in Eq. (2.24) that contain variables from only two bubbles may now be calculated. However, several terms in the equations of motion (Eq. (2.24)) contain variables from three bubbles. Unlike the two-bubble interaction terms, it is not immediately apparent how the variables in these terms should be delayed. Some insight may be gained by examining the distances that appear in terms containing variables from three bubbles. The fifth term in Eq. (2.24b) is

$$-\frac{1}{2}\sum_{i\neq j, i\neq k}\frac{G_i G_k}{R_j R_k D_{ij} D_{ik}}. \tag{2.54}$$

Both distances that appear in this term are relative to the ith bubble, the primary bubble for this equation, thus the interaction is due to the combined effect of the fields produced by bubble j and bubble k. This interaction must be delayed by the distance required for a signal to propagate from each bubble to bubble i, therefore the two-bubble delays τ_{ij} and τ_{ik} given by Eq. (2.36) are employed.

A more complicated three-bubble interaction is found in the last term of Eq. (2.24a),

$$\sum_{j\neq i,k}\frac{R_j G_i G_k}{R_i^2 R_k D_{ij} D_{jk}}. \tag{2.55}$$

The presence of the distance D_{ij} implies an interaction of the type discussed in the previous paragraph between the current bubble i and the bubble j. Thus all terms containing the coordinates from the jth bubble must be delayed by τ_{ij} as previously defined. The distance D_{jk} implies an action of the kth bubble on the jth bubble and must be delayed accordingly. Because the variables of bubble j are already delayed by τ_{ij}, the interaction between bubbles j and k must be delayed further. The interaction described by expression (2.55) can be interpreted as the action of bubble k on bubble i, mediated by bubble j. In other words, a signal propagates from bubble k to bubble j and is passed on by bubble j to act on bubble i.

This interpretation is justified by considering the iterative substitution method used in Ref. 23 to obtain the evolution equations for the generalized coordinates. The equation given for the time derivative of the bubble radius is

$$R_i^3\dot{R}_i = \frac{G_i}{4\pi\rho_0} - \sum_{j\neq i}\frac{R_i^2R_j^2}{D_{ij}}\dot{R}_j + \frac{1}{2}\sum_{j\neq i}\frac{R_i^2R_j^3}{D_{ij}^2}\dot{\mathbf{X}}_i\cdot\mathbf{n}_{ij} - \frac{1}{2}\sum_{j\neq i}\frac{R_i^2R_j^3}{D_{ij}^2}\mathbf{u}_{ej}\cdot\mathbf{n}_{ij}. \tag{2.56}$$

In a compressible liquid, each coupling term is delayed by the time required for a signal to propagate between the bubbles. Equation (2.56) becomes

$$\begin{aligned}R_i^3\dot{R}_i = \frac{G_i}{4\pi\rho_0} &- \sum_{j\neq i}\frac{R_i^2[R_j^2]_{\tau_{ij}}}{[D_{ij}]_{\tau_{ij}}}[\dot{R}_j]_{\tau_{ij}} + \frac{1}{2}\sum_{j\neq i}\frac{R_i^2[R_j^3]_{\tau_{ij}}}{[D_{ij}]^2_{\tau_{ij}}}\dot{\mathbf{X}}_i\cdot[\mathbf{n}_{ij}]_{\tau_{ij}}\\ &- \frac{1}{2}\sum_{j\neq i}\frac{R_i^2[R_j^3]_{\tau_{ij}}}{[D_{ij}]^2_{\tau_{ij}}}[\mathbf{u}_{ej}\cdot\mathbf{n}_{ij}]_{\tau_{ij}}.\end{aligned} \tag{2.57}$$

The time derivatives on the right-hand side are eliminated by iterative substitution. The substitutions are made based on the knowledge of an approximate form of the time derivatives of the generalized coordinates to the required order. Each occurrence of the time derivative on the right-hand side of an equation is replaced by its approximation and higher order terms were eliminated. This results in coupled interactions that cannot immediately be associated with the pressure produced by one bubble acting on another as in the Lagrangian equations of motion.

When the analytic approximations for the time derivatives of the generalized coordinates are used in a compressible liquid, all quantities must be delayed appropriately. When the iterative substitutions are made for the delayed variable $[\dot{R}_j]_{\tau_{ij}}$, all coupling terms must be delayed further, thus to $O(R^2/D^2)$ the second term in Eq. (2.57) is

$$
\begin{aligned}
-\sum_{j\neq i}\frac{R_i^2[R_j]_{\tau_{ij}}^2}{[D_{ij}]_{\tau_{ij}}}[\dot{R}_j]_{\tau_{ij}} &= -\sum_{j\neq i}\frac{R_i^2[R_j]_{\tau_{ij}}^2}{[D_{ij}]_{\tau_{ij}}}\left[\frac{G_j}{4\pi R_j^3\rho_0}-\sum_{k\neq j}\frac{R_j^2\,[R_k]_{\tau_{jk}}^2}{\left[D_{jk}\right]_{\tau_{jk}}}\dot{R}_j\right]_{\tau_{ij}} \\
&= -\sum_{j\neq i}\frac{R_i^2[R_j]_{\tau_{ij}}^2}{[D_{ij}]_{\tau_{ij}}}\left[\frac{G_j}{4\pi R_j^3\rho_0}-\sum_{k\neq j}\frac{R_j^2[R_k]_{\tau_{jk}}^2}{[D_{jk}]_{\tau_{jk}}}\frac{G_j}{4\pi R_j^3\rho_0}\right]_{\tau_{ij}}. \qquad (2.58)
\end{aligned}
$$

By definition, $[[R_i]_{\tau_1}]_{\tau_2} = [R_i(t-\tau_1)]_{\tau_2} = R(t-\tau_1-\tau_2) = [R_i]_{\tau_1+\tau_2}$, therefore the delayed terms may be collected:

$$
\begin{aligned}
&-\sum_{j\neq i}\frac{R_i^2[R_j]_{\tau_{ij}}^2}{[D_{ij}]_{\tau_{ij}}}\left[\frac{G_j}{4\pi R_j^3\rho_0}-\sum_{k\neq j}\frac{R_j^2[R_k]_{\tau_{jk}}^2}{[D_{jk}]_{\tau_{jk}}}\frac{G_j}{4\pi R_j^3\rho_0}\right]_{\tau_{ij}} \\
&\qquad = -\frac{1}{4\pi\rho_0}\sum_{j\neq i}\frac{R_i^2[G_j]_{\tau_{ij}}}{[D_{ij}R_j]_{\tau_{ij}}}+\frac{1}{4\pi\rho_0}\sum_{k\neq j}\frac{[G_j]_{\tau_{ij}}[R_k]_{\tau_{ij}+\tau_{jk}}^2}{[R_j]_{\tau_{ij}}[D_{ij}]_{\tau_{ij}}\left[[D_{jk}]_{\tau_{jk}}\right]_{\tau_{ij}}}. \qquad (2.59)
\end{aligned}
$$

The delayed distance in the denominator of the last term on the right-hand side of the previous equation is interpreted as

$$
\begin{aligned}
\left[[D_{jk}]_{\tau_{ij}}\right]_{\tau_{jk}} &= \left|\left[[\mathbf{X}_k]_{\tau_{jk}}-\mathbf{X}_j\right]_{\tau_{ij}}\right| \\
&= \left|[\mathbf{X}_k]_{\tau_{ij}+\tau_{jk}}-[\mathbf{X}_j]_{\tau_{ij}}\right|. \qquad (2.60)
\end{aligned}
$$

Thus, the interpretation of this class of three-bubble interactions as the indirect effect of bubble k on bubble i through bubble j becomes clear, and the appropriate definition of the delay for the third bubble is obtained.

The three-bubble delay must now be calculated. The physical reasoning follows the two-bubble case. It is convenient to introduce the definition $\tau_{ijk} \equiv$

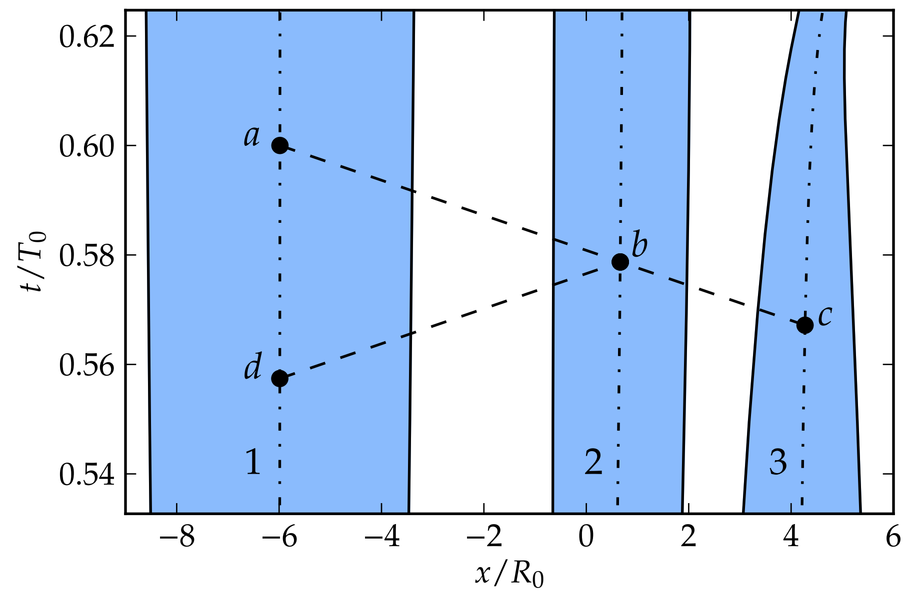

Figure 2.4: Streak plot showing the time evolution of bubble walls and positions for a three-bubble interaction. The propagation characteristics for the bubble interaction signals are included.

$\tau_{ij} + \tau_{jk}$. Henceforth, $\left[[D_{jk}]_{\tau_{ij}}\right]_{\tau_{jk}}$ will be written as $[D_{jk}]_{\tau_{ijk}}$. With the two-bubble delay given in Eq. (2.39), τ_{ijk} is defined implicitly as

$$\begin{aligned}\tau_{ijk} &= \tau_{ij} + \frac{1}{c_0}\left|[\mathbf{X}_k]_{\tau_{ijk}} - [\mathbf{X}_j]_{\tau_{ij}}\right| \\ &= \frac{1}{c_0}\left(\left|[\mathbf{X}_j]_{\tau_{ij}} - \mathbf{X}_i\right| + \left|[\mathbf{X}_k]_{\tau_{ijk}} - [\mathbf{X}_j]_{\tau_{ij}}\right|\right) \qquad (2.61) \\ &= \frac{1}{c_0}\left([D_{ij}]_{\tau_{ij}} + [D_{jk}]_{\tau_{ijk}}\right).\end{aligned}$$

A three-bubble interaction is illustrated in the streak plot in Fig. 2.4. The three bubbles in the plot are numbered 1 to 3 from left to right. The propagation characteristic for the first path of the three-bubble interaction is the segment $\overline{bc}$; this is the action of bubble 3 on bubble 2. The signal resulting from the combination of bubbles 2 and 3 propagates along the characteristic segment $\overline{ab}$ to act on bubble 1 at time t_a. Examination of the plot reveals that the delay $\tau_{123} = t_a - t_b + t_b - t_c = t_a - t_c$. The index constraints of the three-bubble interaction terms are $j \neq i$ and $j \neq k$. It is possible to have $i = k$ and consequently, another possible three-bubble interaction is bubble 1 acting on itself through bubble 2. This interaction signal propagates along the characteristic segment $\overline{bd}$ and then combines with the signal from bubble 2 to propagate along the characteristic segment $\overline{ab}$ to act on bubble 1, and thus $\tau_{121} = t_a - t_b + t_b - t_d = t_a - t_d$.

2.2.5 Modeling coupled bubbles with time delay

With the inclusion of the delays due to the compressibility of the surrounding liquid, the Hamiltonian equations of motion become

$$\dot{R}_i = \frac{1}{4\pi\rho_0}\left(\frac{G_i}{R_i^3} - \sum_{j\neq i}\frac{[G_j]_{\tau_{ij}}}{R_i[R_jD_{ij}]_{\tau_{ij}}} + 3\sum_{j\neq i}\frac{[\mathbf{M}_j\cdot\mathbf{n}_{ij}]_{\tau_{ij}}}{R_i[D_{ij}]^2_{\tau_{ij}}}\right.$$
$$\left. + \sum_{j\neq i,k}\frac{[R_j]_{\tau_{ij}}[G_k]_{\tau_{ijk}}}{R_i[D_{ij}]_{\tau_{ij}}[R_kD_{jk}]_{\tau_{ijk}}}\right), \tag{2.62a}$$

$$\dot{G}_i = \frac{1}{4\pi\rho_0}\left(\frac{3}{2}\frac{G_i^2}{R_i^4} + 9\frac{M_i^2}{R_i^4} - \sum_{j\neq i}\frac{G_i[G_j]_{\tau_{ij}}}{R_i^2[R_jD_{ij}]_{\tau_{ij}}} + \sum_{j\neq i,k}\frac{[R_j]_{\tau_{ij}}G_i[G_k]_{\tau_{ijk}}}{R_i^2[D_{ij}]_{\tau_{ij}}[R_kD_{jk}]_{\tau_{ijk}}}\right.$$
$$\left. - \frac{1}{2}\sum_{i\neq j,k}\frac{G_i[G_k]_{\tau_{ik}}}{[R_jD_{ij}]_{\tau_{ij}}[R_kD_{ik}]_{\tau_{ik}}} + 3\sum_{j\neq i}\frac{G_i[\mathbf{M}_j\cdot\mathbf{n}_{ij}]_{\tau_{ij}}}{R_i^2[D_{ij}]^2_{\tau_{ij}}}\right)$$
$$+ 4\pi R_i^2\left[P_i - P_0 - p_{ei}\right], \tag{2.62b}$$

$$\dot{\mathbf{X}}_i = \frac{3}{2\pi\rho_0}\frac{\mathbf{M}_i}{R_i^3} - \frac{3}{4\pi\rho_0}\sum_{j\neq i}\left[\frac{G_j\mathbf{n}_{ij}}{R_jD_{ij}^2}\right]_{\tau_{ij}} + \mathbf{u}_{ei}, \tag{2.62c}$$

$$\dot{\mathbf{M}}_i = \frac{1}{4\pi\rho_0}\sum_{j\neq i}\frac{G_i[G_j\mathbf{n}_{ij}]_{\tau_{ij}}}{R_i[R_jD_{ij}^2]_{\tau_{ij}}} - \frac{4\pi}{3}R_i^3\nabla p_{ei} - (\nabla\mathbf{u}_{ei})^T\mathbf{M}_i. \tag{2.62d}$$

The addition of propagation delays converts the original system of ordinary differential equations (Eq. (2.24)) into a system of delay differential equations (DDEs). Similar to many nonlinear ordinary differential equations, the delayed equations of motion for the bubble system are analytically intractable and must be integrated numerically. The numerical integration of DDEs requires special care due to the dependence that the current solution has on the past solution. The delay maps past values of the solution to the current value and has two implications. First, the past solution must be known not only at discrete points, but as a continuous function. Second, the accuracy of this interpolated past solution affects the accuracy of the current solution. Therefore, standard methods for numerical integration are not appropriate. Additionally, DDEs may exhibit behavior that is not present in their non-delayed counterpart ordinary differential equations (ODEs), including hyper-chaotic dynamics and synchronization.[64] Additional relevant information on DDEs and the tools used for numerical integration in this work may be found in Appendix B.

The delayed Hamiltonian equations of motion shown here can be classified as a system of state-dependent regular delay differential equations. They are regular because no leading order derivative of any state variable is delayed. Because the delay τ_{ij} is a function of the current and past state variables, the system is classified as state dependent.

Compare the Hamiltonian equations of motion (Eqs. (2.62)) to those obtained by the Lagrangian formalism, shown here with propagation delay, without translation and without the effect of an external source:

$$R_i\ddot{R}_i + \frac{3}{2}\dot{R}_i = \frac{P_i - P_0}{\rho_0} - \sum_{j\neq i}\left[\frac{R_j}{D_{ij}}\left(R_j\ddot{R}_j + 2\dot{R}_j^2\right)\right]_{\tau_{ij}}, \tag{2.63}$$

where the delay τ_{ij} is given by Eq. (2.39). Because the delay is defined in the same way as in the Hamiltonian equations of motion, the delay will be state dependent if bubble translation is considered. However, a key difference between the Hamiltonian and Lagrangian equations is the appearance of delayed leading-order derivatives on the right-hand side of Eq. (2.63).

Delay equations in which the leading order derivatives are delayed are labeled neutral DDEs, thus the Lagrangian formulation produces a set of neutral, state-dependent delay differential equations. This is significant because neutral DDEs can present special difficulties in numerical integration. Many available DDE solvers cannot integrate neutral DDEs, and with those that do it cannot be guaranteed that a solution will be found. An additional complication is the fact that for state-dependent neutral DDEs, the existence of a solution for the general case has not been proven. Thus the regular nature of the delayed Hamiltonian equations of motion provides a significant advantage when seeking numerical solutions. In contrast, the neutral nature of the Lagrangian DDEs limits the solvers that may be used. Bubble simulations performed with the delayed Hamiltonian equations of motion are successful for significantly larger ranges of bubble motion than those performed with the delayed Lagrangian equations of motion.[53]

Because the energy in a system provides a useful metric, it is also necessary to incorporate the effect of delay due to liquid compressibility into the energy expressions. There are no terms representing bubble coupling in the expressions for the potential energy of the system, and therefore these expressions do not change in the presence of compressibility. The expression given for the kinetic energy in Eq. (2.21) must be adapted with the same reasoning used in Section 2.2.4 to include the effects of propagation delay. With the inclusion of the two- and three-bubble delays, the kinetic energy becomes

$$\mathcal{K} = \frac{1}{4\pi\rho_0}\left(\frac{1}{2}\sum_i \frac{G_i^2}{R_i^3} + 3\sum_i \frac{M_i^2}{R_i^3} - \frac{1}{2}\sum_{\substack{i,j\\ i\neq j}} \frac{G_i[G_j]_{\tau_{ij}}}{R_i[R_j D_{ij}]_{\tau_{ij}}}\right.$$
$$\left. +3\sum_{\substack{i,j\\ i\neq j}} \frac{G_i[\mathbf{M}_j \cdot \mathbf{n}_{ij}]_{\tau_{ij}}}{R_i[D_{ij}]^2_{\tau_{ij}}} + \frac{1}{2}\sum_{\substack{i,j,k\\ k\neq i,j}} \frac{[R_j]_{\tau_{ij}} G_i [G_k]_{\tau_{ijk}}}{R_i[D_{ij}]_{\tau_{ij}}[R_k D_{jk}]_{\tau_{ijk}}}\right)$$
$$+\sum_i \mathbf{M}_i \cdot \mathbf{u}_{ei}. \tag{2.64}$$

2.3 Radiation damping due to bubble self-action in a compressible liquid

In addition to delaying bubble interaction, liquid compressibility has an effect on the energy in an oscillating bubble. A compressible medium permits wave propagation. These waves carry energy away from the bubble into the fluid. The radiation of energy from the bubble into the fluid manifests itself in the equations of motion as a damping term. These damping terms are especially important over long time scales, and in large amplitude oscillations when the velocity of the bubble wall is high enough that the Mach number of the bubble wall motion in the liquid is no longer small.

2.3.1 Radiation damping due to self-action of a single bubble

For the case of a single bubble, singular perturbation methods have been used to correct the equations of motion for an incompressible liquid to include the effects of compressibility.[29,32,33] These corrections are expressed as series expansions in powers of $1/c_0$. An elegant and insightful approach was used by Ilinskii and Zabolotskaya[24] to show that the radiation damping is the result of delayed action of the pressure produced by the bubble acting on itself. Corrections to the dynamical equations can be derived from a suitable Taylor expansion of the delayed pressure. See Chicone[65] for a mathematical justification of Taylor expansion of delay differential equations. An understanding of their method is necessary to determine the correct compressibility damping expressions for the Hamiltonian equations of motion.

First recognize that the standard Rayleigh-Plesset equation,

$$\rho_0\left(\ddot{R}R + 2\dot{R}^2\right) - \frac{\rho_0}{2}\dot{R} = P - P_0 - p_e, \tag{2.65}$$

can be written as a pressure balance at the bubble wall,[24]

$$p_1(R,t) + p_2(R,t) + P_0 + p_e = P, \tag{2.66}$$

where P is the pressure just outside the bubble wall given by Eq. (2.3). Here p_1 represents the acoustic, or radiated, pressure produced by the motion of the bubble wall,

$$p_1(r,t) = \frac{\rho_0}{r}(\ddot{R}R^2 + 2\dot{R}^2 R) \tag{2.67}$$

$$= \frac{\rho_0 \ddot{V}}{4\pi r}, \tag{2.68}$$

and p_2 is the Bernoulli pressure due to the motion of the liquid,

$$p_2(r,t) = -\frac{\rho_0}{2}\frac{R^4}{r^4}\dot{R}^2. \tag{2.69}$$

With P_0, p_e, and P considered known, Eq. (2.66) is an exact reformulation of the momentum equation for an incompressible fluid (the Bernoulli equation). The pressures p_1 and p_2 can be termed "self-action" pressures because they are due to the motion of the fluid in response to the motion of the bubble. It was shown in Section 2.2.3 that in a compressible liquid, the acoustic pressure produced by the motion of the bubble wall is delayed by the distance between the bubble center and the receiving point, so that Eq. (2.66) becomes

$$p_1(R, t - R/c_0) + p_2(R, t) + P_0 = P, \tag{2.70}$$

where p_1 is delayed by the distance from the bubble center to the bubble wall. The Bernoulli pressure p_2 is not delayed because it is proportional to $1/r^4$. There is no spherically symmetric solution to the linear wave equation that falls off as $1/r^4$, and thus p_2 represents a non-propagating near-field pressure produced by the inertia of the liquid and is not delayed at this order of approximation. With the definitions in Eqs. (2.67) and (2.69), Eq. (2.70) can be written

$$\text{C1:} \quad \frac{\rho_0}{R}\left[\ddot{R}R^2 + 2\dot{R}^2 R\right]_{t=t-R/c_0} - \frac{\rho_0}{2}\dot{R}^2 = P - P_0 - p_e. \tag{2.71}$$

This approximation for the effects of liquid compressibility is labeled C1 in this work (see Sections 3.3 and 4.1).

Equation (2.71) was obtained by Ilinskii and Zabolotskaya[24] as an intermediate step. As in their work, in order to remove the delay and simplify the problem, it is assumed that the bubble radius is small in comparison to the distance traveled by some acoustic signal in the characteristic time T_0 of the system ($R/c_0T_0 \ll 1$). If this assumption holds, then p_1 on the left-hand side of Eq. (2.70) may be expanded in a Taylor series in the time delay $\tau = R/c_0$. The result of this expansion about $\tau = 0$ is

$$\begin{aligned} p_1(R, t-\tau) &= p_1(R, t) - \tau \frac{\partial p_1}{\partial t} + O(\tau^2) \\ &= \frac{\rho_0}{4\pi R}\ddot{V} - \frac{\rho_0}{4\pi c_0}\dddot{V} + O(1/c_0^2). \end{aligned} \tag{2.72}$$

After this approximation is substituted into Eq. (2.71), expanded, and rearranged, the equation of motion is

$$\rho_0\left(\ddot{R}R + 2\dot{R}^2\right) - \frac{\rho_0}{2}\dot{R} = P - P_0 - p_e + \frac{\rho_0}{4\pi c_0}\dddot{V}. \tag{2.73}$$

This is the modified form of the Rayleigh-Plesset equation for single bubble dynamics in a compressible method that was derived by Ilinskii and Zabolotskaya.[24] In Eq. (2.73) a pressure correction proportional to the third derivative of the bubble volume appears at $O(1/c_0)$. It should be noted that corrections to equations of motion for the position and the translational momentum should occur at $O(1/c_0^2)$, and therefore are not considered here.[66] Interpreting this correction as a modification of the pressure at the bubble surface guides the incorporation of self-action radiation damping into the Hamiltonian bubble model.

Numerical integration of Eq. (2.73) is difficult due to the small $[O(1/c_0)]$ coefficient of the leading-order derivative. It is necessary to use an iterative substitution method to obtain a second-order equation valid to the same order in the expansion parameter $1/c_0$. This is accomplished by solving Eq. (2.73) for $\ddot{R}$ and then differentiating to find an expression for $\dddot{R}$ valid to $O(1/c_0)$, and the result is then substituted into Eq. (2.73) and terms up to the desired order in $1/c_0$ are kept. If necessary, this procedure is repeated until all higher-order derivatives are eliminated.

This approach recovers the commonly used damping terms derived by singular perturbation methods.[32] The result of the recursive substitution is the following form of the Keller-Miksis equation,[29]

$$\text{C2:} \quad \left(1 - \frac{\dot{R}}{c_0}\right) R\ddot{R} + \frac{3}{2}\left(1 - \frac{\dot{R}}{3c_0}\right)\dot{R}^2 = \frac{1}{\rho_0}\left(1 + \frac{\dot{R}}{c_0} + \frac{R}{c_0}\frac{d}{dt}\right)(P - P_0 - p_e)\,. \tag{2.74}$$

This approximation was obtained by Taylor expansion and iterative substitution of the C1 approximation for including the effects of liquid compressibility, and is labeled C2 (or C3 in later chapters). It should be noted that the distinction between the approximations labeled C2 and C3 is only relevant in systems of coupled bubbles, thus C2 is used here.

A similar procedure may be used to incorporate the effects of radiation damping into the Hamiltonian equations of motion. The Hamiltonian equivalent of the Rayleigh-Plesset equation is

$$\dot{R} = \frac{1}{4\pi\rho_0}\frac{G}{R^3}, \tag{2.75a}$$

$$\dot{G} = \frac{3}{8\pi\rho_0}\frac{G^2}{R^4} + 4\pi R^2 (P - P_0 - p_e)\,, \tag{2.75b}$$

where P is the pressure just outside the bubble without the effect of the external source, given by Eq. (2.3). The pressure balance at the surface of the bubble in Eq. (2.71) is rewritten as a force balance in Eq. (2.75b) (recall that the force is the time derivative of the momentum). The first term on the right-hand side of Eq. (2.75b) is the force produced by the motion of the surrounding fluid (Bernoulli pressure times bubble surface area), and the remaining terms are due to the internal, ambient, and external source pressures, respectively.

The pressure correction for bubble self-action in a compressible liquid is added to the pressure terms in the right-hand side Eq. (2.75b) to obtain a set of equations for the dynamics of a single bubble in a compressible medium,

$$\dot{R} = \frac{1}{4\pi\rho_0}\frac{G}{R^3}, \tag{2.76a}$$

$$\dot{G} = \frac{3}{8\pi\rho_0}\frac{G^2}{R^4} + 4\pi R^2\left(P - P_0 - p_e + \frac{\rho_0}{4\pi c_0}\dddot{V}\right). \tag{2.76b}$$

Equations (2.76) should be used instead of Eqs. (2.75) to include the effects of liquid compressibility. The third-order derivative on the right-hand side of Eq. (2.76b) must be eliminated before this equation can be used to simulate the system with numerical integration by standard methods. An alternate expression for $\dddot{V}$ in terms of the state variables is found by differentiating Eq. (2.75a) twice and iteratively substituting Eqs. (2.24) on the right-hand side to eliminate time derivatives. Only term to $O(1/c_0)$ are kept, and the result is

$$\dddot{V} = \frac{G}{4\pi\rho_0^3 R^3}\left[R\frac{\partial P}{\partial R} + 2\left(P - P_0 - p_e\right)\right] - \frac{\partial p_e}{\partial t}\frac{R}{\rho_0} - \frac{3G^3}{16\pi^2\rho_0^3 R^9}. \tag{2.77}$$

This expression is then substituted into Eq. (2.76) to obtain a numerically integrable system of differential equations describing the radial motion of the bubble,

$$\text{C2:} \quad \dot{R} = \frac{1}{4\pi\rho_0}\frac{G}{R^3}, \tag{2.78a}$$

$$\begin{aligned}\dot{G} &= \frac{3}{8\pi\rho_0}\frac{G^2}{R^4} + 4\pi R^2\left(P - P_0 - p_e\right)\\ &\quad + \frac{1}{c_0}\left\{\frac{G}{4\pi\rho_0^3 R}\left[R\frac{\partial P}{\partial R} + 2\left(P - P_0 - p_e\right)\right] - \frac{\partial p_e}{\partial t}\frac{R^3}{\rho_0} - \frac{3G^3}{16\pi^2\rho_0^3 R^7}\right\}.\end{aligned} \tag{2.78b}$$

Whereas the C1 approximation in Eq. (2.71) and the C2 approximation in Eq. (2.74) were expressed in the coordinates of the Lagrangian formulation, this equation is written in the coordinates and momenta of the Hamilton formulation. Because it was obtained by Taylor expansion and iterative substitution to eliminate higher-order derivatives, it is a C2 approximation like Eq. (2.74). Equations (2.78) are equivalent to the Keller-Miksis equation for a single bubble given in Eq. (2.74).

2.3.2 Radiation damping due to self-action in systems of coupled bubbles

In previous studies of coupled bubbles in compressible media,[38–40,46,47,66] the effect of radiation damping was included by adding the single-bubble damping term to the equations of motion. In this section and in the next chapter it will be shown that this method does not fully describe the effects of bubble self-action and radiation damping in systems of coupled bubbles.

If the method used to incorporate radiation losses in the single-bubble case is applied to the coupled-bubble case, the effect of radiation damping is included in the dynamical equations for a system of interacting bubbles by adding the $\dddot{V}_i$ pressure correction to the radial momentum equation. An iterative method must again be used to eliminate third-order derivatives from the equations of motion. In the coupled-bubble case, this process is considerably more difficult due to the the interaction terms. It is necessary to use a computer algebra system to carry out the calculations required to obtain the correct expressions for radiation damping in coupled-bubble systems. To illustrate the magnitude of the problem, at one point the calculation requires that the product of two expressions each containing approximately 4000 individual terms, many of which contain one or more sums, be expanded. The computer algebra package Maxima[67] was used for this work. A special set of Maxima utilities was developed to carry out the necessary calculations. These utilities use the Hamiltonian of the system to calculate the equations of motion, perform the iterative substitutions, and generate Fortran code, thus eliminating human errors.

After the result of these calculations is included, the equation for the radial momentum (Eq. (2.24b)) modified to include viscosity and compressibility becomes

$$\begin{aligned}
\text{C2:}\quad \dot{G}_i = \frac{1}{4\pi\rho_0}\Bigg[& \frac{3}{2}\frac{G_i^2}{R_i^4} + 9\frac{M_i^2}{R_i^4} - \sum_{j\neq i}\frac{G_iG_j}{R_i^2R_jD_{ij}} + \sum_{k\neq i,j}\frac{R_kG_iG_j}{R_i^2R_jD_{ik}D_{jk}} \\
& - \frac{1}{2}\sum_{i\neq j,k}\frac{G_iG_k}{R_jR_kD_{ij}D_{ik}} + 3\sum_{j\neq i}\frac{G_i(\mathbf{M}_j\cdot\mathbf{n}_{ij})}{R_i^2D_{ij}^2}\Bigg] \\
& + 4\pi R_i^2\left(P_i - P_0 - p_{ei}\right) \\
& + 4\eta\left[-\frac{G_i}{R_i^2\rho_0} + \sum_{i\neq j}\frac{G_j}{D_{ij}R_j\rho_0} - \sum_{j\neq i,k}\frac{R_jG_k}{D_{ij}D_{jk}R_k\rho_0}\right] \\
& + C_i^{(c,0)} + C_i^{(c,1)} + C_i^{(c,2)} + C_i^{(\eta,0)} + C_i^{(\eta,1)} + C_i^{(\eta,2)},
\end{aligned} \tag{2.79}$$

where the $C_i^{(c,n)}$ represent the corrections for compressibility to $O(1/c_0)$ and nth order in R/D. The $C_i^{(\eta,n)}$ represent the corrections for compressibility to $O(1/c_0)$ and nth order in R/D that also contain the viscosity coefficient η. Currently, only terms up to second order in R/D and first order in $1/c_0$ are considered. In this work, an approximation for compressibility effects obtained by Taylor expansion of the C1 approximation given in Eq. (2.79) and iterative substitutions of the result to eliminate higher-order derivatives while retaining terms up to $O(R^2/D^2)$ and $O(1/c_0)$ is labeled C2. Thus, Eq. (2.79) is a C2 approximation. The $C_i^{([c,\eta],n)}$ are defined as follows:

$$
\begin{aligned}
C_i^{(c,0)} = \frac{1}{\rho_0 c_0}\Bigg\{ & -\frac{G_i^3}{16\pi^2\rho_0 R_i^7} + 2\frac{G_i}{R_i}\left(P_i - P_0 - p_{ei}\right) + \frac{\partial P_i}{\partial R_i}G_i \\
& - 4\pi\rho_0 R_i^3\frac{\partial p_{ei}}{\partial t} - \frac{9G_i|\mathbf{M}_i|^2}{4\pi^2 R_i^7\rho_0} - 4\pi\rho_0 R_i^3 \boldsymbol{\nabla} p_{ei}\cdot\mathbf{u}_{ei} \\
& -12\mathbf{M}_i\cdot\boldsymbol{\nabla} p_{ei} - \frac{9[(\boldsymbol{\nabla}\mathbf{u}_{ei})^T\mathbf{M}_i]\cdot\mathbf{M}_i}{2\pi R_i^3}\Bigg\},
\end{aligned}
\tag{2.80}
$$

$$
\begin{aligned}
C_i^{(c,1)} = \sum_{i\neq j}\frac{1}{\rho_0 c_0 D_{ij}}\Bigg\{ & \frac{3G_i^2 G_j}{16\pi^2\rho_0 R_i^5 R_j} - \frac{G_i G_j^2}{16\pi^2\rho_0 R_i R_j^5} + \frac{R_i^3 G_j^3}{16\pi^2\rho_0 R_j^9} \\
& - \frac{2R_i G_j}{R_j}(P_i - P_0 - p_{ei}) - \left[\frac{2G_i R_j}{R_i} + \frac{2R_i^3 G_j}{R_j^3}\right](P_j - P_0 - p_{ej}) \\
& - \frac{R_i^2 G_j}{R_j}\frac{\partial P_i}{\partial R_i} - \frac{R_i^3 G_j}{R_j^2}\frac{\partial P_j}{\partial R_j} + 4\pi\rho_0 R_i^3 R_j\frac{\partial p_{ej}}{\partial t} + \frac{9|\mathbf{M}_i|^2 G_j}{4\pi^2 R_i^5 R_j\rho_0} \\
& - \frac{9|\mathbf{M}_j|^2 G_i}{8\pi^2 R_i R_j^5\rho_0} + \frac{9|\mathbf{M}_j|^2 G_j R_i^3}{4\pi^2 R_j^9\rho_0} + \frac{12R_i^3\mathbf{M}_j\cdot\boldsymbol{\nabla} p_{ej}}{R_j^2} \\
& + 4\pi\rho_0 R_i^3 R_j\boldsymbol{\nabla} p_{ej}\cdot\mathbf{u}_{ej} + \frac{9R_i^3\left[(\boldsymbol{\nabla}\mathbf{u}_{ej})^T\mathbf{M}_j\right]\cdot\mathbf{M}_j}{2\pi R_j^5}\Bigg\},
\end{aligned}
\tag{2.81}
$$

$$
\begin{aligned}
C_i^{(c,2)} = \sum_{i\neq j,k} \frac{1}{c_0\rho_0 D_{ij}D_{ik}} \Bigg[& -\frac{3G_iG_jG_k}{16\pi^2\rho_0 R_i^3 R_j R_k} - \frac{5R_iG_j^2G_k}{64\pi^2\rho_0 R_j^5 R_k} + \frac{9R_iG_jG_k^2}{64\pi^2\rho_0 R_j R_k^5} \\
& - \frac{5R_iR_jG_k}{2R_k}(P_j - P_0 - p_{ej}) + \frac{9R_iG_jR_k}{2R_j}(P_k - P_0 - p_{ek}) \\
& + \frac{9}{32\pi^2\rho_0}\left(\frac{9|\mathbf{M}_k|^2 R_i G_j}{R_j R_k^5} - \frac{5|\mathbf{M}_j|^2 R_i G_k}{R_j^5 R_k} \right) \Bigg] \\
+ \sum_{i\neq j,k} \frac{1}{c_0\rho_0 D_{ij}D_{jk}} \Bigg[& \frac{G_iG_jG_k}{8\pi^2\rho_0 R_i R_j^3 R_k} - \frac{3G_i^2R_jG_k}{16\pi^2\rho_0 R_i^5 R_k} - \frac{3R_i^3G_j^2G_k}{16\pi^2\rho_0 R_j^7 R_k} \\
& + \frac{G_iR_jG_k^2}{16\pi^2\rho_0 R_i R_k^5} + \frac{R_i^3G_jG_k^2}{16\pi^2\rho_0 R_j^3 R_k^5} - \frac{R_i^3R_jG_k^3}{16\pi^2\rho_0 R_k^9} \\
& + \frac{2R_iR_jG_k}{R_k}(P_i - P_0 - p_{ei}) + \frac{2R_i^3G_k}{R_jR_k}(P_j - P_0 - p_{ej}) \\
& + \left(\frac{2G_iR_jR_k}{R_i} + \frac{2R_i^3G_jR_k}{R_j^3} + \frac{2R_i^3R_jG_k}{R_k^3} \right)(P_k - P_0 - p_{ek}) \\
& + \frac{R_i^2R_jG_k}{R_k}\frac{\partial P_i}{\partial R_i} + \frac{R_i^3G_k}{R_k}\frac{\partial P_j}{\partial R_j} + \frac{R_i^3R_jG_k}{R_k^2}\frac{\partial P_k}{\partial R_k} - \frac{9R_i^3G_k|\mathbf{M}_j|^2}{4\pi^2R_j^7R_k\rho_0} \\
& - 4\pi\rho_0R_i^3R_jR_k\frac{\partial p_{ek}}{\partial t} - 4\pi\rho_0R_i^3R_jR_k\mathbf{u}_{ek}\cdot\boldsymbol{\nabla}p_{ek} \\
& - \frac{9R_jG_k|\mathbf{M}_i|^2}{4\pi^2R_i^5R_k\rho_0} + \frac{9|\mathbf{M}_k|^2}{8\pi^2R_k^5\rho_0}\left(\frac{G_iR_j}{R_i} + \frac{G_jR_i^3}{R_j^3} - \frac{2R_i^3R_jG_k}{R_k^4} \right) \\
& - \frac{12R_i^3R_j}{R_k^2}\mathbf{M}_k\cdot\boldsymbol{\nabla}p_{ek} - \frac{9R_i^3R_j}{2\pi R_k^5}\left[(\boldsymbol{\nabla}\mathbf{u}_{ek})^T\mathbf{M}_k\right]\cdot\mathbf{M}_k \Bigg]
\end{aligned}
$$

continued on next page

$$
\begin{aligned}
&+\sum_{i\neq j}\frac{1}{\rho_0 c_0 D_{ij}^2}\Bigg[-\frac{3G_j^2\mathbf{M}_i\cdot\mathbf{n}_{ij}}{8\pi^2R_j^5\rho_0}-\frac{3R_i^3\mathbf{M}_j\cdot\mathbf{n}_{ij}}{4\pi^2\rho_0}\left(\frac{G_j^2}{R_j^8}+\frac{3G_i^2}{4R_i^8}\right)+\frac{3G_iG_j\mathbf{M}_i\cdot\mathbf{n}_{ij}}{2\pi^2R_i^4R_j\rho_0}\\
&\quad+\frac{3G_iG_j\mathbf{M}_j\cdot\mathbf{n}_{ij}}{4\pi^2R_iR_j^4\rho_0}-\frac{27|\mathbf{M}_i|^2\mathbf{M}_j\cdot\mathbf{n}_{ij}}{4\pi^2R_i^5\rho_0}-\frac{27|\mathbf{M}_j|^2\mathbf{M}_i\cdot\mathbf{n}_{ij}}{4\pi^2R_j^5\rho_0}\\
&\quad+\frac{27R_i^3|\mathbf{M}_j|^2\mathbf{M}_j\cdot\mathbf{n}_{ij}}{4\pi^2R_j^8\rho_0}+6R_i(\mathbf{M}_j\cdot\mathbf{n}_{ij})(P_i-P_0-p_{ei})\\
&\quad+\frac{12}{R_j^2}(P_j-P_0-p_{ej})\left(R_i^3\mathbf{M}_j-R_j^3\mathbf{M}_i\right)\cdot\mathbf{n}_{ij}+3R_i^2(\mathbf{M}_j\cdot\mathbf{n}_{ij})\frac{\partial P_i}{\partial R_i}\\
&\quad-\frac{2R_j^3G_i}{R_i}\boldsymbol{\nabla}p_{ej}\cdot\mathbf{n}_{ij}+\frac{5R_i^3G_j}{R_j}\left(\boldsymbol{\nabla}p_{ei}-\boldsymbol{\nabla}p_{ej}\right)\cdot\mathbf{n}_{ij}-6R_i^3\{[\boldsymbol{\nabla}(\boldsymbol{\nabla}p_{ej})]\mathbf{M}_j\}\cdot\mathbf{n}_{ij}\\
&\quad-4\pi\rho_0R_i^3R_j^3\left(\frac{\partial}{\partial t}\boldsymbol{\nabla}p_{ej}\right)\cdot\mathbf{n}_{ij}+8\pi R_jR_i^3(P_j-P_0-p_{ej})\left(\mathbf{u}_{ej}-\mathbf{u}_{ei}\right)\cdot\mathbf{n}_{ij}\\
&\quad-4\pi\rho_0R_i^3R_j^3\{[\boldsymbol{\nabla}(\boldsymbol{\nabla}p_{ej})]\mathbf{u}_{ej}\}\cdot\mathbf{n}_{ij}-4\pi\rho_0R_i^3R_j^3[(\boldsymbol{\nabla}(\mathbf{u}_{ej})^T\boldsymbol{\nabla}p_{ej}]\cdot\mathbf{n}_{ij}\\
&\quad+\frac{R_i^3G_j^2}{4\pi R_j^5}(\mathbf{u}_{ej}-\mathbf{u}_{ei})\cdot\mathbf{n}_{ij}+\frac{G_iG_j}{2\pi R_iR_j}\left(\mathbf{u}_{ej}-\mathbf{u}_{ei}\right)\cdot\mathbf{n}_{ij}\\
&\quad+\frac{9R_i^3}{2\pi R_j^5}|\mathbf{M}_j|^2(\mathbf{u}_{ej}-\mathbf{u}_{ei})\cdot\mathbf{n}_{ij}+\frac{R_i^3G_j}{R_j}\frac{\partial}{\partial t}\left(\mathbf{u}_{ej}-\mathbf{u}_{ei}\right)\cdot\mathbf{n}_{ij}\\
&\quad-\frac{3R_i^3G_i}{2\pi R_i^4}\left[(\boldsymbol{\nabla}\mathbf{u}_{ej})^T\cdot\mathbf{M}_j\right]\cdot\mathbf{n}_{ij}+\frac{3R_i^3G_j}{2\pi R_j^4}\left\{\left[\boldsymbol{\nabla}\mathbf{u}_{ej}-(\boldsymbol{\nabla}\mathbf{u}_{ej})^T\right]\cdot\mathbf{M}_j\right\}\cdot\mathbf{n}_{ij}\\
&\quad+\frac{3G_j}{2\pi R_j}\left\{\left[(\boldsymbol{\nabla}\mathbf{u}_{ei})^T-\boldsymbol{\nabla}\mathbf{u}_{ei}\right]\mathbf{M}_i\right\}\cdot\mathbf{n}_{ij}+3R_i^3([(\boldsymbol{\nabla}\mathbf{u}_{ej})^2]^T\mathbf{M}_j)\cdot\mathbf{n}_{ij}\\
&\quad+\frac{R_i^3G_j}{R_j}[(\boldsymbol{\nabla}\mathbf{u}_{ej})\mathbf{u}_{ej}-(\boldsymbol{\nabla}\mathbf{u}_{ei})\mathbf{u}_{ei}]\cdot\mathbf{n}_{ij}-3R_i^3\left\{\left[\frac{\partial}{\partial t}(\boldsymbol{\nabla}\mathbf{u}_{ej})^T\right]\cdot\mathbf{M}_j\right\}\cdot\mathbf{n}_{ij}\\
&\quad+3R_i^3\left(\boldsymbol{\nabla}\left\{\left[\boldsymbol{\nabla}\left(\mathbf{u}_{ej}\cdot\mathbf{M}_j\right)\right]\cdot\mathbf{n}_{ij}\right\}\right)\cdot\left(\frac{\mathbf{M}_j}{2\pi\rho_0R_j^3}-\mathbf{u}_{ej}\right)\Bigg].
\end{aligned}
\tag{2.82}
$$

Direct tensor notation is employed in the previous expressions. The velocity gradient $\nabla\mathbf{u}$ is a second-order tensor, and the right-hand product of a tensor and a vector $[(\nabla\mathbf{u})\mathbf{M}]$ is a vector. The center dot $(\cdot)$ represents the dot product between vectors, and a superscript T represents the tensor transpose. The third-order tensor expression in the last term of Eq. (2.82) may be written in standard index notation as

$$(\nabla\{[\nabla(\mathbf{u}\cdot\mathbf{M})]\cdot\mathbf{n}\})\cdot\left(\frac{\mathbf{M}}{2\pi\rho_0 R^3}-\mathbf{u}\right)=\sum_{i,j,k=1}^{3}\frac{\partial^2 u_i}{\partial x_j\partial x_k}M_i n_j\left(\frac{M_k}{2\pi\rho_0 R^3}-u_k\right). \tag{2.83}$$

All three indices are summed from 1 to 3. Here the indices refer not to the bubble number, but to vector components. The M_i are the components of a single-bubble momentum vector $\mathbf{M}$, n_i represent the components of a unit normal vector $\mathbf{n}$, and u_i are the components of the velocity vector field. All expressions containing u_i are evaluated at the bubble center.

The viscosity terms are

$$C_i^{(\eta,0)}=\frac{\chi\eta}{3\rho_0 c_0}\left[\frac{G_i^2}{2\pi\rho_0 R_i^5}+\frac{16\eta G_i}{\rho_0 R_i^3}-16\pi R_i(P_i-p_{ei}-P_0)-\frac{36|\mathbf{M}_i|^2}{\pi\rho_0 R_i^5}\right], \tag{2.84}$$

$$\begin{aligned}C_i^{(\eta,1)}=&\sum_{i\neq j}\frac{\chi\eta}{3\rho_0 c_0 D_{ij}}\left[-\frac{G_iG_j}{\pi\rho_0 R_i^3 R_j}+\frac{2G_iG_j}{\pi\rho_0 R_i R_j^3}+\frac{R_iG_j^2}{2\pi\rho_0 R_j^5}-\frac{R_i^3G_j^2}{2\pi\rho_0 R_j^7}\right.\\&\left.+16\pi R_i^2\left(\frac{R_j}{R_i}+\frac{R_i}{R_j}\right)(P_j-P_0-p_{ej})+\frac{9R_i^3|\mathbf{M}_j|^2}{\pi\rho_0 R_j^5}\left(\frac{1}{R_i^2}+\frac{4}{R_j^2}\right)\right]\\&-\sum_{i\neq j}\frac{16\chi\eta^2}{c_0\rho_0^2 D_{ij}}\left[\frac{G_j}{R_iR_j}+\frac{R_iG_j}{R_j^3}+\frac{R_i^3G_j}{R_j^5}\right],\end{aligned} \tag{2.85}$$

and

$$
\begin{aligned}
C_i^{(\eta,2)} = &\sum_{i\neq j,k} \frac{\chi\eta}{3\rho_0 c_0 D_{ij} D_{ik}} \left(\frac{G_j G_k}{2\pi\rho_0 R_i R_j R_k} + \frac{5R_i G_j G_k}{2\pi\rho_0 R_j^3 R_k} - \frac{9R_i G_j G_k}{2\pi\rho_0 R_j R_k^3} \right) \\
&+ \sum_{j\neq i,k} \frac{\chi\eta}{3\rho_0 c_0 D_{ij} D_{jk}} \left\{ \frac{G_i R_j G_k}{\pi\rho_0 R_i^3 R_k} - \frac{2G_i G_k}{\pi\rho_0 R_i R_j R_k} - \frac{R_i G_j G_k}{\pi\rho_0 R_j^3 R_k} + \frac{R_i^3 G_j G_k}{\pi\rho_0 R_j^5 R_k} \right. \\
&\qquad - \frac{2G_i R_j G_k}{\pi\rho_0 R_i R_k^3} - \frac{2R_i^3 G_j G_k}{\pi\rho_0 R_j^3 R_k^3} - \frac{R_i R_j G_k^2}{2\pi\rho_0 R_k^5} - \frac{R_i^3 G_k^2}{2\pi\rho_0 R_j R_k^5} + \frac{R_i^3 R_j G_k^2}{2\pi\rho_0 R_k^7} \\
&\qquad - 16\pi \left[R_i R_j R_k + \frac{R_i^3 R_k}{R_j} + \frac{R_i^3 R_j}{R_k} \right] (P_k - P_0 - p_{ek}) \\
&\qquad \left. - \frac{9R_i^3 |\mathbf{M}_k|^2}{\pi\rho_0 R_k^5} \left(\frac{1}{R_j} + \frac{R_j}{R_i^2} + \frac{4R_j}{R_k^2} \right) \right\} \\
&+ \sum_{j\neq i,k} \frac{16\chi\eta^2}{3\rho_0^2 c_0 D_{ij} D_{jk}} \left[\frac{R_j G_k}{R_i R_k} + \frac{R_i G_k}{R_j R_k} + \frac{R_i^3 G_k}{R_j^3 R_k} + \frac{R_i R_j G_k}{R_k^3} + \frac{R_i^3 G_k}{R_j R_k^3} + \frac{R_i^3 R_j G_k}{R_k^5} \right] \\
&+ \sum_{i\neq j} \frac{\chi\eta}{3\rho_0 c_0 D_{ij}^2} \left[\frac{3}{\pi} \left(\frac{G_i}{R_i^3} - \frac{3G_i}{R_i R_j^2} - \frac{2G_j R_i}{R_j^4} - \frac{4G_j R_i^3}{R_j^6} \right) \mathbf{M}_j \cdot \mathbf{n}_{ij} \right. \\
&\qquad + \left(\frac{15G_j}{\pi R_i^2 R_j} + \frac{12G_j}{\pi R_j^3} \right) \mathbf{M}_i \cdot \mathbf{n}_{ij} + \left(\frac{4R_i G_j}{R_j} + \frac{8R_i^3 G_j}{R_j^3} \right) \mathbf{u}_{ei} \cdot \mathbf{n}_{ij} \\
&\qquad - \left(\frac{4R_i G_j}{R_j} + \frac{8R_i^3 G_j}{R_j^3} \right) \mathbf{u}_{ej} \cdot \mathbf{n}_{ij} \\
&\qquad + \left(16\pi R_i R_j^3 + 24\pi R_i^3 R_j \right) \nabla p_{ej} \cdot \mathbf{n}_{ij} \\
&\qquad \left. + \left(\frac{36R_i^3}{R_j^2} + 12R_i \right) [(\nabla \mathbf{u}_{ej})^T \mathbf{M}_j] \cdot \mathbf{n}_{ij} \right].
\end{aligned}
\tag{2.86}
$$

As was explained in Section 2.1.6 following Eq. (2.28), χ varies depending on the Reynolds number of the flow. The relative importance of these additional expressions will be considered in Chapter 3.

It should be mentioned that the model equations given in Eqs. (A44)–(A48) of Fuster and Colonius[17] appear to be analogous to the model equations in Eqs. (2.62) and (2.79), but written in terms of bubble radius R_i, radial velocity $\dot{R}_i$, and radial acceleration $\ddot{R}_i$. Fuster and Colonius do not use a Lagrangian or a Hamiltonian formulation to derive their equations of motion. Their equations are obtained by an expansion of the coupled velocity potential for the medium surrounding the bubbles. The equations of Fuster and Colonius contain terms to the same order in $1/c_0$ and R/D, but neglect translation and are valid only to $O(R/D)$, whereas the model equations presented in this chapter include translation and are valid to $O(R^2/D^2)$. Even without the effects of translation in Eqs. (2.62) and (2.79), the large number of terms in both sets of equations precludes direct comparison.

If in Eq. (2.79) all coupling terms associated with liquid compressibility (terms of $O(1/c_0)$ that are also $O(R/D)$) are neglected, then only $C_i^{(c,0)}$ remains. This requires the assumption that the interaction between the bubbles in the cluster does not influence the radiation damping of the bubbles in the system, and hence the expression for the single-bubble radiation damping may be used. $C_i^{(c,0)}$ can be recognized as the compressibility terms in Eq. (2.78b), augmented to include the effects of bubble translation. This approximation is labeled C3 in this work. If the time delays in bubble interaction are neglected in the C3 approximation, then the result is labeled C4. The labels assigned to the various approximations for liquid compressibility effects used in this work are summarized in Table 2.1. All labels with corresponding equations are presented together in Appendix C.

Label	Description	Equations
C1	Delayed self-action pressure, delays in bubble interaction	Eq. (2.71) (single), Eq. (3.12) (coupled)
C2	Delayed self-action pressure expanded in Taylor series, terms up to $O(1/c_0) \times O(R^2/D^2)$ kept, delays in bubble interaction	Eqs. (2.62) and (2.79)
C3	Delayed self-action pressure expanded in Taylor series, terms of $O(1/c_0) \times O(R/D)$ discarded, delays in bubble interaction	Eqs. (2.62) and (2.79), only $C_i^{(c,0)}$ in Eq. (2.79)
C4	C3 without delays in bubble interaction	Eqs. (2.62) and (2.79), only $C_i^{(c,0)}$ in Eq. (2.79), no delays
C1-L	Linearized form of C1	Eq. (3.13)
C2-L	Linearized form of C2	Eq. (3.23)
C3-L	Linearized form of C3	Eq. (3.15)
C4-L	Linearized form of C4	Eq. (3.24)

Table 2.1: Summary of labels assigned to methods of approximation for the effects of liquid compressibility along with equations in which the approximations are given.

2.4 Summary

The Hamiltonian model developed by Ilinskii et al.[23] was presented and adapted to include the effect of compressibility in the host medium and viscosity. The liquid compressibility manifests itself through a delay in the bubble interaction, and radiation damping due to the delayed action of a bubble on itself. When compared with the equations of motion obtained by a Lagrangian formalism, the Hamiltonian equations of motion afford several advantages. In an incompressible medium, numerical matrix inversion is not required. In a compressible medium, the Hamiltonian equations of motion are regular delay differential equations instead of neutral delay differential equations as are obtained in the Lagrangian case. Thus in the case of a compressible liquid, the Hamiltonian differential equations are better suited to numerical integration with existing software tools. Also, in problems requiring iterative substitutions to eliminate higher-order derivatives, as in Section 2.3.2, the Hamiltonian equations provide a simpler approach. This property will again be useful in developing approximations for the implicitly defined delays and the delay equations, which is discussed in Chapter 5.

Four possible expressions for the bubble interaction time delay were presented, along with the physical motivation for choosing Eq. (2.39) as the most appropriate expression. A physical interpretation of the three-bubble interaction terms in the Hamiltonian equations of motion was presented and used to motivate the selection of suitable delays for the elements of these terms. The effect of radiation damping was considered first for the single-bubble Hamiltonian model and then for the coupled-bubble system.

The method of Ilinskii and Zabolotskaya,[68] wherein the self-acting radiated pressure produced by a bubble is delayed by the time required for the pressure to propagate from the bubble center to the bubble wall, was employed. This approximation for compressibility effects (Eq. (2.71)) was labeled C1. A new expression for the radiation damping due to the self-action of a bubble in the Hamiltonian equations of motion for a system of coupled bubbles was presented in the form of a series expansion to first order in $1/c_0$ and second order in R/D. This approximation for liquid compressibility effects, consisting of delays in bubble interactions and the approximate series expansion for the delayed self-action, was labeled C2 (Eq. (2.79)). The related approximation for compressibility effects in which the effect of bubble interactions on the bubble self-action expansion is neglected was labeled C3. The C3 approximation is obtained by retaining only the term $C_i^{(c,0)}$ in the last line of Eq. (2.79).

Chapter 3

Stability and Dynamics of One- and Two-Bubble Systems in a Compressible Liquid

Results of numerical integration of the Hamiltonian equations of motion for a single bubble, modified to include radiation damping due to liquid compressibility (Eqs. (2.76)), are compared to results from integration of the corresponding Lagrangian (Keller-Miksis) equation of motion, an accepted standard for single-bubble dynamics in a compressible fluid, to demonstrate that radiation damping is taken into account consistently in the Hamiltonian formulation. Metrics to evaluate and compare coupled-bubble systems are presented. Three linearized models that include time delay and radiation damping due to liquid compressibility at differing orders of approximation in systems of interacting bubbles are developed. The linearized model for coupled bubbles with single-bubble radiation damping and without time delay is included for comparison. An eigenvalue analysis of the linearized models is used to evaluate the relative importance of the corresponding four levels of approximation that were discussed in Chapter 2 (C1, C2, C3, C4; see Table 2.1) for the self-action and time delay due to liquid compressibility in a two-bubble system. Nonlinear time-domain motion predicted by the C2 model for a compressible liquid and compared to the predictions of the C4 model with single-bubble radiation damping, and without time delay in bubble interactions. The pressure produced by a system of two bubbles excited by a tone burst is predicted by the C2 model for a compressible medium is compared to the predictions of the C4 model for a range of bubble separation distances and excitation amplitudes.

3.1 Verification of single-bubble radiation damping in the Hamiltonian formulation

In order to demonstrate that the corrections for radiation damping in a Hamiltonian bubble system agree with commonly used models, results from the numerical integration of both the new Hamiltonian system in Eq. (2.78) and the Keller-Miksis equation given in Eq. (2.74) are compared. The Keller-Miksis model is chosen for comparison not because it is most accurate, but rather because it is most frequently used to include the effects of liquid compressibility.[32,33] A single bubble with an equilibrium radius of $R_0 = 20\,\mu$m, characteristic period $T_0 = 6.08\,\mu$s, an initial radius of $10R_0$, and initially at rest is simulated in free response using both models, with the results shown in Fig. 3.1. The bubble radius accelerates into a collapse at $t/T_0 \approx 3$, after which the bubble rebounds and undergoes successively smaller oscillations. Because the effects of liquid viscosity are neglected, the majority of the damping occurs during the initial collapse ($t/T_0 \approx 3$) due to the enormous acceleration, and corresponding radiation of a high-amplitude acoustic pulse. The subsequent damping due to acoustic radiation is much lower. Part (a) of the figure shows the bubble radius normalized by the equilibrium radius R_0, and part (b) shows the difference between the Hamiltonian model presented here and the Keller-Miksis model that is often used. This case was chosen to illustrate the agreement between the two models during a violent collapse when compressibility effects are especially strong. Part (b) of the figure shows that the two models provide the same result to within the numerical tolerances.

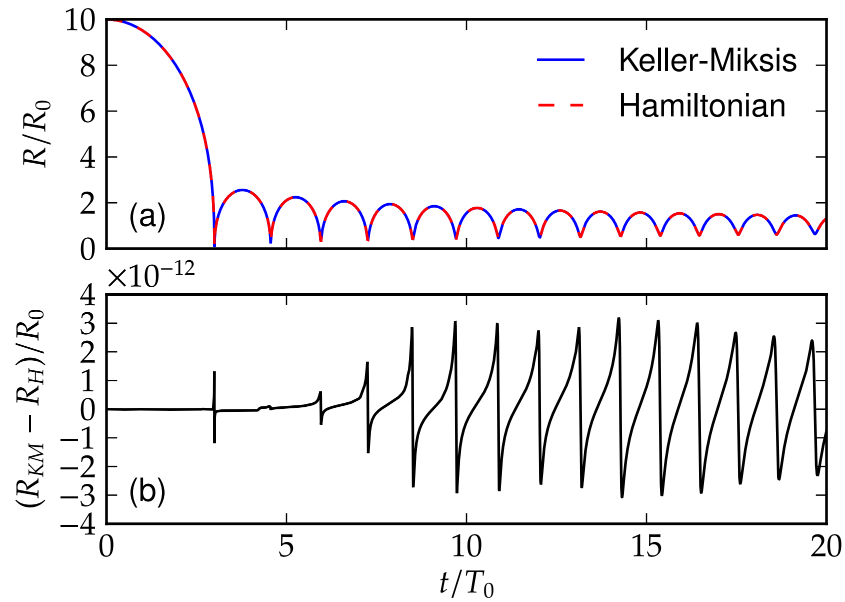

Figure 3.1: Comparison of radiation damping in Keller-Miksis and Hamiltonian formulations of single bubble motion. The free response of a bubble released from rest with an initial radius of $10R_0$, where $R_0 = 20\,\mu$m, is shown. The normalized bubble radii [part (a)] agree within numerical precision. The difference between the Keller-Miksis prediction (R_{KM}) and the Hamiltonian prediction (R_H) is shown in part (b).

3.2 Bubble system metrics

While comparison of single bubble systems is simple, comparisons of systems containing multiple bubbles are considerably more complicated. Direct comparison of the radius-time curves can be difficult for a two-bubble system, confusing for a three-bubble system, and nearly impossible for a ten-bubble system, even when the bubbles do not translate. To provide concise means for comparing different systems, several metrics are employed for the bubble radii, positions, and combined quantities that characterize the system. Because no single metric completely characterizes the system, it is often necessary to use several metrics together in order to gain insight into the behavior of the system.

3.2.1 Radial metrics

Two previously used metrics are the average bubble radius,[66] given by

$$R_{\text{avg}} = \frac{1}{N} \sum_{i=1}^{N} R_i, \tag{3.1}$$

and the effective bubble radius,[50] which is the radius of a sphere with the same volume as that of all of the bubbles in the system when added together,

$$R_{\text{eff}} = \left[\sum_{i=1}^{N} R_i^3 \right]^{1/3}. \tag{3.2}$$

It is useful to reference these metrics to an appropriate equilibrium radius calculated by applying the metric to the equilibrium state of the system,

$$R_{0,\text{avg}} = \frac{1}{N} \sum_{i=1}^{N} R_{0i}, \tag{3.3}$$

$$R_{0,\mathrm{eff}} = \left[\sum_{i=1}^{N} R_{0i}^3 \right]^{1/3}, \tag{3.4}$$

to obtain measures of relative displacement from equilibrium, $R_{\mathrm{avg}} - R_{0,\mathrm{avg}}$ and $R_{\mathrm{eff}} - R_{0,\mathrm{eff}}$. Both of these metrics suffer from the same shortcoming, which is that they may return small values for systems that contain bubbles in anti-phase motion. In these cases, a similar but more sensitive metric is the average radial displacement,

$$R_{\mathrm{disp}} = \frac{1}{N} \sum_{i=1}^{N} |R_i - R_{0i}|. \tag{3.5}$$

These three metrics are compared in Figs. 3.2 and 3.3. Both figures show the three metrics applied to the free response of a two-bubble system consisting of two equal-sized bubbles with equilibrium radius of 20 μm, separated by 200 μm and initially at rest. In Fig. 3.2, the bubbles are released in phase from $1.1R_0$. In Fig. 3.3, the bubbles are initially in anti-phase, meaning that one bubble starts with a radius of $0.9R_0$ and the other bubble starts with a radius of $1.1R_0$.

Figure 3.2 shows that, for in-phase motion, the three metrics give fairly similar results, with the average radial displacement approximating a rectified version of the average bubble radius. However, the anti-phase case shown in Fig. 3.3 exhibits significant differences between between the three metrics. Both the average radius and the effective radius show apparently small variations from equilibrium, while the average radial displacement correctly characterizes the motion of the bubble system as being nearly identical in amplitude to the in-phase case. The dramatic difference in the damping of the in- and anti-phase cases will be discussed later in the chapter.

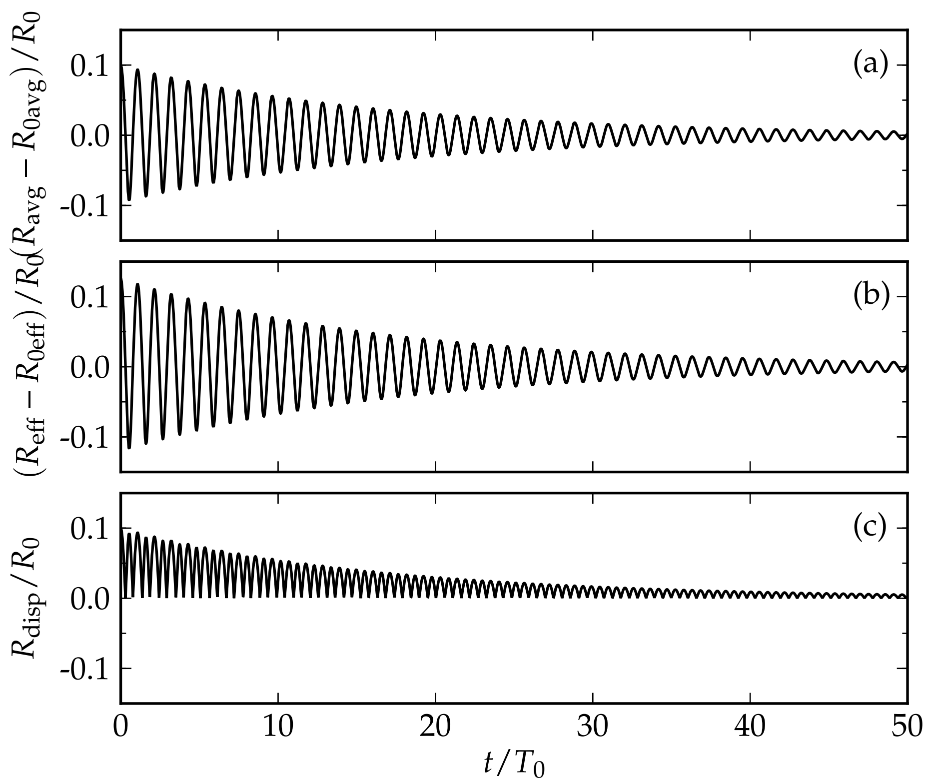

Figure 3.2: Comparison of three different metrics for the radii in a bubble system. The three metrics are applied to a pair of bubbles each with a radius of 20 μm, separated by 20 bubble radii (200 μm). The bubbles are in in-phase free response from $1.1R_0$ and released from rest. Part (a) shows the average radius given by Eq. (3.1), part (b) shows the effective radius given by Eq. (3.2), and part (c) shows the average radial displacement given by Eq. (3.5). All metrics are normalized by the equilibrium radius $R_0 = 20\,\mu$m.

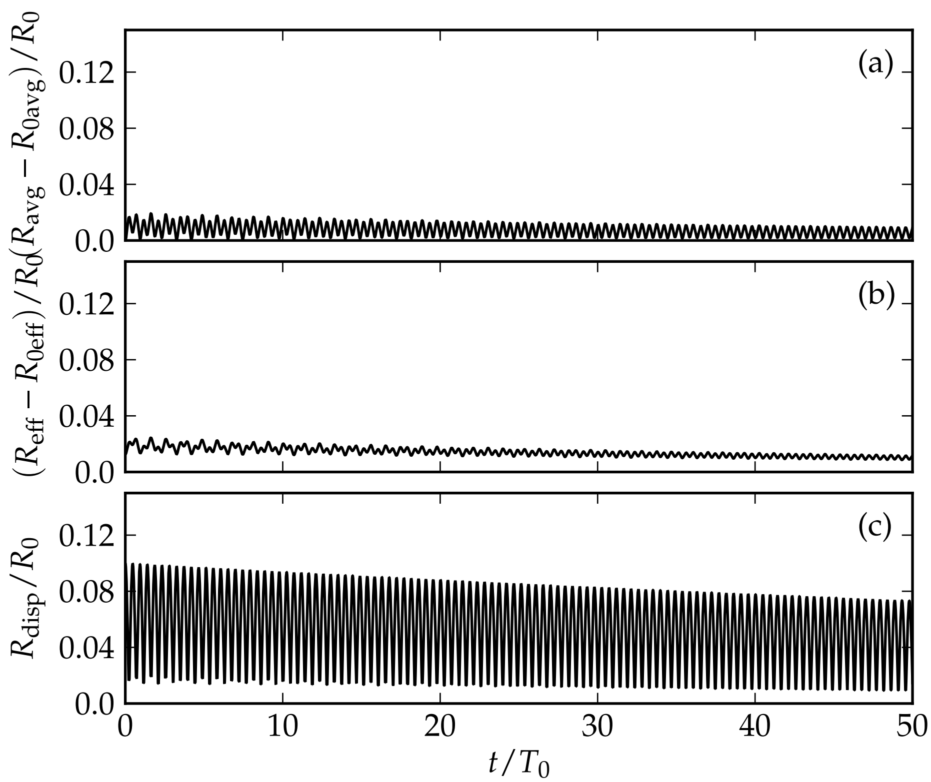

Figure 3.3: Comparison of three different metrics for the radii in a bubble system. The three metrics are applied to a pair of bubbles each with a radius of 20 μm, separated by 20 bubble radii (200 μm). The bubbles are in anti-phase free response from $1.1R_0$ and $0.9R_0$ and released from rest. Part (a) shows the average radius given by Eq. (3.1), part (b) shows the effective radius given by Eq. (3.2), and part (c) shows the average radial displacement given by Eq. (3.5). All metrics are normalized by the equilibrium radius $R_0 = 20\,\mu$m.

3.2.2 Positional metrics

The most natural positional metric for a two-bubble system is the center-to-center distance,

$$D = |\mathbf{X}_2 - \mathbf{X}_1|. \tag{3.6}$$

This metric can only be applied to two-bubble systems. Related metrics for multi-bubble systems will be discussed in Chapter 4. Two other metrics can be used as indicators for the amount of displacement experienced by bubbles in a system. The average displacement is

$$D_{\text{avg}} = \frac{1}{N} \sum_{i=1}^{N} |\mathbf{X}_i - \mathbf{X}_{i0}|, \tag{3.7}$$

where $\mathbf{X}_{i0} = \mathbf{X}_i|_{t=t_0}$ is the initial position of the bubble, and the average total displacement is found by integrating,

$$D_{\text{tot}} = \frac{1}{N} \sum_{i=1}^{N} \int_{t_0}^{t} |\dot{\mathbf{X}}_i| \, dt. \tag{3.8}$$

Together, the average displacement and average total displacement can serve as indicators of translational trends within the system. For example, a small average displacement combined with a large average total displacement would be indicative of oscillatory motion in the bubble positions, while similar values for both displacement quantities would suggest bulk translation of the system. Clearly, for models without translation, all of these positional metrics will be constant.

3.2.3 Combined metrics

It is also useful to define combined metrics that indicate the overall state of the system. An especially useful combined metric is the total energy in the bubble system, which is equal to the Hamiltonian of the system defined by Eq. (2.22),

$$
\begin{aligned}
E = \frac{1}{4\pi\rho_0} & \left[\frac{1}{2} \sum_i \frac{G_i^2}{R_i^3} + 3 \sum_i \frac{M_i^2}{R_i^3} - \frac{1}{2} \sum_{\substack{i,j \\ i \neq j}} \frac{G_i G_j}{R_i R_k D_{ij}} \right. \\
& \left. + 3 \sum_{\substack{i,j \\ i \neq j}} \frac{G_i \mathbf{M}_j \cdot \mathbf{n}_{ij}}{R_i D_{ij}^2} + \frac{1}{2} \sum_{\substack{i,j,k \\ k \neq i,j}} \frac{R_j G_i G_k}{R_i R_k D_{ij} D_{jk}} \right] \\
& + \sum_i \mathbf{M}_i \cdot \mathbf{u}_{ei} + \sum_i \mathcal{V}_i,
\end{aligned}
\tag{3.9}
$$

where $\mathcal{V}_i$ is given by Eq. (2.4). The total energy in the system can be decomposed into kinetic energy due to the bubbles, $\mathcal{K}_{\text{bub}}$, potential energy in the bubbles, $\mathcal{V}_{\text{bub}}$, and energy due to the external acoustic source, E_{src}, such that $E = \mathcal{K}_{\text{bub}} + \mathcal{V}_{\text{bub}} + E_{\text{src}}$. It is often convenient to subtract the equilibrium energy,

$$
E_0 = \sum_i \mathcal{V}_i \Big|_{R_i = R_{0i}}, \tag{3.10}
$$

from the total energy so that the resultant quantity is zero when the system is at rest.

For low-amplitude oscillations, it is possible to identify a damping coefficient by fitting an exponential curve to the energy in the system. The damping coefficient provides a single number metric which facilitates comparison of systems across large variations in parameters. Unfortunately, for high-amplitude radial motion, the energy dissipation no longer follows an exponential trend and thus a standard damping coefficient cannot be calculated. Thus the damping coefficient may only be used as a metric for systems in low-amplitude motion. Generally, there is a damping coefficient associated with each individual mode of a system. The presence of multiple modes can complicate the analysis of a system using damping coefficients as metrics.

Another physical quantity that is useful as a metric is the pressure produced by the bubble system. The pressure at the point $\mathbf{x}$ is

$$\begin{aligned} p_s(\mathbf{x}, t) &= \sum_i \frac{\rho_0 \ddot{V}_i(t - \tau_i)}{4\pi |\mathbf{X}_i(t - \tau_i) - \mathbf{x}|} \\ &= \sum_i \frac{\rho_0}{|\mathbf{X}_i(t - \tau_i) - \mathbf{x}|} \left[R_i^2 \ddot{R}_i + 2R_i \dot{R}_i^2 \right]_{t=t-\tau_i}, \end{aligned} \tag{3.11}$$

where the delay τ_i is defined implicitly by $\tau_i = (|[\mathbf{X}_i]_{\tau_i} - \mathbf{x}|)/c_0$. The pressure produced by a bubble system is a useful metric because it often provides the clearest indicator of the effect that the system will have on the surrounding environment.

3.3 Analysis of compressibility coupling terms

3.3.1 Stability analysis of linearized systems

Section 2.3.2 describes corrections for the effects of liquid compressibility in systems of coupled bubbles. The present section develops a linearized model to evaluate the relative importance of these corrections. Initial analysis is most easily conducted using a Lagrangian (modified Rayleigh-Plesset) system. In this section only the effects of liquid compressibility are considered. The effects of viscosity, thermal damping, and surface tension are neglected here and included in Section 4.2.

For a linearized system without bubble translation, it is possible to derive expressions that allow comparisons of the corrections for compressibility effects presented in Chapter 2. The derivation begins by combining the single bubble equation for the delayed self-action of a bubble (Eq. (2.63)) and the time-delayed Lagrangian equations of motion (Eq. (2.71)) to obtain

$$\frac{1}{R_i}\left[R_i^2\ddot{R}_i + 2R_i\left(\dot{R}_i\right)^2\right]_{t=t-R_i/c_0} - \frac{1}{2}\left(\dot{R}_i\right)^2 = \frac{P_i - P_0 - p_{ei}}{\rho_0} - \sum_{i\neq j}\left[\frac{R_j}{D_{ij}}\left(R_j\ddot{R}_j + 2\dot{R}_j\right)\right]_{t=t-\tau_{ij}}. \tag{3.12}$$

Equation (3.12) is linearized by defining $R_i = R_{0i} + \xi_i$, where $|\xi_i|$ is the radial displacement of the ith bubble. It is then necessary to assume $\xi_i \ll R_{0i}$ and expand Eq. (3.12), retaining only terms up to $O(\xi)$. The result is

$$\text{C1-L:}\quad \ddot{\xi}_i(t - R_{0i}/c_0) + \omega_{0i}^2\xi_i(t) + \sum_{i\neq j}\frac{R_{0j}^2}{D_{ij}R_{0i}}\ddot{\xi}_j(t-\tau_{ij}) = -\frac{p_{ei}(t)}{R_{0i}\rho_0}, \tag{3.13}$$

where $\omega_{0i}^2 = 3\gamma P_0/R_{0i}^2\rho_0$ is the square of the natural angular frequency in the absence of losses and surface tension, often called the Minnaert frequency.[55] The approximation for the effects of liquid compressibility obtained by appropriately delaying the self-action term is labeled C1 in the current work (see Table 2.1). The linearized version in Eq. (3.13) is labeled C1-L. All labeled approximations are collected in Appendix C. The delay in bubble interactions is

$$\tau_{ij} = \frac{D_{ij}}{c_0}. \tag{3.14}$$

In previous work,[46,47] rewritten in the current notation and neglecting thermal and viscous damping the following approximations of Eq. (3.13) is used:

$$\text{C3-L:}\quad \ddot{\xi}_i(t) + \omega_{0i}\delta_{i,\mathrm{rad}}\dot{\xi}_i(t) + \omega_{0i}^2\xi_i(t) + \sum_{i\neq j}\frac{R_{0j}^2}{D_{ij}R_{0i}}\ddot{\xi}_j(t-\tau_{ij}) = -\frac{p_{ei}(t)}{R_{0i}\rho_0} \tag{3.15}$$

and the associated time-harmonic version produced by introducing $e^{j\omega t}$ time dependence on the right-hand side[38–40] have been used to model coupled bubbles. In the time-harmonic version, the time delayed terms on the left-hand side become the phase terms $e^{-jkD_{ij}}$. This approximation for the effects of liquid compressibility is labeled C3 here, and the linearized version is labeled C3-L. Note that Eqs. (3.13) and (3.15) differ only in the first term on the left-hand side of Eq. (3.13) and the first two terms on the left-hand side of Eq. (3.15). The constant $\delta_{i,\mathrm{rad}}$ is the nondimensional radiation damping coefficient defined by Leighton[55] as

$$\delta_{i,\mathrm{rad}} = \frac{\omega_{0i} R_{0i}}{c_0}. \tag{3.16}$$

Thus the second term on the left-hand side of Eq. (3.15) is the common damping expression for the radiation damping of a single bubble derived by Devin[69] and which appears in Ref. 55.

In order to relate Eq. (3.13) to Eq. (3.15) it is necessary to expand the first term on the left-hand side of Eq. (3.13) in a Taylor series for small values of the delay R_{0i}/c_0 to find the approximate form

$$\ddot{\xi}_i(t) - \frac{R_{0i}}{c_0}\dddot{\xi}_i(t) + \omega_{0i}^2 \xi_i(t) + \sum_{i \neq j} \frac{R_{0j}^2}{D_{ij} R_{0i}} \ddot{\xi}_j(t - \tau_{ij}) = -\frac{p_{ei}(t)}{R_{0i}\rho_0}. \tag{3.17}$$

Equation (3.15) is obtained if it can assumed that

$$\dddot{\xi}_i(t) = -\omega_{0i}^2 \dot{\xi}_i(t). \tag{3.18}$$

The validity of this assumption may be tested by solving Eq. (3.17) for $\ddot{\xi}_i$ and differentiating the result to obtain an expression for $\dddot{\xi}_i$,

$$\dddot{\xi}_i(t) = -\omega_{0i}^2 \dot{\xi}_i(t) - \frac{1}{R_{0i}\rho_0}\frac{\partial p_{ei}}{\partial t} - \sum_{i \neq j} \frac{R_{0j}^2}{D_{ij} R_{0i}} \dddot{\xi}_j(t - \tau_{ij}) + O(1/c_0). \tag{3.19}$$

Because this expression will be multiplied by R_{0i}/c_0 in the equation of motion, all terms of $O(1/c_0)$ here will be $O(1/c_0^2)$ in the equation of motion and only terms of $O(1/c_0)$ will be kept in the final equation, all terms of $O(1/c_0)$ are neglected here. Comparison of Eqs. (3.18) and (3.19) reveals the implicit assumption in Eq. (3.15) that the neighboring bubbles and the external source have a negligible impact on the radiation damping. The current chapter will demonstrate that assuming bubble interactions and source coupling do not affect the radiation damping is not always appropriate.

Iterative substitution of Eq. (3.19) into itself to eliminate third-order derivatives on the right-hand side while neglecting $O(1/c_0)$ terms and retaining terms up to $O(R_0^2/D_{ij}^2)$ results in an alternate expression,

$$\dddot{\xi}_i(t) = -\omega_{0i}^2\dot{\xi}_i(t) - \frac{1}{R_{0i}\rho_0}\frac{\partial p_{ei}}{\partial t} + \sum_{i\neq j}\frac{R_{0j}^2}{D_{ij}R_{0i}}\left(\omega_{0j}^2\dot{\xi}_j(t-\tau_{ij}) + \frac{1}{R_{0j}\rho_0}\frac{\partial p_{ej}}{\partial t}(t-\tau_{ij})\right)$$
$$- \sum_{j\neq i,k}\frac{R_{0j}R_{0k}^2}{D_{ij}D_{jk}R_{0i}}\left(\omega_{0k}^2\dot{\xi}_k(t-\tau_{ij}-\tau_{jk}) + \frac{1}{R_{0k}\rho_0}\frac{\partial p_{ek}}{\partial t}(t-\tau_{ij}-\tau_{jk})\right). \quad (3.20)$$

With this expression, the damping term in Eq. (3.17) is

$$-\frac{R_{0i}}{c_0}\dddot{\xi}_i(t) = \frac{R_{0i}\omega_{0i}^2}{c_0}\dot{\xi}_i(t) + \frac{1}{\rho_0 c_0}\frac{\partial p_{ei}}{\partial t} - \sum_{i\neq j}\frac{R_{0j}^2}{c_0 D_{ij}}\left(\omega_{0j}^2\dot{\xi}_j(t-\tau_{ij}) - \frac{R_{0i}}{R_{0j}\rho_0}\frac{\partial p_{ej}}{\partial t}(t-\tau_{ij})\right)$$
$$+ \sum_{j\neq i,k}\frac{R_{0j}R_{0k}^2}{c_0 D_{ij}D_{jk}}\left(\omega_{0k}^2\dot{\xi}_k(t-\tau_{ij}-\tau_{jk}) + \frac{1}{\rho_0}\frac{\partial p_{ek}}{\partial t}(t-\tau_{ij}-\tau_{jk})\right). \quad (3.21)$$

Similar to the Keller-Miksis equation (Eq. (2.74)), the time derivative of the source pressure enters the dynamical equations through the iterative substitution. The first term on the right-hand side of Eq. (3.21) is the leading order contribution to the single-bubble radiation damping. The remaining terms are corrections to the radiation damping due to bubble-bubble interactions and source effects.

For free response the damping term is

$$-\frac{R_{0i}}{c_0}\dddot{\xi}_i(t) = \frac{R_{0i}\omega_{0i}^2}{c_0}\dot{\xi}_i(t) - \sum_{i\neq j}\frac{R_{0j}^2}{c_0 D_{ij}}\omega_{0j}^2\dot{\xi}_j(t-\tau_{ij})$$
$$+\sum_{j\neq i,k}\frac{R_{0j}R_{0k}^2}{c_0 D_{ij}D_{jk}}\omega_{0k}^2\dot{\xi}_k(t-\tau_{ij}-\tau_{jk}). \tag{3.22}$$

The contribution of each of these terms to the damping in the system can now be analyzed. The first term on the right-hand side is the commonly used expression for linear radiation damping, and it has a purely resistive effect on the radial motion. The sign of the second term leads to the conclusion that in-phase arrivals from other bubbles in the system tend to reduce the radiation damping, while arrivals that are out of phase tend to increase the radiation damping. The third term is a three-bubble interaction with the opposite effect (note that for negligible time delay, the terms have opposite signs).

The expanded damping term in Eq. (3.21) is substituted into Eq. (3.17) to obtain the the linearized equations of motion with coupling corrections for radiation damping,

$$\text{C2-L:}\quad \ddot{\xi}_i(t) + \frac{R_{0i}\omega_{0i}^2}{c_0}\dot{\xi}_i(t) + \omega_{0i}^2\xi_i(t) + \sum_{i\neq j}\frac{R_{0j}^2}{D_{ij}R_{0i}}\ddot{\xi}_j(t-\tau_{ij})$$

$$-\sum_{i\neq j}\frac{\omega_{0j}^2 R_{0j}^2}{c_0 D_{ij}}\dot{\xi}_j(t-\tau_{ij}) + \sum_{j\neq i,k}\frac{\omega_{0k}^2 R_{0j} R_{0k}^2}{c_0 D_{ij} D_{jk}}\dot{\xi}_k(t-\tau_{ij}-\tau_{jk})$$

$$= -\frac{p_{ei}(t)}{R_{0i}\rho_0} - \frac{1}{\rho_0 c_0}\frac{\partial p_{ei}}{\partial t}(t) - \sum_{i\neq j}\frac{R_{0i}R_{0j}}{\rho_0 c_0 D_{ij}}\frac{\partial p_{ej}}{\partial t}(t-\tau_{ij})$$

$$+\sum_{j\neq i,k}\frac{R_{0j}R_{0k}^2}{\rho_0 c_0 D_{ij} D_{jk}}\frac{\partial p_{ek}}{\partial t}(t-\tau_{ij}-\tau_{jk}), \tag{3.23}$$

which has been rearranged to place all source terms on the right-hand side of the equation. The approximation resulting from retention of terms to first order in $1/c_0$ and second order in R/D in the iterative substitution used to eliminate the third-order derivative in the Taylor expansion of the C1 approximation is labeled the C2 approximation. The linearized form in Eq. (3.23) is labeled C2-L. The first term in the second row on the right-hand side of Eq. (3.23) is the single-bubble radiation damping expression used in Eq. (3.15) (the C3-L approximation). The remaining terms are corrections for bubble interaction effects. It can now be seen that the C3-L approximation results from neglecting terms of $O(R/D)$ that are also $O(1/c_0)$.

If the time delays in bubble interaction are neglected in the C3 model, the resulting model is labeled C4. The C4-L model is presented here for reference.

$$\text{C4-L:}\quad \ddot{\xi}_i(t) + \omega_{0i}\delta_{i,\mathrm{rad}}\dot{\xi}_i(t) + \omega_{0i}^2\xi_i(t) + \sum_{i\neq j}\frac{R_{0j}^2}{D_{ij}R_{0i}}\ddot{\xi}_j(t) = -\frac{p_{ei}(t)}{R_{0i}\rho_0}. \tag{3.24}$$

The homogeneous equations of motion for the four linearized approximations are:

$$\text{C1-L:}\quad \ddot{\xi}_i(t - R_{0i}/c_0) + \omega_{0i}^2 \xi_i(t) + \sum_{i\neq j} \frac{R_{0j}^2}{D_{ij} R_{0i}} \ddot{\xi}_j(t - \tau_{ij}) = 0, \tag{3.25}$$

$$\begin{aligned} \text{C2-L:}\quad & \ddot{\xi}_i(t) + \frac{R_{0i}\omega_{0i}^2}{c_0}\dot{\xi}_i(t) + \omega_{0i}^2 \xi_i(t) + \sum_{i\neq j} \frac{R_{0j}^2}{D_{ij} R_{0i}} \ddot{\xi}_j(t - \tau_{ij}) \\ & - \sum_{i\neq j} \frac{\omega_{0j}^2 R_{0j}^2}{c_0 D_{ij}} \dot{\xi}_j(t - \tau_{ij}) + \sum_{j\neq i,k} \frac{\omega_{0k}^2 R_{0j} R_{0k}^2}{c_0 D_{ij} D_{jk}} \dot{\xi}_k(t - \tau_{ij} - \tau_{jk}) = 0, \end{aligned} \tag{3.26}$$

$$\text{C3-L:}\quad \ddot{\xi}_i(t) + \frac{R_{0i}\omega_{0i}^2}{c_0}\dot{\xi}_i(t) + \omega_{0i}^2 \xi_i(t) + \sum_{i\neq j} \frac{R_{0j}^2}{D_{ij} R_{0i}} \ddot{\xi}_j(t - \tau_{ij}) = 0, \tag{3.27}$$

$$\text{C4-L:}\quad \ddot{\xi}_i(t) + \frac{R_{0i}\omega_{0i}^2}{c_0}\dot{\xi}_i(t) + \omega_{0i}^2 \xi_i(t) + \sum_{i\neq j} \frac{R_{0j}^2}{D_{ij} R_{0i}} \ddot{\xi}_j(t) = 0. \tag{3.28}$$

In this form the C2-L (Eq. (3.26)) and C3-L (Eq. (3.27)) approximations can be compared. The C2-L approximation contains two coupling terms that do not appear in the C3-L approximation. These two terms appear on the second row of the right-hand side of Eq. (3.26) and represent corrections for bubble interactions in a compressible medium.

The homogeneous equations of motion will now be analyzed to compare the damping in the C1-L, C2-L, and C3-L equations of motion. The change in the damping of a system is most easily seen by an eigenvalue analysis of the governing homogeneous differential equations. To simplify the analysis, a two bubble system with equally sized bubbles is considered. Both the approximate model and the analytical model are analyzed. For the system of two equal bubbles Eq. (3.25) reduces to

$$\ddot{\xi}_1(t - R_0/c_0) + \omega_0^2 \xi_1 + \frac{R_0}{D}\ddot{\xi}_2(t - \tau) = 0 \tag{3.29a}$$

$$\ddot{\xi}_2(t - R_0/c_0) + \omega_0^2 \xi_2 + \frac{R_0}{D}\ddot{\xi}_1(t - \tau) = 0, \tag{3.29b}$$

where τ is given by

$$\tau = \frac{D}{c_0}. \tag{3.30}$$

A decoupled system of equations may be found by adding and subtracting Eqs. (3.29a) and (3.29b) and defining $\xi_+ = \xi_1 + \xi_2$ and $\xi_- = \xi_1 - \xi_2$. The new variables correspond to the in-phase mode (r_+) and the anti-phase mode (r_-) of the system. When written in terms of the new variables, the C1-L equations of motion are

$$\ddot{\xi}_+(t - R_0/c_0) + \omega_0^2 \xi_+(t) + \frac{R_0}{D}\ddot{\xi}_+(t - \tau) = 0, \tag{3.31a}$$

$$\ddot{\xi}_-(t - R_0/c_0) + \omega_0^2 \xi_-(t) - \frac{R_0}{D}\ddot{\xi}_-(t - \tau) = 0. \tag{3.31b}$$

The solutions to Eq. (3.31) are assumed to be of the form $\xi = \chi e^{st}$, where χ is a constant. Substitution of this *ansatz* into Eq. (3.31) produces the characteristic equations for the C1-L approximation:

$$s_+^2 \left(e^{-s_+ R_0/c_0} + \frac{R_0}{D} e^{-s_+ \tau} \right) + \omega_0^2 = 0, \tag{3.32a}$$

$$s_-^2 \left(e^{-s_- R_0/c_0} - \frac{R_0}{D} e^{-s_- \tau} \right) + \omega_0^2 = 0. \tag{3.32b}$$

The roots of these equations are the eigenvalues of the system; s_+ is the eigenvalue of the in-phase mode and s_- is the eigenvalue of the anti-phase mode.

The same procedure applied to the C2-L model (Eq. (3.23)) produces the characteristic equations

$$s_+^2\left(1+\frac{R_0}{D}e^{-s_+\tau}\right)+s_+\frac{R_0\omega_0^2}{c_0}\left(1-\frac{R_0}{D}e^{-s_+\tau}+\frac{R_0^2}{D^2}e^{-s_+\tau}\right)+\omega_0^2=0 \tag{3.33a}$$

$$s_-^2\left(1-\frac{R_0}{D}e^{-s_-\tau}\right)+s_-\frac{R_0\omega_0^2}{c_0}\left(1+\frac{R_0}{D}e^{-s_-\tau}+\frac{R_0^2}{D^2}e^{-s_-\tau}\right)+\omega_0^2=0. \tag{3.33b}$$

The analogous characteristic equations for the C3-L model (Eq. (3.15)) are

$$s_+^2\left(1+\frac{R_0}{D}e^{-s_+\tau}\right)+s_+\frac{R_0\omega_0^2}{c_0}+\omega_0^2=0 \tag{3.34a}$$

$$s_-^2\left(1-\frac{R_0}{D}e^{-s_-\tau}\right)+s_-\frac{R_0\omega_0^2}{c_0}+\omega_0^2=0. \tag{3.34b}$$

In general, the eigenvalues are complex, $s = -\delta\omega/2 \pm i\omega$, where δ is the nondimensional damping coefficient (reciprocal of the quality factor) and ω is the natural frequency of the corresponding mode. Although Eqs. (3.32)–(3.34) are transcendental and in general will have an infinite number of eigenvalues, the stability of the system is determined by the right-most root in the complex plane. The remainder of the current section will be concerned with the right-most eigenvalues of the two natural modes, or eigenvalues for which δ is negative.

It is known that for small-amplitude oscillations, bubbles moving in phase produce a mutual load on each other that results in an increased effective mass of the oscillating system.[68] The increased effective mass reduces the natural frequency of the bubbles in the system relative to the natural frequency of a single bubble. An opposite effect occurs for bubbles moving in anti-phase, where the bubble motion reduces the effective mass and raises the natural frequency of the system.

It has also been observed[38–40,46,47] that the inclusion of time delays due to liquid compressibility in coupled-bubble interaction models can either increase or decrease the damping relative to the damping of each bubble in isolation. The change in damping occurs because the propagation delay alters the relative phase of the bubble interactions and is thus highly dependent on the distance between the bubbles.

For two closely-spaced (less than half an acoustic wavelength) bubbles oscillating in-phase, the pressure produced by one bubble acts on the other bubble by increasing the pressure the other bubble experiences, and vice versa. This increased pressure can increase the damping of the bubble system by up to a factor of two. On the other hand, for bubbles in the same configuration, but oscillating in anti-phase, the pressure produced by the motion of one bubble reduces the pressure experienced by the other bubble, and hence the damping is reduced significantly.

To evaluate the effect of the approximations for liquid compressibility (C1, C2, C3, and C3; see Table 2.1 and Eqs. (3.25)–(3.28)) without the additional effects produced by including time delays in bubble interactions, the time delay in bubble interactions is removed by setting $\tau = 0$ in Eqs. (3.32)–(3.34). As a note, later in this work, a suffix N will be appended to the label of models in which the delay is neglected. As an example, the characteristic equation for the C1-L approximation with $\tau = 0$ is

$$s_+^2\left(e^{-s_+R_0/c_0} + \frac{R_0}{D}\right) + \omega_0^2 = 0, \tag{3.35a}$$

$$s_-^2\left(e^{-s_-R_0/c_0} - \frac{R_0}{D}\right) + \omega_0^2 = 0,. \tag{3.35b}$$

The characteristic equations are solved numerically for s and the damping coefficient δ and natural frequency f are calculated from the real and imaginary parts of each eigenvalue ($s = \delta\omega/2 + i\omega$). The resulting natural frequencies and damping coefficients are shown in Fig. 3.4 for a system of two bubbles with an equilibrium radius of 20 μm and with separation distances ranging from 2 to 1000 bubble radii. Although the models in Eqs. (3.32)–(3.34) require $R^2/D^2 \ll 1$ and thus are not strictly valid for closely spaced bubbles, the results are presented for separation distances ranging for $2R_0$ (bubble walls touching) to $1000R_0$. No viscous or thermal losses are included in the system; the effects of viscous and thermal damping will be considered in Chapter 4. The only damping in the system is due to acoustic radiation. The calculated damping and natural frequency of the two-bubble system are marked with a subscript 2. In the figures, both the natural frequency of the two-bubble system $\omega_{0,2} = \mathrm{Im}\{s_\pm\}$ and the effective radiation damping coefficient $\delta_{\mathrm{rad},2} = 2\mathrm{Re}\{s_\pm\}/\omega_{0,2}$ are normalized by the natural frequency

$$\omega_0 = \frac{1}{R_0}\sqrt{\frac{3\gamma P_0}{\rho_0}} \tag{3.36}$$

and radiation damping coefficient of a single bubble at resonance,

$$\delta_{\mathrm{rad}} = \frac{\omega_0 R_0}{c_0}. \tag{3.37}$$

For an air bubble in water, $\delta_{\mathrm{rad}} = 0.014$, a constant and independent of R_0 in the long wavelength limit. Three cases are shown in Fig. 3.4, the C1-L case, Eq. (3.32) (solid), the C2-L case, Eq. (3.33) (dashed), and the C3-L case, Eq. (3.34) (dash-dot). In all three cases the interaction delay τ is set to zero. The C4-L case is not shown because without delay, the C3-L and C4-L cases are equivalent. The top row shows the natural frequency of the two-bubble system for in-phase motion on the left and anti-phase motion on the right. For all three cases the natural frequency behaves as expected. The frequency of the in-phase mode (part (a)) decreases for more closely spaced bubbles while the frequency of the anti-phase mode (part (b)) increases.

The bottom row shows the damping coefficient of the system, again with in-phase motion on the left and anti-phase motion on the right. The C1-L approximation, Eq. (3.32) (solid), slightly decreases the damping of the in-phase mode compared to the system without the radiation damping corrections, Eq. (3.34) (dash-dot). The result of the C2-L approximation, Eq. (3.33) (dashed) agrees well with the C1-L approximation.

In contrast, for the anti-phase mode, shown on the right, the damping coefficient for the C1-L approximation is as much twice as large as the system with the C3-L for closely spaced bubbles. The C2-L approximation matches the C1-L approximation well and thus it is apparent that the corrections for bubble interaction in a compressible medium introduced by the C2-L approximation significantly affect the damping of closely spaced bubbles.

The importance of using the C1-L or C2-L approximation when modeling bubble dynamics in compressible media is emphasized when time delays in bubble interactions are included. Figure 3.5 shows the natural frequencies (top row) and damping coefficient (bottom row) of the system with delayed bubble interactions with the C1-L and C3-L approximations. Stable regions of the parameter space

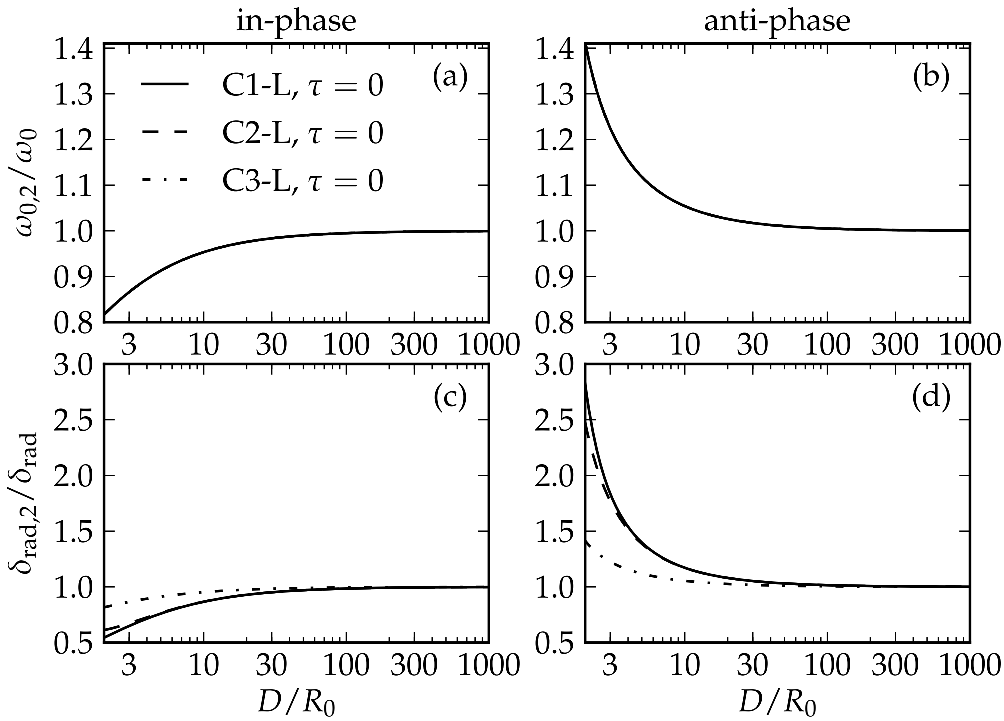

Figure 3.4: Comparison of systems with the C1-L approximation for compressibility effects (solid lines), the C2-L approximation (dashed lines) and the C3-L approximation (dash-dot lines) for in-phase (left column) and anti-phase motion (right column). The bubble-interaction delay τ is zero. The upper row shows the natural frequency of the coupled system normalized by the natural frequency of a single bubble (the three curves overlay each other). The lower row shows the effective nondimensional radiation damping coefficient normalized by the nondimensional radiation damping coefficient of a single bubble.

are indicated by a white background, unstable regions are indicated by a colored background. The C3-L approximation without delays in bubble interactions is included for comparison. For convenience, the special case of a C3 model without delays has been given the label C4. Thus, C4-L represents a model with single-bubble radiation damping without interaction delays. The characteristic equations for the C4-L approximation are

$$\omega_0^2 + s_+ \frac{R_0\omega_0^2}{c_0} + s_+^2\left(1 + \frac{R_0}{D}\right) = 0 \tag{3.38a}$$

$$\omega_0^2 + s_- \frac{R_0\omega_0^2}{c_0} + s_-^2\left(1 - \frac{R_0}{D}\right) = 0. \tag{3.38b}$$

The inclusion of liquid compressibility effects has a negligible effect on the natural frequency of either oscillation mode shown in parts (a) and (b) of Fig. 3.5. The C1-L approximation (solid line) slightly decreases the damping of the in-phase mode (part (c)). The damping of the anti-phase mode is shown in part (d). The effect of the C1-L approximation on the damping of the anti-phase mode is more significant as the damping is dramatically reduced in comparison to the C4-L case (dash-dot line). This agrees with the results of Feuillade.[38–40] Indeed, the model with the C3-L approximation (dashed line) for liquid compressibility exhibits a negative damping coefficient for closely spaced bubbles, and thus the C3-L model system is unstable.

Instability in model two-bubble systems with delay has been observed by Heckman et al.[52] and Sinden et al.[53] However, no work was done to determine whether the instability was due to an incomplete model or correlated with a physical phenomenon. The damping of the system with the C1-L approximation does not become negative, but rather approaches zero. Thus, the C1-L or C2-L approximation eliminates the observed instability and therefore must be included in simulations. The work performed here shows that the instability is due to the incomplete incorporation of the effects of liquid compressibility in the C3-L model.

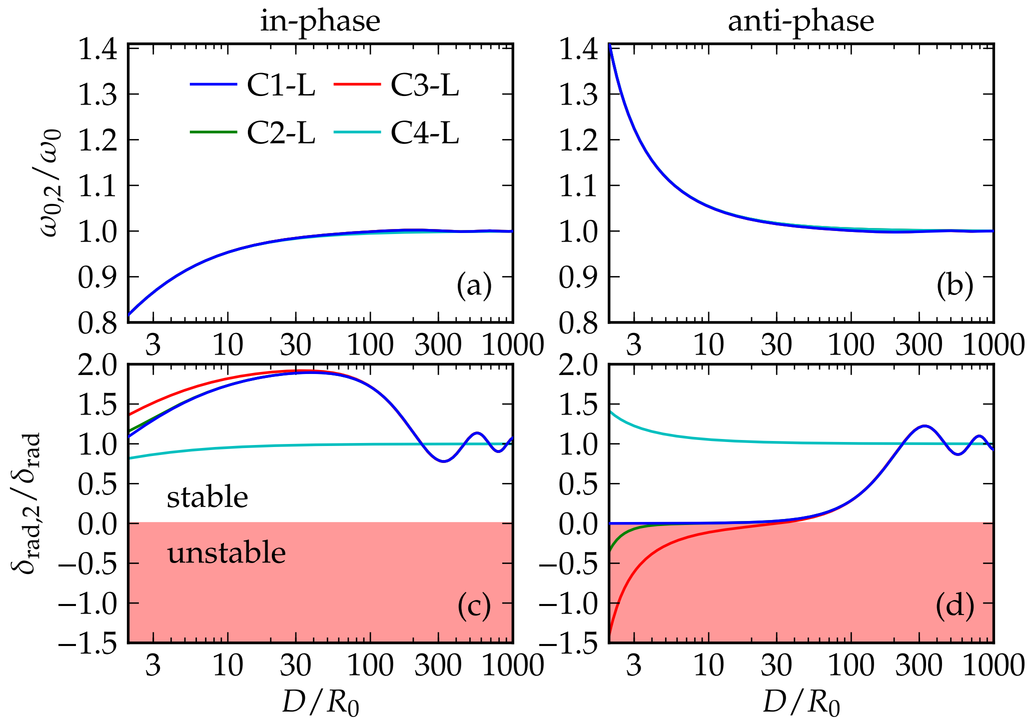

Figure 3.5: Comparison of normalized natural frequencies and damping coefficients predicted by the C1-L model (blue lines), the C2-L model (green lines), the C3-L model (red lines), and the C3-L model without interaction delays (light blue lines). The upper row shows the natural frequency of the coupled system normalized by the natural frequency of a single bubble (the four curves overlay each other). The lower row shows the nondimensional damping coefficient. Stable regions of the parameter space are indicated by a white background, unstable regions are indicated by a colored background.

Figure 3.6 compares the results of the linearized C1-L model in Eq. (3.32) to the result obtained by numerical integration of the Hamiltonian delay differential equations given in Chapter 2 with the C2-L approximation and the C3-L approximation. Only small-amplitude oscillations are considered here and the effects of viscous and thermal damping are neglected. The results produced by the C1-L model are plotted with a blue line, and the results produced by the C4-L model are plotted with a light blue line. Stable regions of the parameter space are indicated by a white background, unstable regions are indicated by a colored background. Again the natural frequencies remain the same for all systems (parts (a) and (b)). The behavior of the numerically obtained damping coefficient of the in-phase mode shown in part (c) agrees with the behavior shown in part (c) of Fig. 3.5. As expected, for the anti-phase mode (part (d)) the numerical model with the C3-L approximation (red line) displays instability for closely spaced bubble configurations. The result of numerical integration with C2-L approximation (green lines) does not display the same instability. Instead there is a slight increase in the calculated damping coefficient for small bubble separation distances. The difference between the C1-L model based on a modified Rayleigh-Plesset equation and the numerical model based on a Hamiltonian formalism may be attributed to the fact that both are valid to $O(R^2/D^2)$. The fact that the difference between the two occurs only when R^2/D^2 is not necessarily small suggests that the discrepancy is due to series truncation effects.

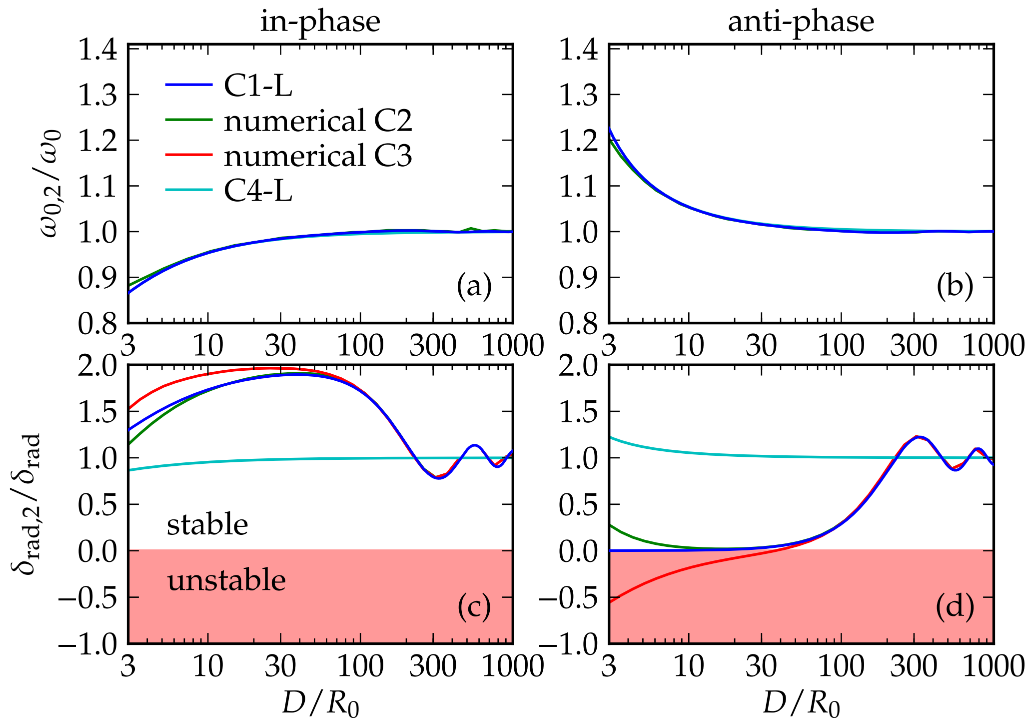

Figure 3.6: Comparison of the natural frequency and damping coefficient predicted by the C1-L model (blue lines) and the C4-L model (light blue lines) to the natural frequency and damping coefficient calculated from numerical simulations produced by integrating the Hamiltonian equations of motion (Eq. (2.62)) with the C2-L approximation (green lines) and the C3-L approximation (red lines) for in-phase (left column) and anti-phase motion (right column). The upper row shows the natural frequency of the two-bubble system normalized by the natural frequency of a single bubble (the four curves overlay each other). The lower row shows the nondimensional damping coefficient normalized by the nondimensional radiation damping coefficient for a single bubble. Stable regions of the parameter space are indicated by a white background, unstable regions are indicated by a colored background.

3.3.2 High-amplitude free-response motion

The equations of motion presented in Chapter 2 were derived for the fully nonlinear case and can be applied to cases in which the linearized equations of motion used in Section 3.3.1 are not applicable. Figures 3.7 and 3.8 show the medium-amplitude free response of a system of two bubbles separated by $10R_0$ predicted by the C2 model for bubbles in a compressible medium (Eqs. (2.62) and (2.79)) and the model produced by using the C3 model without delays in the bubble interaction (Eqs. (2.24) and (2.78b)). For convenience the C3 model without time delays in bubble interactions is labeled C4. Neither viscous or thermal damping is included in systems in this section. The a numerical implementation of the C1 model has not yet been developed.

As was discussed in the previous section, the damping of two bubbles oscillating in-phase is increased, while the damping of the same two bubbles oscillating in anti-phase is reduced. The eigenvalue analysis of the linearized equations of motion in the previous section confirmed this behavior. Now the effect of the same phenomenon is examined in the predictions of the nonlinear equations of motion.

The results of simulations with three different initial conditions are shown, in-phase (left column), where both bubbles start at $2R_0$, mixed-phase (center column), where one starts at $2.1R_0$ and the other at $2R_0$, and anti-phase (right column), where one starts at $2R_0$ and the other at $0.2R_0$. The top row contains plots of the total energy in the system. The bottom row contains plots of the average radial displacement normalized by the equilibrium radius R_0. The energy plot in part (a) of Fig. 3.7 show that for the in-phase case, the damping is increased in the C2 model (black curves) relative to the C4 model (red curves), as expected. Part (c) shows that for the anti-phase case, the damping is decreased in the C2 model relative to the C4 model, as expected. In the mixed-phase case shown in part (b) both the in- and anti-phase modes are excited. It can be seen that the damping of the C2 model is initially greater while the in-phase portion of the initial excitation is damped. After this initial period, the damping of the C2 model is lower because only the anti-phase portion of the initial disturbance remains, and the anti-phase portion is damped more slowly than in the C4 model. The behavior shown in the average radial displacement curves in the bottom row of Fig. 3.7 (parts (d)-(f)) agrees with the energy plots in the top row. In-phase motion is damped more quickly, anti-phase motion more slowly, and in mixed-phase motion the in-phase component of the initial state is damped more quickly while the anti-phase component is damped more slowly.

The motion of the individual bubble radii as a function of time is shown in Fig. 3.8 with the lines for one bubble shown in green and the lines for the other in blue. The C2 model is shown on the top row and the C4 model is shown on the bottom row. Scrutiny of the radius-time curves in Fig. 3.8 reveals that for the in-phase case, the bubbles do indeed remain in phase and the radial motion is damped much more quickly for the C2 model (part (a)) than the C4 model (part (d)). In the mixed case, for the C2 model (part (b)) the in-phase portion is quickly damped out, and the remaining motion appears to be dominated by the anti-phase mode. It is interesting to note that the beat frequency of the C2 model is higher than the C4 model (part (e)). The reason for the difference in beat frequencies is unknown, although it may be due to the presence of other natural frequencies in the delayed system.[70] For the anti-phase case, the C2 model (part (c)) is damped more slowly than, but does not exhibit the same beating as, the C4 model (part (f)). The reduced damping is expected, but the reason for the absence of beats in the C2 model is unknown. The previous section presented the minimum damping case for each mode of the system. However, due to the transcendental nature of the characteristic equations (Eqs. (3.32) and (3.33)) it is possible for other eigenvalues and corresponding natural frequencies to exist in the system.[70] In the anti-phase case, despite the high-amplitude, non-sinusoidal radial motion, the two bubbles remain in anti-phase and the C2 model exhibits reduced damping compared to the C4 model.

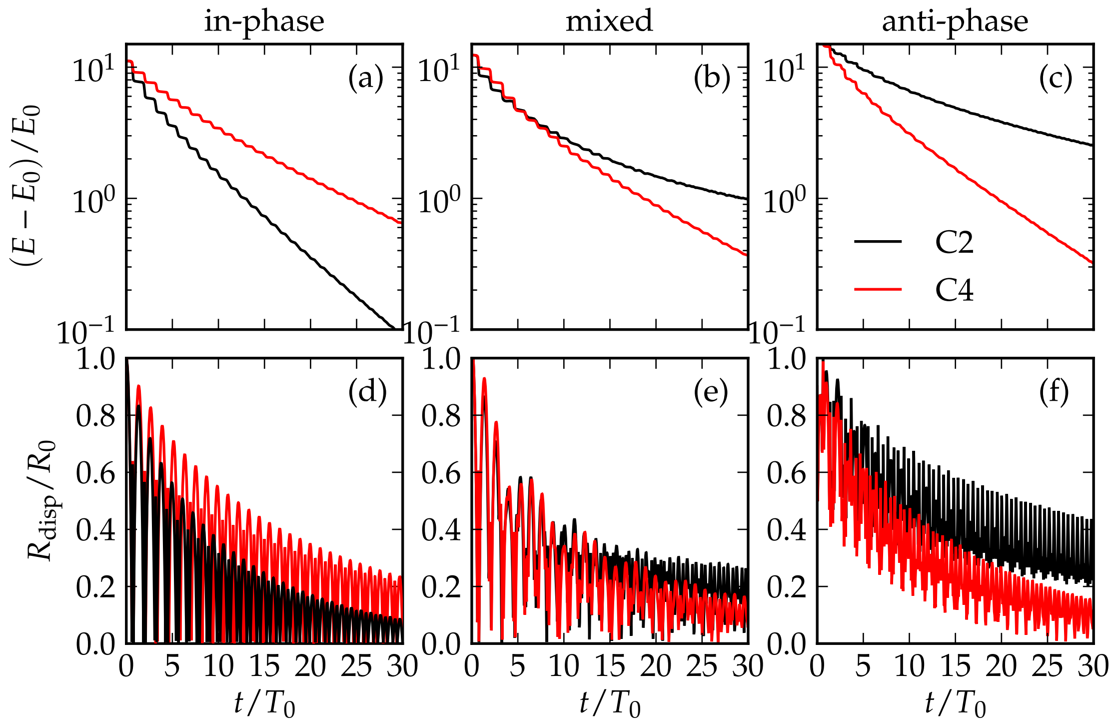

Figure 3.7: Comparison of models for bubbles in a compressible medium (C2) and an incompressible medium with single-bubble radiation damping (C4). The in-phase systems start with both bubbles at $2R_0$, the mixed systems start with one at $2.1R_0$ and the other at $2R_0$, and the anti-phase systems start with one at $2.0R_0$ and the other at $0.2R_0$. Shown are the total energy (top row), the average displacement (bottom row).

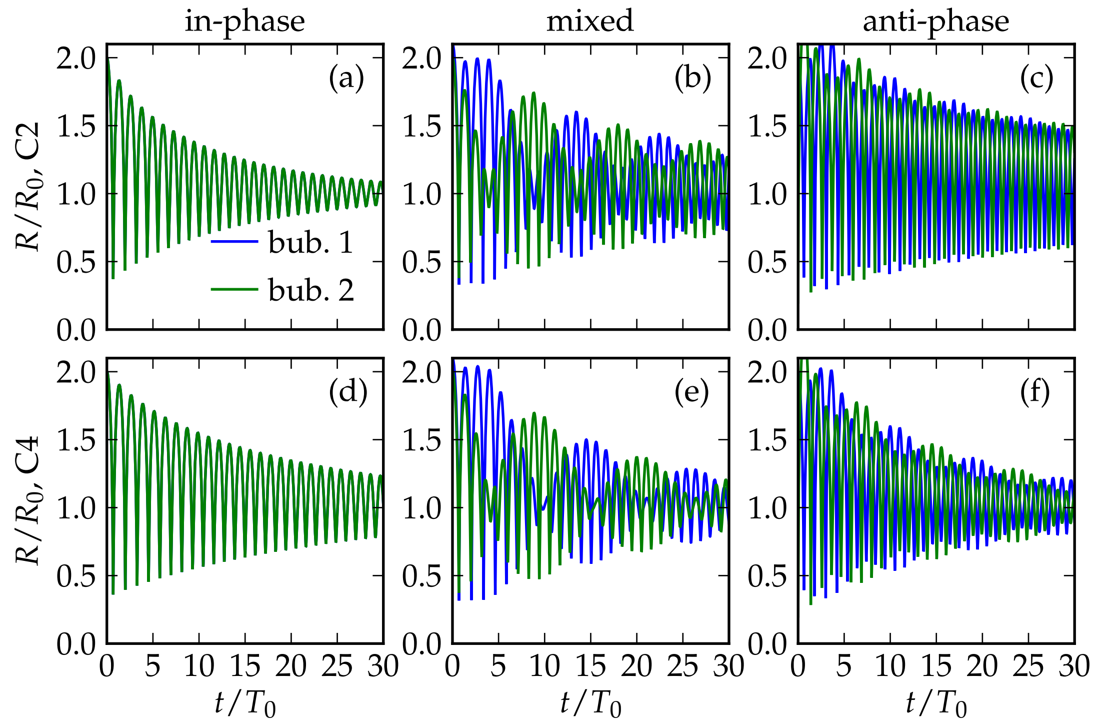

Figure 3.8: Comparison of models for bubbles in a compressible medium (C2) and an incompressible medium with single-bubble radiation damping (C4). The in-phase systems start with both bubbles at $2R_0$, the mixed systems start with one at $2.1R_0$ and the other at $2R_0$, and the anti-phase systems start with one at $2.0R_0$ and the other at $0.2R_0$. The motion of the individual bubbles is shown for the C2 (top row) and C4 (bottom row) models.

3.4 Forced response

In this chapter it has been shown that the C2 model for bubble motion in a compressible medium derived in Section 2.3.2 agrees well with an C1-L model when the amplitude of the radial oscillations is small, and that the corrections for liquid compressibility are significant in high-amplitude, nonlinear motion. The importance of including the effects of liquid compressibility in systems driven by an external acoustic source typical of biomedical treatment applications is analyzed in the present section. The bubble system response to short, high-amplitude pulses that produce inertial bubble growth is considered in this section.

In the presence of an external acoustic source, the evaluation of the equations of motion with the C2 approximation for liquid compressibility requires knowledge of the pressure and particle velocity due to the source as well as their spatial and temporal derivatives up to order 2. For a planar source with a pressure waveform

f the necessary quantities are

$$p_e = f(t - \mathbf{x} \cdot \mathbf{n}/c_0), \tag{3.39a}$$

$$\frac{\partial p_e}{\partial t} = f'(t - \mathbf{x} \cdot \mathbf{n}/c_0), \tag{3.39b}$$

$$\frac{\partial^2 p_e}{\partial t^2} = f''(t - \mathbf{x} \cdot \mathbf{n}/c_0), \tag{3.39c}$$

$$\boldsymbol{\nabla} p_e = -\frac{\mathbf{n}}{c_0} f'(t - \mathbf{x} \cdot \mathbf{n}/c_0), \tag{3.39d}$$

$$\frac{\partial}{\partial t}\boldsymbol{\nabla} p_e = -\frac{\mathbf{n}}{c_0} f''(t - \mathbf{x} \cdot \mathbf{n}/c_0), \tag{3.39e}$$

$$\boldsymbol{\nabla}(\boldsymbol{\nabla} p_e) = \frac{\mathbf{n} \otimes \mathbf{n}}{c_0} f''(t - \mathbf{x} \cdot \mathbf{n}/c_0), \tag{3.39f}$$

$$\mathbf{u}_e = \frac{\mathbf{n}}{\rho_0 c_0} f(t - \mathbf{x} \cdot \mathbf{n}/c_0), \tag{3.39g}$$

$$\frac{\partial \mathbf{u}_e}{\partial t} = \frac{\mathbf{n}}{\rho_0 c_0} f'(t - \mathbf{x} \cdot \mathbf{n}/c_0), \tag{3.39h}$$

$$\frac{\partial^2 \mathbf{u}_e}{\partial t^2} = \frac{\mathbf{n}}{\rho_0 c_0} f''(t - \mathbf{x} \cdot \mathbf{n}/c_0), \tag{3.39i}$$

$$\boldsymbol{\nabla} \mathbf{u}_e = -\frac{\mathbf{n} \otimes \mathbf{n}}{\rho_0 c_0^2} f'(t - \mathbf{x} \cdot \mathbf{n}/c_0), \tag{3.39j}$$

$$\frac{\partial}{\partial t}\boldsymbol{\nabla} \mathbf{u}_e = -\frac{\mathbf{n} \otimes \mathbf{n}}{\rho_0 c_0^2} f''(t - \mathbf{x} \cdot \mathbf{n}/c_0), \tag{3.39k}$$

$$\boldsymbol{\nabla}(\boldsymbol{\nabla} \mathbf{u}_e) = \frac{\mathbf{n} \otimes (\mathbf{n} \otimes \mathbf{n})}{\rho_0 c_0^3} f''(t - \mathbf{x} \cdot \mathbf{n}/c_0), \tag{3.39l}$$

where the prime indicates differentiation with respect to the argument and $\otimes$ represents the tensor or outer product defined so that $(\mathbf{a} \otimes \mathbf{b}) \cdot \mathbf{c} = (\mathbf{b} \cdot \mathbf{c})\,\mathbf{a}$, where $\mathbf{a}$, $\mathbf{b}$, and $\mathbf{c}$ are vectors.

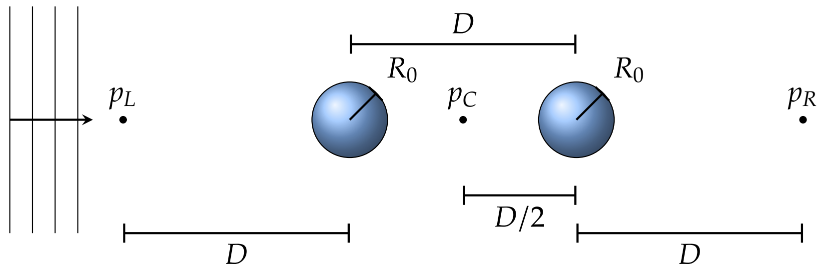

Figure 3.9: Geometry of two bubbles excited by an externally applied pressure field. The bubbles are separated by a distance D. The pressure produced by the bubbles is calculated at three locations, a distance D to the left of the left-most bubble (p_L), in between the bubbles (p_C), and a distance D to the right of the right-most bubble (p_R).

The maximum pressure predicted by the C2 model is compared to the maximum pressure predicted by the C4 model for two equally sized bubbles placed a distance D apart. The geometry of the bubbles is shown in Fig. 3.9. The bubbles are initially at rest, the excitation is produced by a 5.8 μs duration, single-cycle tone burst (this corresponds to a frequency of 173 kHz) with amplitude p_0, propagating along the shared axis of the bubbles The amplitude p_0 of the pulse ranges from 0.1 to 2 MPa. In these simulations, both bubbles have an equilibrium radius of 10 μm. The effect of viscosity as given by Eq. (2.25) is included in both models. The pressure produced by the bubbles is calculated at three locations, a distance D to the left of the left-most bubble (p_L), in between the bubbles (p_C), and a distance D to the right of the right-most bubble (p_R). These thee points are marked in the figure.

The percent difference between the pressure predicted by the two models is shown in Fig. 3.10 for a range of values of D. The percent difference is defined as

$$\frac{p_{\text{max}}^{(\text{C2})} - p_{\text{max}}^{(\text{C4})}}{p_{\text{max}}^{(\text{C4})}} \times 100\%, \tag{3.40}$$

where $p_{\max}^{(C4)}$ is the maximum pressure predicted by the C4 model for bubbles in a incompressible liquid with single-bubble radiation damping, and $p_{\max}^{(C2)}$ is the maximum pressure predicted by the C2 model for bubbles in a compressible liquid. The figure shows the results for the pressure at a distance D behind the bubbles (p_L, part (a)), in between the two bubbles (p_C, part (b)), and a distance D in front of the bubbles (p_R, part (c)). In Fig. 3.10, dark red indicates regions where the pressure predicted by the C2 model is larger than that predicted by the C4 model, and dark blue indicates regions where the pressure predicted by the C2 model is smaller than that predicted by the C4 model. The white area represents the region of the parameter space where the bubbles collide and the simulation is halted.

Comparison of parts (a)-(c) in Fig. 3.10 shows that the inclusion of compressibility effects in the bubble model significantly changes the predicted pressure. Whether the resultant pressure is increased or decreased is highly dependent on the separation of the two bubbles, the drive amplitude, and the amplitude of the bubble motion.

The change in the resultant pressure due to the inclusion of liquid compressibility effects observed in Fig. 3.10 is most easily analyzed in the case of two bubbles undergoing a violent collapse. Consider that the collapse of the two bubbles is slightly staggered due to the different times at which the driving pulse reaches each bubble. If the bubble separation and collapse occur such that the pulse produced by the collapse of the first bubble arrives during the collapse phase of the second bubble, the collapse of the second bubble can be significantly accelerated. This acceleration increases the pressure produced by the collapse of the second bubble. In

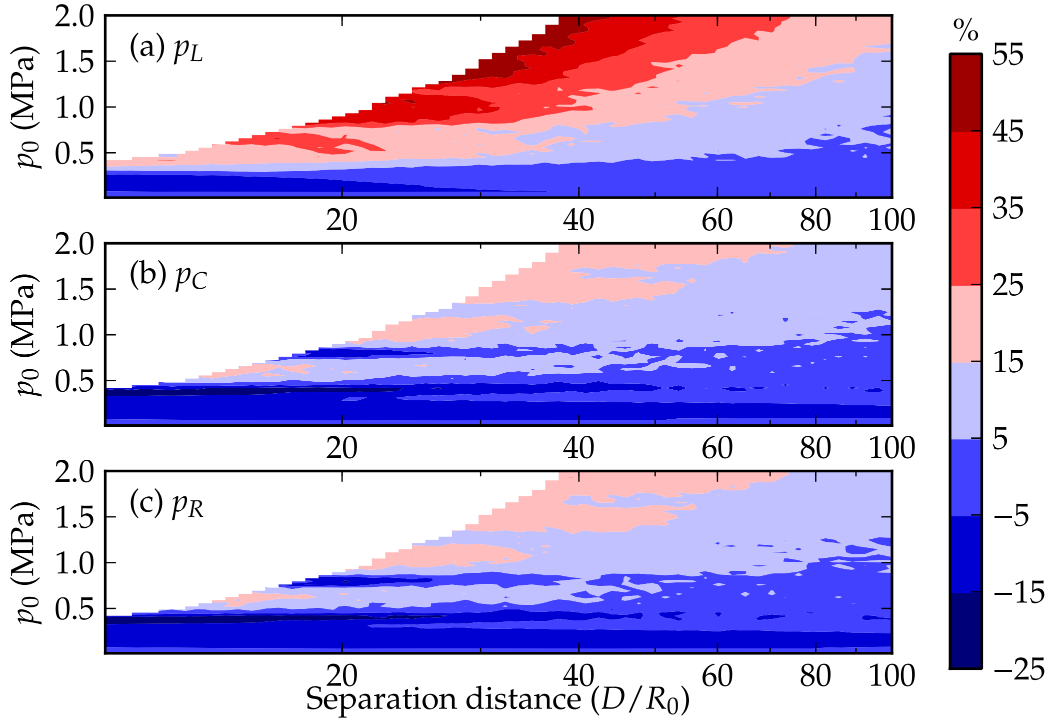

Figure 3.10: Comparison of pressure predicted by C2 and C4 models for two bubbles of 10 μm radius driven by a 5.8 μs duration, single-cycle tone burst with amplitude p_0. The percent difference between the two models is shown for a range of separation distances ($D = 10R_0$–$100R_0$) and source pressures ($p_0 = 0.01$–2 MPa) at three locations left of the bubbles (p_L) in the center of the bubbles (p_C) and to the right of the bubbles (p_R).

contrast, if the bubble separation and collapse occur such that the pulse produced by the collapse of the first bubble arrives during the rebound of the second bubble, the growth of the second bubble can be retarded or reversed, and this reduces the pressure produced by the second bubble. This explanation is supported by the fact that regions of reduced pressure in Fig. 3.10 are very narrow. This occurs because suppression is strongest when the pulse from the first bubble arrives during the rebound of the second bubble. This is a very narrow window since the rebound occurs quickly. In contrast, the initial inertial collapse of a bubble is relatively long, and any positive pressure pulse that arrives during this collapse will accelerate the collapse and increase the resultant pressure. Consequently, the regions of increased pressure are much larger than the regions of reduced pressure. In addition to the delay effects, the additional interaction terms in the C2 approximation for compressibility increases the strength of the interaction between the bubbles.

The acceleration and deceleration of the radial motion that results in an increase or decrease in pressure can be observed in plots of the bubble radius as a function of time. An instance of reduced pressure occurs when the drive pressure is approximately 0.35 MPa and the bubbles are separated by $10.4R_0$ (104 μm). Figure 3.11 shows the bubble radii (a) and pressure in between the bubbles (b) for this case at the time of the first collapse. The times at which the bubble rebound occurs are different, thus it is difficult to distinguish significant differences between the shape of the radial curves for the C2 (solid) and C4 (dashed) models at the time of rebound. The curve for the second bubble (blue) predicted by the C2 model is slightly more rounded at the point of rebound, and the minimum bubble radius is slightly larger than the rebound predicted by the C4 model (dashed curve). This indicates a less violent collapse. It can also be seen that the rebound of the second bubble (blue curve) occurs approximately 0.07 μs after the rebound of the first (green curve). The pressure pulse caused by the rebound of the first bubble takes 0.071 μs to arrive at the second, and thus the second bubble experiences a significant positive pressure during its rebound. This positive pressure decelerates the bubble during its rebound and reduces the radiated pressure. Thus the significant reduction in the radiated pressure produced by the pair is caused by the fact that the motion of the first bubble at these amplitudes has a collapse at just the right time to inhibit the rebound of the second when the delay due to propagation is included.

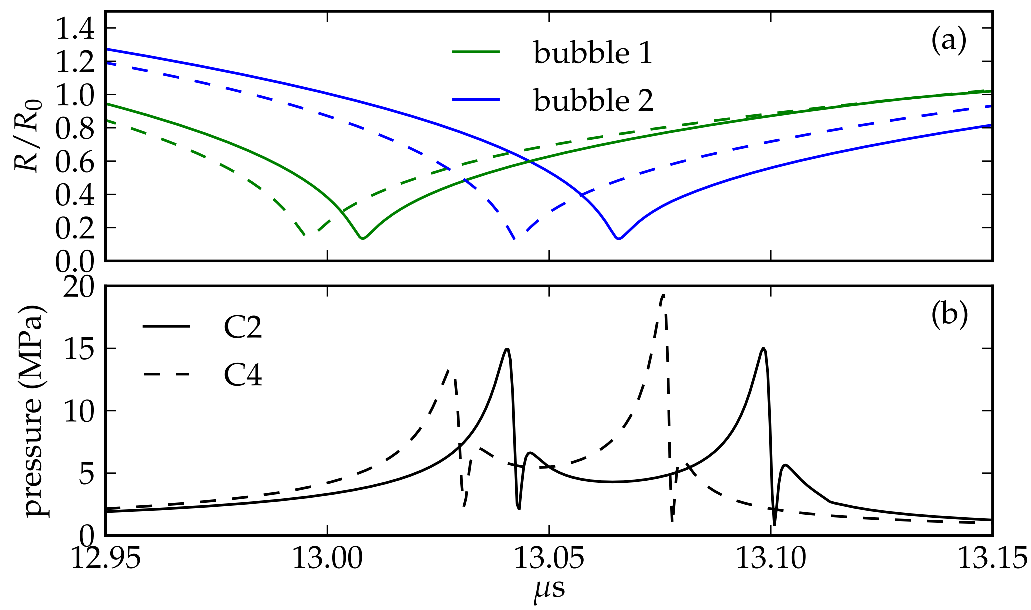

Figure 3.11: Bubble radii (a) and pressure between two bubbles (b) predicted by C2 and C4 models. The bubbles have an equilibrium radius of 10 μm and are separated by $10.4R_0$ (104 μm). They are driven by a 5.8 μs duration, single-cycle, sinusoidal pulse with an amplitude of 0.35 MPa. Only the first rebound is shown.

Now consider Fig. 3.12, which shows the first rebound of two bubbles subjected to a pulse with the same waveform, but with an amplitude of 2.0 MPa. The bubbles are separated by $50R_0$ (500 μm). In part (a) of Fig. 3.12 it can be seen that the pulse generated by the collapse of the first bubble (green curve) arrives at the second bubble (blue curve) while it is still collapsing. The time at which the pressure produced by the initial collapse of the first bubble arrives at the second is indicated by arrow A for the C4 case and arrow B for the C2 case. The sudden change in pressure produces an abrupt change in the radial motion of bubble 2 predicted by the model for a compressible liquid and the corresponding collapse becomes significantly more violent. The pressure in between the two bubbles is shown in part (b) of Fig. 3.12. The pressure produced by the collapse of the second bubble is approximately 40% higher for the model for a compressible liquid (C2) than for the incompressible liquid with single-bubble radiation damping (C4). This increase in pressure is due to the more violent collapse caused by the stronger coupling and the propagation delay in bubble interaction in the model for a compressible liquid.

The increased coupling strength between the bubbles due to the C2 approximation for fluid compressibility can also be observed by noting that there is no abrupt change in the radial motion of the second bubble predicted by the C4 model (arrow A) when the first bubble collapses. As mentioned previously, there is an abrupt change in the motion predicted by the C2 model (arrow B). It is also possible to discern an arrested expansion when the pulse produced by the collapse of bubble 2 arrives at bubble 1. This event is marked by arrow D. The corresponding location in the motion of bubble 2 is indicated by arrow C. There is no similar abrupt change at point C. Were the coupling strength between the two bubbles similar in both models, then more significant changes would be expected in the C4 simulations at the points marked by arrows A and C. Thus the corrections in the C2 model for a compressible liquid increase the strength of the interaction between the bubbles relative to the model for an incompressible liquid with single-bubble radiation damping (C4).

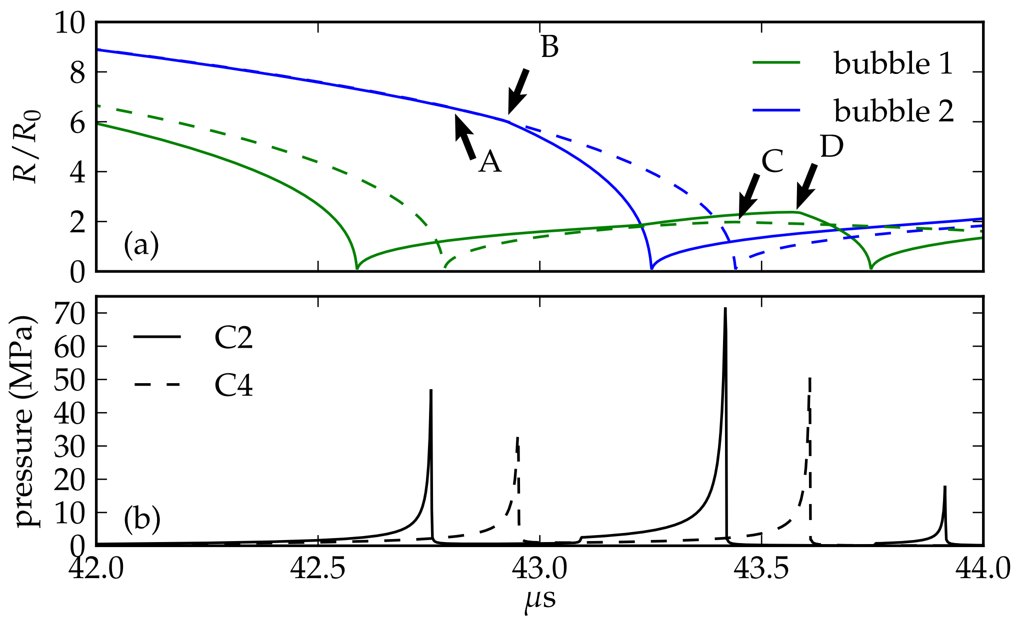

Figure 3.12: Bubble radii (a) and pressure between two bubbles (b) predicted by the models for compressible and incompressible liquids. The bubbles have an equilibrium radius of 10 μm and are separated by $50R_0$ (500 μm). They are driven by a 5.8 μs duration, single-cycle, sinusoidal pulse with an amplitude of 2.0 MPa. Only the first rebound is shown.

Fujikawa and Takahira[49] noted that the inclusion of acoustic propagation delay in a model of two-bubble dynamics resulted in the production of significantly higher pressures for certain configurations undergoing large oscillations. Their study was conducted for bubble pairs in free response without the inclusion of viscosity, and the C3 method was used to include compressibility effects. The numerical approach used is not clear. The trends of the results shown here agree with their results in cases where the pressure is increased. In addition to the cases with increased pressure, there are also cases in which the effects of liquid compressibility significantly reduce the pressure produced by the bubble system. Examination of the first collapse of bubble 1 (green curve) in Figs. 3.11 and 3.12 suggests that the first collapse of bubble 1 predicted by the C2 model is slightly more violent than the prediction of the C4 model. This effect can also be seen in the calculated pressure at the center of the bubble pair, where the pressure predicted by the C2 model is higher than the pressure predicted by the C4 model. This is because the retarded interaction due to propagation delay allows the bubbles in the C2 model to develop greater inertia before experiencing the effects of the other bubble in the system, and thus they collapse more violently.

3.5 Comparison with experimental results

Acoustic scattering by a system of two bubbles was considered experimentally by Kapodistrias and Dahl.[43] In their work they compared experimental results obtained by measuring the field scattered by a system of two bubbles to the predictions of multiple scattering theory. It is possible to compare the models developed here to the results obtained by Kapodistrias and Dahl. In their experiment, the bubbles were of approximately equal size, and measurements were taken for a range of separation distances. The source was positioned so that the bubbles experienced approximately the same field and thus oscillated in unison.

For low-amplitude excitation, the same system may be modeled with either of the approximations in Eqs. (3.25) and (3.26). A similar approach was used by Feuillade[38] to analyze bubble pairs. The C1-L model is chosen here for the comparison. For a pair of bubbles oscillating in phase, the C1-L equation of motion (Eq. (3.13)) for one of the bubbles in the system can be reduced to a single equation:

$$\ddot{\xi}(t - R_0/c_0) + \omega_0^2\xi(t) + \frac{R_0}{D}\ddot{\xi}(t-\tau) = -\frac{p_e(t)}{R_0\rho_0}. \tag{3.41}$$

It is assumed that the system is in steady state and that the external source pressure p_e is time-harmonic with amplitude p_0 and angular frequency ω_s ($p_e(t) = p_0 e^{-i\omega_s t}$). In this case, the response of each bubble is also harmonic with a solution of the form $\xi(t) = \chi e^{-i\omega_s t}$. With the assumptions of time-harmonic source and response, Eq. (3.41) can be rewritten as

$$-\omega_s^2\chi e^{i(k_s R_0 - \omega_s t)} + \omega_0^2\chi e^{-i\omega_s t} - \omega_s^2\frac{R_0}{D}\chi e^{i(k_s D - \omega_s t)} = -\frac{p_0}{\rho_0 R_0}, \tag{3.42}$$

where $k_s = \omega_s/c_0$. Equation (3.42) can be solved for the complex radial displacement amplitude χ:

$$\chi = -\frac{p_0}{\rho_0 R_0}\left[\omega_0^2 - \omega_s^2\left(e^{ik_s R_0} + \frac{R_0}{D}e^{ik_s D}\right)\right]^{-1}. \tag{3.43}$$

In the work of Kapodistrias and Dahl, the experimental results are presented in terms of target strength (TS) defined as

$$\mathrm{TS} = 10\log_{10}\left|\frac{p_T}{p_0}r\right|^2 \text{ dB re 1 m}, \tag{3.44}$$

where p_T is the pressure measured far from the system and r is the distance at which the measurement is made, which is the same for each bubble due to the symmetric geometry of the experiment. Thus, in order to compare with their work, the pressure produced by the system must also be calculated. The pressure produced by a single bubble is

$$p(r,t) = \frac{\rho_0\ddot{V}(t - r/c_0)}{4\pi r}. \tag{3.45}$$

For the small-amplitude, time-harmonic oscillations considered here linearization yields

$$\ddot{V} = -4\pi R_0^2 \omega_s^2 \xi. \tag{3.46}$$

The pressure produced by the motion of the bubbles at a point r equidistant from the two bubbles is

$$\begin{aligned} p_T &= 2\frac{\rho_0 R_0^2 \omega_s^2 \chi}{r} \\ &= 2p_0 \frac{R_0}{r}\left[\left(\frac{\omega_0}{\omega_s}\right)^2 - \left(e^{ik_s R_0} + \frac{R_0}{D} e^{ik_s D}\right)\right]^{-1}. \end{aligned} \tag{3.47}$$

With this expression for the pressure produced by the bubbles, the target strength can be calculated from Eq. (3.44) as

$$\mathrm{TS} = 10\log_{10}\left[4R_0^2\left|\left(\frac{\omega_0}{\omega_s}\right)^2 - \left(e^{ik_s R_0} + \frac{R_0}{D} e^{ik_s D}\right)\right|^{-2}\right] \mathrm{dB\,re\,1\,m}. \tag{3.48}$$

Equation (3.48) is to be compared with Fig. 9 of Kapodistrias and Dahl at the source frequency 136 kHz (the results for all other frequencies in their Fig. 9 are virtually identical). Their nominal bubble radius is 585 μm, for which the natural frequency is in the neighborhood of 3 kHz. For these frequencies the term $(\omega_0/\omega_s)^2$ in Eq. (3.48) is negligible, and therefore the limiting value of the target strength for large bubble separation ($R_0/D \ll 1$) is $\mathrm{TS} = 20\log_{10} R_0 + 6$ dB, which for their bubble radius yields TS = −58.7 dB.

Shown in Fig. 3.13(a) are the results from Fig. 9 of Kapodistrias and Dahl at 136 kHz, in which the circles are measurements and the curves are calculations based on their scattering theory for $R_0 = 550$ μm (lower curve), $R_0 = 585$ μm (middle curve), and R_0 = 620 μm (upper curve). The horizontal coordinate kd in our notation equals $kD/2$, because their quantity d is half the separation distance D. Shown in Fig. 3.13(b) is the result from Eq. (3.48) for R_0 = 585 μm. The agreement with their results for R_0 = 585 μm is good, although Eq. (3.48) predicts a $\sim$ 1 dB higher target strength.

3.6 Summary

In this chapter, the expression for single-bubble radiation damping in the Hamiltonian model given in Section 2.3.1 was compared to the commonly used Keller-Mikisis model for a single bubble in a compressible liquid, and agreement between the two models was shown to be within numerical precision.

Three levels of approximation for liquid compressibility effects in the linearized equations of motion for a bubble system were presented. The analysis was conducted using linearized forms of the modified Rayleigh-Plesset equations rather than the Hamiltonian equations of motion presented in Chapter 2. The first approximation is an extension of the method used by Ilinskii and Zabolotskaya,[24] in which the radiated pressure produced by a bubble and acting on itself (self-action) is delayed by the time required to propagate from the center of the bubble to the bubble wall. This approximation was labeled C1-L (L for linearized). Ilinskii and Zabolotskaya expanded the delay differential equation associated with the C1 method using a Taylor expansion for small delays. A similar Taylor expansion of the delayed self-action term was used here. The third-order derivatives produced by the Taylor expansion were eliminated by an iterative substitution of the linearized

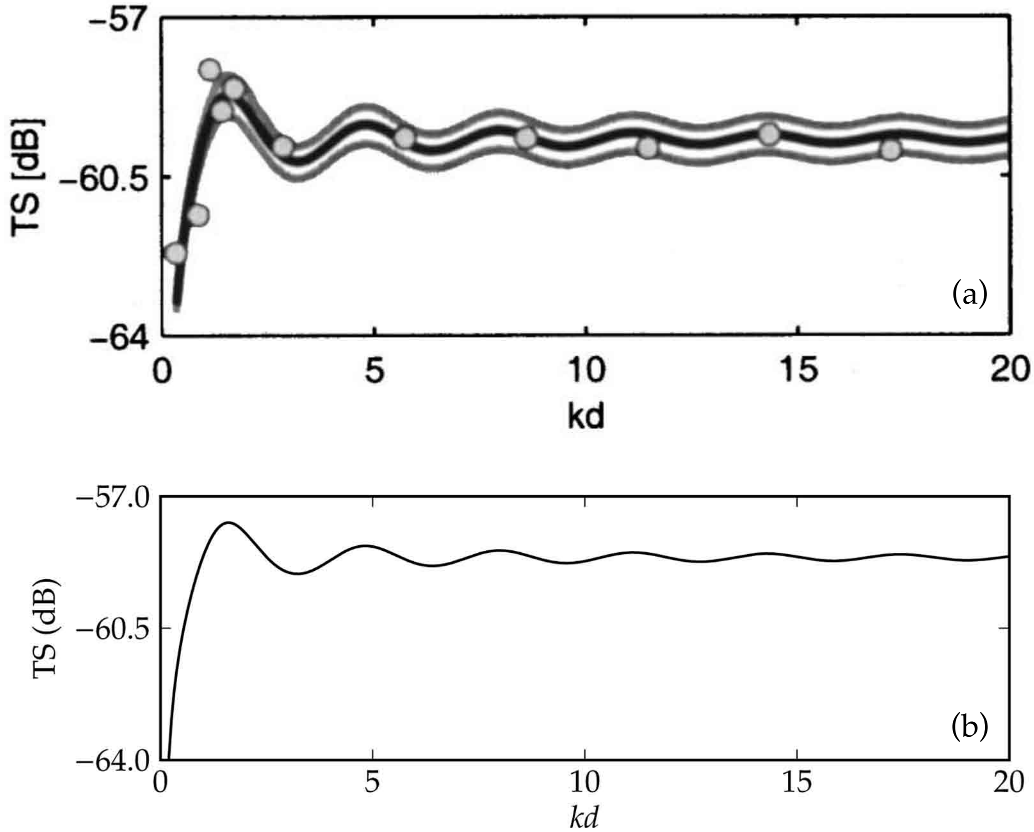

Figure 3.13: Part (a) shows experimental and theoretical results for the target strength of a system of two bubbles, taken from the plot for 136 kHz in Fig. 9 in Kapodistrias and Dahl.[43] Theoretical results were obtained using multiple scattering theory. Part (b) shows target strength computed using the C1 model as given in Eq. (3.48).

equations of motion analogous to the method by which higher-order derivatives were eliminated from the equations of motion in Section 2.3.2. When, during the iterative substitution, terms of $O(R^2/D^2)$ and $O(1/c_0)$ were retained, then the resulting approximation was labeled C2-L. The accuracy of the C2-L equations of motion obtained here is equivalent to that of the C2 approximation given in Section 2.3.2. When terms of $O(R/D)$ that were also $O(1/c_0)$ were neglected in the iterative substitution, the resulting approximation was labeled C3-L. The approximation for a incompressible host liquid in which the single-bubble radiation damping expression is used, but delays in bubble interaction are neglected is labeled C4, or C4-L for the linearized case.

The remainder of the chapter focused on two-bubble systems. An eigenvalue analysis of the linearized equations of motion was used to show that bubble interaction has a significant impact on the damping and stability of a coupled bubble system and cannot be neglected as is the case in the C3 approximation. The C3 approximation has been used by others to include the effects of liquid compressibility in bubble models.[38–40,46,47,50,51,71] It was shown that the C2 approximation for liquid compressibility produces a stable model for two-bubble systems with much smaller separation distances than the C3 model. Also, the low-amplitude predictions of the nonlinear C2 model from Chapter 2 were compared to the C1-L model with good agreement. Results from numerical integration of the nonlinear C2 and C4 (single-bubble radiation damping, no delay) models were used to demonstrate the presence of reduced damping of anti-phase motion and increased damping of in-phase motion in moderate-amplitude, nonlinear free response in the C2 model as compared to the C4 model, as is expected. The high-amplitude response of a bubble pair to an external pressure source was considered. It was observed that the inclusion of time delay and the compressibility corrections resulted in either higher or lower amplitude pressures being predicted by the model for a compressible liquid relative to the model for an incompressible liquid. Whether the radiated pressure is higher or lower is dependent on the separation distance of the bubbles and the amplitude of the driving pressure and subsequent bubble motion. Finally, the predictions of the C1-L model were compared to the experimental and theoretical results of Kapodistrias and Dahl[43] with excellent agreement.

Chapter 4

Stability and Dynamics of Multi-Bubble Systems in a Compressible Liquid

The effect of time delay and bubble self-action on stability and damping in a multi-bubble system in a compressible liquid is examined through an eigenvalue analysis of the linearized equations of motion. An eigenvalue analysis of thermally and viscously damped motion of bubble arrays and clusters with varying numbers of bubbles is conducted to compare the three levels of approximation for the effects of liquid compressibility obtained in Chapters 2 and 3 by Taylor expansion of delayed self-action terms. The results are compared to previous work on coupled bubble systems in a compressible liquid. Also, the response of a cluster undergoing nonlinear motion is presented. Finally, the pressure produced by high-amplitude motion of an acoustically driven system of two bubbles near a rigid wall is predicted using models for bubble motion in both incompressible and compressible liquids, and the results are compared to evaluate the impact of compressibility effects on the resultant pressure.

4.1 Compressibility effects in multi-bubble systems

This section extends the analysis of two-bubble systems presented in Section 3.3 to systems containing an arbitrary number of bubbles. Three possible methods for including the effects of liquid compressibility were presented in Chapter 3, the results from which are used here. The homogeneous forms of the C1, C2, and C3 approximations given in Eqs. (3.25)–(3.27) are used to analyze the stability of systems containing multiple bubbles. The approximation labels are summarized in Table 2.1 and the corresponding equations are collected in Appendix C for reference.

In this section, an eigenvalue analysis of the linearized, homogeneous equations of motion is used to investigate the stability of the three approximations for the effect of bubble self action in a compressible liquid. With the *ansatz* $\xi_i = \chi_i e^{st}$, where χ_i are the elements of a vector $\boldsymbol{\chi} = [\chi_1\, \chi_2\, \cdots\, \chi_N]^T$, the linearized equations of motion can be written in matrix form as

$$(\mathbf{S} + \mathbf{C})\,\boldsymbol{\chi} e^{st} = \mathbf{0}, \tag{4.1}$$

where $\mathbf{0}$ is the zero vector, and $\mathbf{S}$ and $\mathbf{C}$ may be functions of s. The matrix $\mathbf{S}$ contains single-bubble terms and the matrix $\mathbf{C}$ contains coupling terms. Equation (4.1) will only have nontrivial solutions if $\mathbf{S} + \mathbf{C}$ is singular. Thus a necessary and sufficient condition for nontrivial solutions is that

$$\det(\mathbf{S} + \mathbf{C}) = 0. \tag{4.2}$$

This is the characteristic equation for the system, and the values of s that are roots of Eq. (4.2) are the eigenvalues of the system. The characteristic equation is equivalent to Eqs. (3.32)–(3.34) given in Section 3.3. However, the equations in Section 3.3 are for composite variables representing the distinct modes of the system. In general it is not convenient to separate the individual modes of an N-bubble system, and therefore the characteristic equation is left in determinant form.

The homogeneous equations of motion for a system of bubbles in an incompressible liquid without damping are

$$\ddot{\xi}_i(t) + \omega_{0i}^2 \xi_i(t) + \sum_{i \neq j} \frac{R_{0j}^2}{D_{ij} R_{0i}} \ddot{\xi}_j(t) = 0. \tag{4.3}$$

For these equations the matrices $\mathbf{S}$ and $\mathbf{C}$ are

$$\mathbf{S}_{[ij]} = \begin{cases} \omega_{0i}^2 + s^2, & i = j \\ 0, & i \neq j, \end{cases} \tag{4.4a}$$

$$\mathbf{C}_{[ij]} = \begin{cases} 0, & i = j \\ s^2 \frac{R_{0j}^2}{D_{ij} R_{0i}}, & i \neq j. \end{cases} \tag{4.4b}$$

For the equations of motion with the C1-L approximation (Eq. (3.13)), the elements of $\mathbf{S}$ and $\mathbf{C}$ are given by

$$\mathbf{S}_{[ij]} = \begin{cases} \omega_{0i}^2 + s^2 e^{-sR_{0i}/c_0}, & i = j \\ 0, & i \neq j, \end{cases} \tag{4.5a}$$

$$\mathbf{C}_{[ij]} = \begin{cases} 0, & i = j \\ s^2 \frac{R_{0j}^2}{D_{ij} R_{0i}} e^{-s\tau_{ij}}, & i \neq j. \end{cases} \tag{4.5b}$$

The equations of motion for the C2-L approximation are more complicated. In order to write the equations of motion in matrix form it is useful to let $\mathrm{diag}(a_i)$ represent the diagonal matrix

$$\mathrm{diag}(a_i) = \begin{bmatrix} a_1 & 0 & \cdots & 0 \\ 0 & a_2 & \cdots & 0 \\ \vdots & \vdots & \ddots & \vdots \\ 0 & 0 & \cdots & a_N \end{bmatrix}.$$

It is also convenient to define a matrix of delayed signal amplitudes:

$$\mathbf{D}_{[ij]} = \begin{cases} 0, & i = j \\ \frac{e^{-s\tau_{ij}}}{D_{ij}}, & i \neq j. \end{cases} \tag{4.6}$$

The matrices **S** and **C** are written as

$$\mathbf{S} = \mathrm{diag}(\omega_{0i}^2) + \frac{s}{c_0}\mathrm{diag}(R_{0i}\omega_{0i}^2) + s^2\mathbf{1}, \tag{4.7a}$$

$$\mathbf{C} = \frac{s}{c_0}\left[\mathbf{D}\,\mathrm{diag}(R_{0i})\,\mathbf{D}\,\mathrm{diag}(\omega_{0i}^2 R_{0i}) - \mathbf{D}\,\mathrm{diag}(\omega_{0i}^2 R_{0i}^2)\right]$$

$$+ s^2\mathrm{diag}(1/R_{0i})\,\mathbf{D}\,\mathrm{diag}(R_{0i}^2), \tag{4.7b}$$

where **1** is the identity matrix. With the C3-L approximation, the equations of motion in Eq. (3.15) may be written in matrix form by defining

$$\mathbf{S}_{[ij]} = \begin{cases} \omega_{0i}^2 + s^2 + s\frac{R_{0i}\omega_{0i}^2}{c_0}, & i = j \\ 0, & i \neq j, \end{cases} \tag{4.8a}$$

$$\mathbf{C}_{[ij]} = \begin{cases} 0, & i = j \\ s^2\frac{R_{0j}^2}{D_{ij}R_{0i}}e^{-s\tau_{ij}}, & i \neq j. \end{cases} \tag{4.8b}$$

For a system of N bubbles without compressibility effects (Eq. (4.3)), **S** and **C** are given by Eqs. (4.4a) and (4.4b). In this case Eq. (4.1) can be manipulated to obtain

$$\left(\mathbf{A} - s^2\mathbf{1}\right)\chi e^{st} = \mathbf{0}, \tag{4.9}$$

where $\mathbf{A} = -(\mathbf{1} + s^{-2}\mathbf{C})^{-1}\mathrm{diag}(\omega_{0i}^2)$. Because **C** is defined as a constant, real matrix multiplied by s^2, **A** is a real matrix. The eigenvalues s of the system are given by the square root of the eigenvalues of **A**. For the undamped bubble system without delays, the eigenvalues s are purely imaginary.

When propagation delays are included in the bubble interactions, the characteristic equation becomes transcendental and, in general, possesses an infinite number of roots. It is still possible to study the stability in spite of the infinite number of eigenvalues. The presence of even one eigenvalue in the right half of the complex plane indicates an unstable mode, and therefore an unstable system.

An eigenvalue analysis of the stability of a two-bubble system was considered in Section 3.3 and it was shown that no instability occurs in the model with the C1-L approximation for liquid compressibility. The anti-phase mode of the model with the C3-L approximation becomes unstable when the bubble separation distance is less than $\sim 50R_0$. In contrast, the model with the C2-L approximations, derived in Section 2.3, is stable.

A similar analysis will be conducted here for a system of N bubbles. In a two-bubble system the relevant parameter for the coupled dynamics is the separation distance between the bubbles. Because in this case there is only one parameter, it is possible to analyze the behavior of the system over the parameter space of interest for the eigenvalues of all (two) modes with the lowest damping. It is impossible to conduct an equivalent analysis of the set of possible configurations even for a three-bubble system. Thus, a statistical analysis is required for multi-bubble systems.

The behavior of a 20-bubble system is examined by calculating the damping coefficient corresponding to the eigenvalue with the smallest value of δ (the right-most eigenvalue in the complex plane). The minimum damping coefficient is calculated by solving Eq. (4.2) numerically with **S** and **C** given by Eq. (4.5), Eq. (4.8), or Eq. (4.7). Test cases are generated by placing bubbles with a radius of 3.5 mm at random locations within a sphere. This size was chosen to facilitate comparison with previous work on bubbles in a compressible medium[46,47,54] that will be discussed in Sections 4.2.1 and 4.2.2. Because the bubbles are all of equal size, the subscript i of the equilibrium radius R_{0i} and natural frequency ω_{0i} is suppressed. Although the results are nominally computed for bubbles with an equilibrium radius of 3.5 mm, because the effects of surface tension, and viscous and thermal damping are neglected here and the calculations are performed at the natural frequency, the equations can be written in a form that is independent of the bubble radius. Thus the results presented here are valid for bubbles of any size.

The damping coefficient is computed for clusters with a radius R_{cl} ranging from $10R_0$ to $1000R_0$. The calculations are carried out for 100 realizations at each distinct bubble cluster radius. The spread of the damping coefficients calculated with all three approximations is shown in Fig. 4.1. These figures summarize the behavior of 10,000 distinct bubble cluster geometries. The horizontal axis is the nominal cluster radius R_{cl} normalized by the equilibrium bubble radius R_0, and the vertical axis is the minimum damping coefficient normalized by the nondimensional radiation damping coefficient for a single bubble (Eq. (3.37)), shown on a symmetric log scale (both negative and positive values are log-scaled). The value of δ_{rad} is approximately 0.014 for air bubbles in water.[55] Stable regions of the parameter space are indicated by a white background, unstable regions are indicated by a colored background.

The full range of values is shown in light gray, the range of the second and

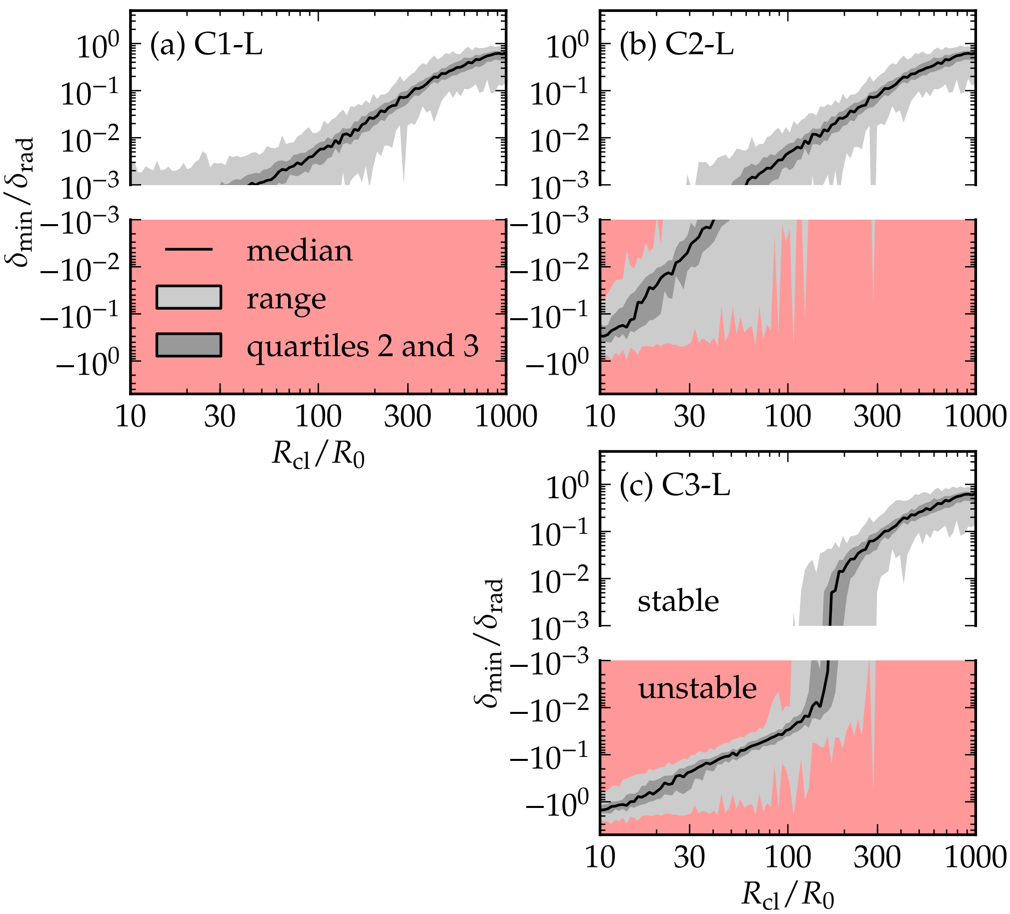

Figure 4.1: Quartiles of the distribution of damping coefficients calculated for clusters containing 20 bubbles as a function of the cluster radius R_{cl}. The quartiles are obtained from the calculated damping coefficients of 100 realizations of random bubble configurations for each cluster radius. Stable regions of the parameter space are indicated by a white background, unstable regions are indicated by a colored background.

third quartiles is shown in dark gray, and the median value is indicated by the solid black line. Part (a) corresponds to the C1-L approximation (Eq. (4.5)), part (b) to the C2-L approximation (Eq. (4.7)), and part (c) to the C3-L approximation (Eq. (4.8)).

The model with the C1-L approximation is uniformly stable. Presumably this occurs because the C1 approximation relies only on the assumption that the bubble radius is much smaller than the acoustic wavelength in the surrounding medium, which is always true here. In contrast, the C2 approximation to C1 is only valid to $O(R^2/D^2)$, $O(1/c_0)$, and $O(R^2/(D^2 c_0))$ for both the self-action of the bubble and the interaction with other bubbles. For the C2-L model shown in part (b), before the cluster radius reaches $50R_0$, the majority of the bubble configurations are stable (positive damping coefficient). After this point, for most configurations the damping predicted by the C2-L model closely follows the prediction of the C1-L model. However, there are a few outlying configurations that remain unstable until the cluster radius is nearly $300R_0$. In contrast, for the C3-L model shown in part (c) of Fig. 4.1, at least half of the realizations are unstable for cluster radii less than $\sim 200R_0$, and some realizations are unstable even for cluster radii of nearly $300R_0$. It should be noted that in the C3-L approximation, terms of $O(R/D)$ that are also $O(1/c_0)$ are neglected.

Similar to the two-bubble anti-phase case shown in Fig. 3.5, the model with the C3-L approximation is unstable for larger bubble spacing. All clusters with radii less than $\sim 100R_0$ are unstable with the C3-L approximation. The model with the C2-L approximation performs significantly better than the C3-L model, but the large range of values of R_{cl} and the isolated outlying values for which the models predict unstable systems suggest that the cluster radius is not the relevant length scale for system stability.

Additional insight into the behavior of the bubble systems can be gained by considering the damping as a function of other characteristic lengths. Several possibilities include the minimum separation distance D_{min} between bubbles in the cluster, the mean separation distance D_{mean} between bubbles, the minimum separation distance normalized by the cluster radius $D_{\mathrm{min}}/R_{\mathrm{cl}}$, and the mean separation distance normalized by the cluster radius $D_{\mathrm{mean}}/R_{\mathrm{cl}}$.

The ranges of $D_{\mathrm{min}}/R_{\mathrm{cl}}$ and $D_{\mathrm{mean}}/R_{\mathrm{cl}}$ for clusters containing 10, 20, and 30 bubbles are shown in Fig. 4.2. $D_{\mathrm{min}}/R_{\mathrm{cl}}$ may be very small for large clusters that happen to have a pair of closely spaced bubbles. Because the bubbles cannot overlap, the minimum possible value of D_{min} is $2R_0$. Therefore, as the cluster radius decreases, $D_{\mathrm{min}}/R_{\mathrm{cl}}$ increases. This increase can be observed in Fig. 4.2. In the configurations considered here, the smallest cluster has a radius of $R_{\mathrm{cl}} = 10R_0$. Thus, the minimum value of $D_{\mathrm{min}}/R_{\mathrm{cl}}$ approaches 0.2. The curvature of the minimum value of $D_{\mathrm{min}}/R_{\mathrm{cl}}$ as R_{cl} approaches $10R_0$ is due to the presence of R_{cl} in the denominator. The value of $D_{\mathrm{mean}}/R_{\mathrm{cl}}$ exhibits greater variation for clusters containing fewer bubbles. As the number of bubbles in the cluster increases, $D_{\mathrm{mean}}/R_{\mathrm{cl}}$ approaches 1. This occurs because there are more pairs separated by distances greater than R_{cl} than by distances less than R_{cl}, or in other words, there is a greater number of more distant bubble pairs than of close bubble pairs.

The minimum damping coefficient δ_{min} normalized by the single bubble radiation damping coefficient δ_{rad} is shown in Fig. 4.3 as a function of $D_{\mathrm{min}}/R_{\mathrm{cl}}$ (left column) and $D_{\mathrm{mean}}/R_{\mathrm{cl}}$ (right column). These are the same data that were presented in Fig. 4.1. The scattered data demonstrate virtually no correlation between either $\delta_{\mathrm{min}}/\delta_{\mathrm{rad}}$ and $D_{\mathrm{min}}/R_{\mathrm{cl}}$ or $\delta_{\mathrm{min}}/\delta_{\mathrm{rad}}$ and $D_{\mathrm{mean}}/R_{\mathrm{cl}}$. The lack of correlation with either length suggests that neither $D_{\mathrm{mean}}/R_{\mathrm{cl}}$ nor $D_{\mathrm{mean}}/R_{\mathrm{cl}}$ is the appropriate length scale for the cluster system stability.

The minimum separation distance D_{min} and mean separation distance D_{mean} are now considered. Figure 4.4 shows the spread of the minimum damping coefficient predicted by the C2-L model (top row) and the C3-L model (bottom row) as a function of the two different characteristic lengths. The left column in Fig. 4.4 shows the damping as a function of the minimum separation distance D_{min} in a cluster, while the right column shows the damping as a function of the mean separation distance D_{mean}. It can be seen in part (b) of Fig. 4.4 that the damping coefficient is negative for a large range of parameter values and at several outlying points. This suggests that D_{mean}/R_0 is not the relevant length parameter for the stability of the C2-L model. Part (a) in Fig. 4.4 shows that the C2-L model is stable for all configurations having a minimum separation distance greater than $10R_0$. This result is reasonable considering the expansion to $O(R^2/D^2)$ that was used to obtain the C2 approximation. This suggests that the unstable modes in the C2-L model are due to truncation errors in the expansion. It appears that unstable modes only occur when R^2/D^2 is not much less than 1. Thus, the characteristic parameter for the system stability is D_{min}/R_0.

In contrast, the C3-L model shown in part (b) of Fig. 4.1 and parts (c) and (d) of Fig. 4.4 is unstable for much higher values of all three characteristic lengths.

Instability occurs for cluster radii and mean separation distances of $100R_0 - 400R_0$ and for minimum separation distances greater than $50R_0$.

The same effects can be seen in clusters with different numbers of bubbles. The minimum damping coefficients for the 10- and 30-bubble clusters shown in Fig. 4.2 are shown in Figs. 4.5 and 4.6, respectively. As was the case for the 20-bubble system, the C2-L approximation for both the 10- and 30-bubble systems (part (a) in Figs. 4.5 and 4.6, respectively) produces unstable systems when $D_{\mathrm{min}} < 10R_0$. Again, the C3-L approximation produces unstable systems (part (c) in Figs. 4.5 and 4.6) when $D_{\mathrm{min}} < 50R_0$.

Doinikov et al.[46] and Ooi et al.[47] performed a similar analysis of the change in damping produced by the inclusion of time delay in bubble-bubble interactions. Their work was performed using the C3-L model (Eq. (4.8)) but no instabilities were observed. Their work included the effects of liquid viscosity and thermal damping, which are not included in the present section. Simulations of bubble clusters with the effects of liquid viscosity and thermal damping are considered in Section 4.2, where a direct comparison to the results of Doinikov et al. and Ooi et al. is made.

Figures 4.1 and 4.4–4.6 illustrate that the instabilities observed in the simple two-bubble case are not merely artifacts of the symmetries present in a two-bubble system, but are also present in large, asymmetric systems. Therefore, the C1-L model must be used to accurately predict the behavior of a system of bubbles in a compressible medium. For systems in which the minimum bubble separation distance is large enough, the C2-L model may be used.

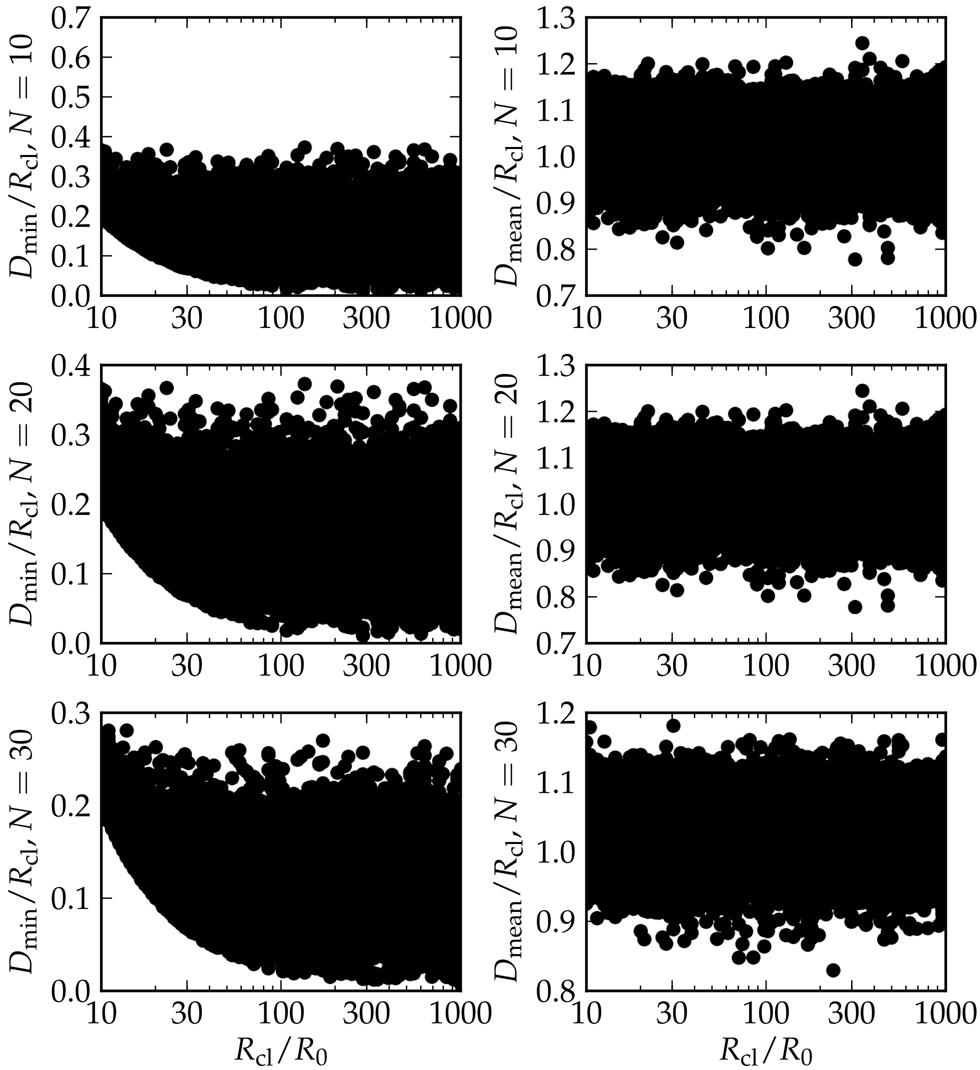

Figure 4.2: Scatter plots of $D_{\mathrm{min}}/R_{\mathrm{cl}}$ (left) and $D_{\mathrm{mean}}/R_{\mathrm{cl}}$ (right) as a function of R_{cl}/R_0 for clusters containing 10, 20, and 30 bubbles. The cluster radius ranges from $10R_0$ to $1000R_0$.

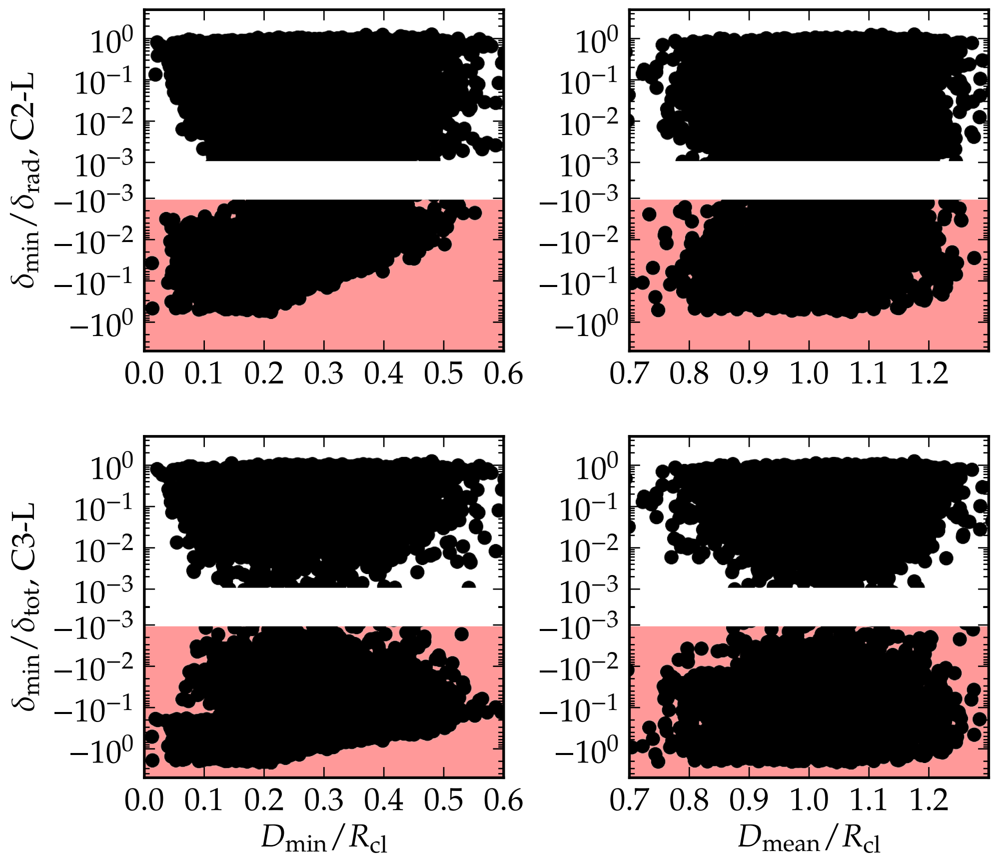

Figure 4.3: Scatter plots of the minimum damping coefficient as a function of $D_{\min}/R_{\mathrm{cl}}$ (left) and $D_{\mathrm{mean}}/R_{\mathrm{cl}}$ (right) for a cluster containing 20 bubbles. The C2-L approximation is used for the top row and the C3-L approximation for the bottom row. The cluster radius ranges from $10R_0$ to $1000R_0$. Stable regions of the parameter space are indicated by a white background, unstable regions are indicated by a colored background.

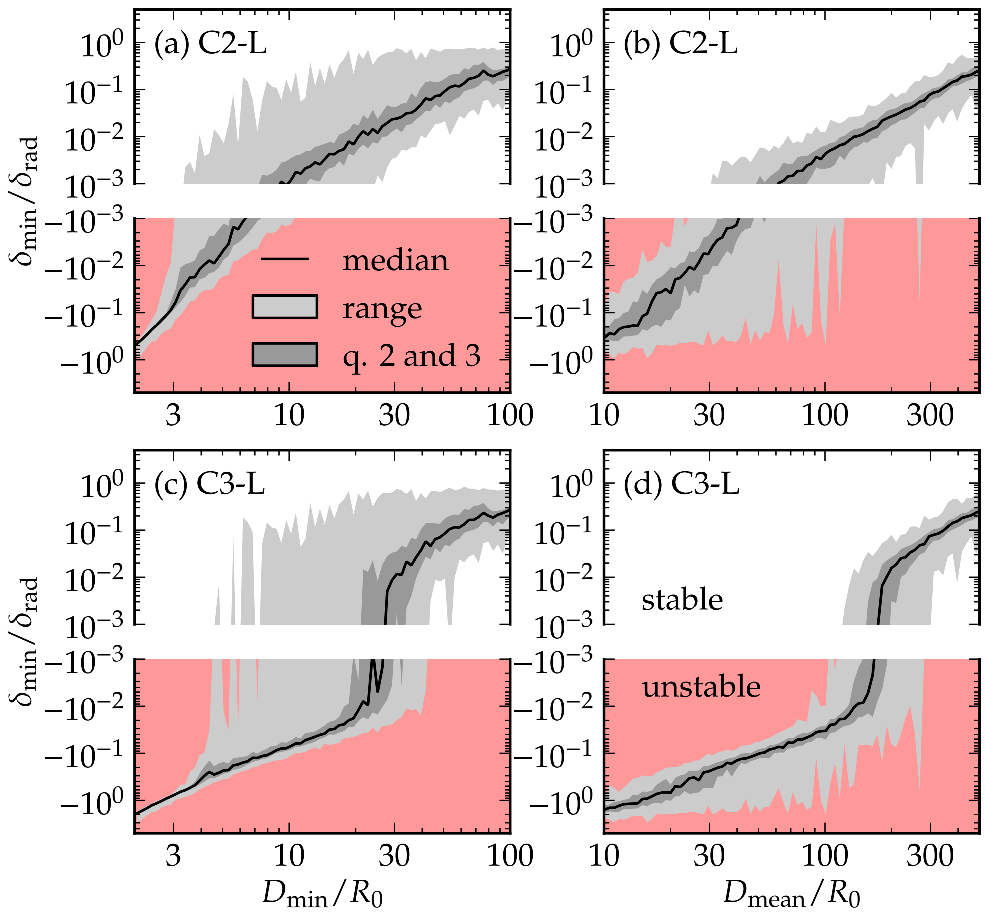

Figure 4.4: Quartiles of the minimum damping coefficient for a 20 bubble cluster as a function of the minimum bubble separation distance $D_{\min}$ (left column) and mean bubble separation distance D_{mean} (right column). The top row was produced by the C2-L model (Eq. (4.7)) and the bottom row was produced by the C3-L model (Eq. (4.8)). Stable regions of the parameter space are indicated by a white background, unstable regions are indicated by a colored background.

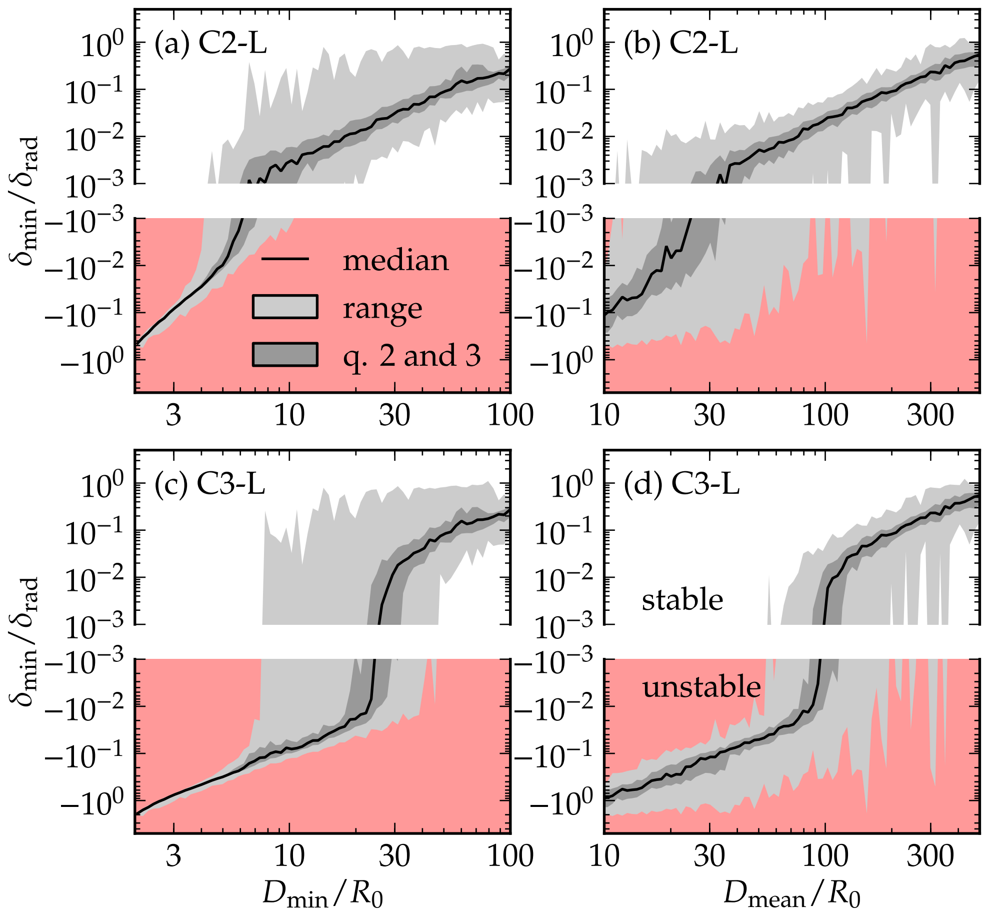

Figure 4.5: Quartiles of the minimum damping coefficient for a 10-bubble cluster as a function of the minimum bubble separation distance $D_{\min}$ (left column) and mean bubble separation distance D_{mean} (right column). The top row was produced by the C2-L model (Eq. (4.7)) and the bottom row was produced by the C3-L model (Eq. (4.8)). Stable regions of the parameter space are indicated by a white background, unstable regions are indicated by a colored background.

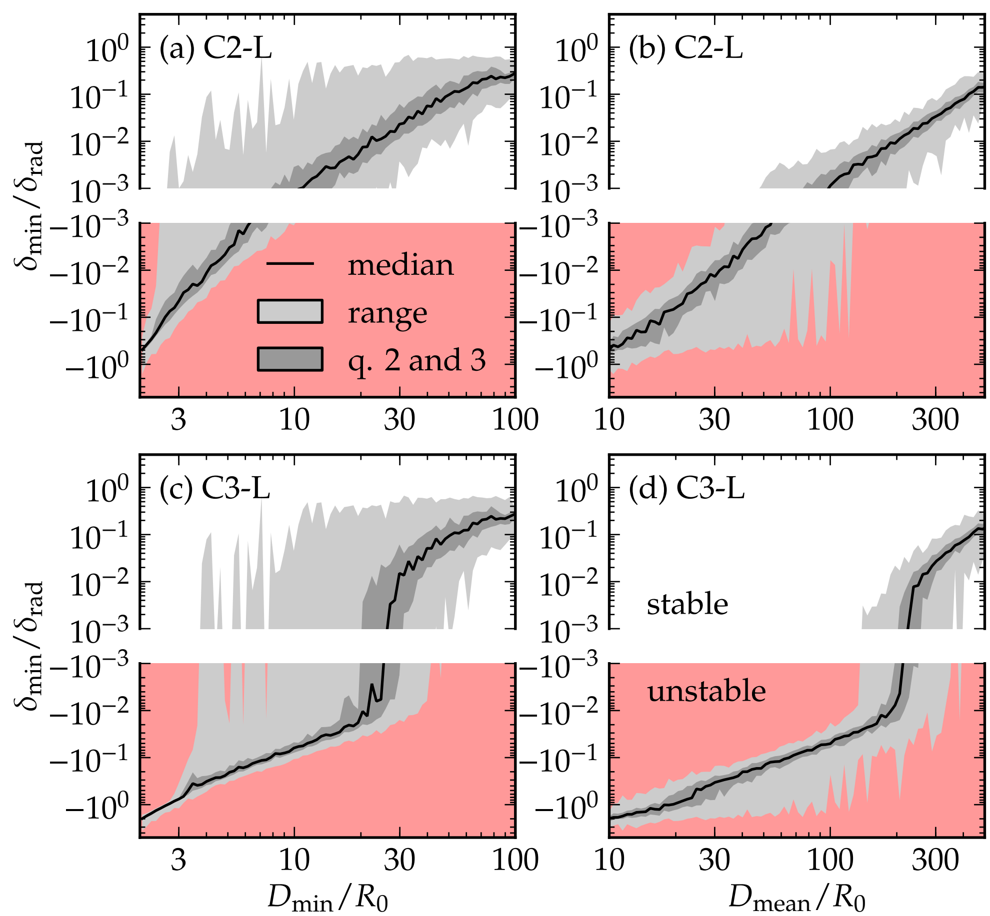

Figure 4.6: Quartiles of the minimum damping coefficient for a 30-bubble cluster as a function of the minimum bubble separation distance D_{min} (left column) and mean bubble separation distance D_{mean} (right column). The top row was produced by the C2-L model (Eq. (4.7)) and the bottom row was produced by the C3-L model (Eq. (4.8)). Stable regions of the parameter space are indicated by a white background, unstable regions are indicated by a colored background.

4.2 Compressibility effects with viscous and thermal damping in multi-bubble systems

The effects of liquid viscosity and thermal damping were not included in the linearized equations of motion analyzed in the previous section. In order to simulate real physical systems and compare with experiments, it is necessary to modify the equations of motion to include viscous and thermal damping effects.

The viscous damping term for the nonlinear equations of radial motion was given in Eq. (2.25). Equation (2.25) can be converted to an expression that accounts for viscous damping in the linear approximation. The viscous effects are included by adding

$$\frac{4\eta\dot{\xi}_i(t)}{\rho_0 R_{0i}^2} \tag{4.10}$$

to the left-hand side of each relevant equation (Eqs. (3.13), (3.15), (3.23), and (4.3)). For example, Eq. (4.3) becomes, without the coupling terms and for a single bubble,

$$\ddot{\xi} + \delta_{\mathrm{visc}}\omega_0\dot{\xi} + \omega_0\xi = 0, \tag{4.11}$$

where

$$\delta_{\mathrm{visc}} = \frac{4\eta}{\rho_0 R_0^2 \omega_0} \tag{4.12}$$

is the viscous damping coefficient. In this form, δ_{visc} is the reciprocal of the quality factor and is thus consistent with Eq. (3.37) for δ_{rad}. Equations (3.13), (3.15), and (3.23) are modified in the same way. The definition in Eq. (4.12) is identical to the expressions given by Clay and Medwin[72] and Leighton.[55] Unlike the viscous and radiation damping coefficients, which are constants at our order of approximation, the thermal damping coefficient is a function of frequency. For solutions of the form $\xi(t) = \chi e^{st}$, where $\omega = \mathrm{Im}\{s\}$, Eq. (4.11) becomes, when augmented to account for radiation and thermal damping,

$$\left\{s^2 + [\delta_{\mathrm{rad}} + \delta_{\mathrm{visc}} + \delta_{\mathrm{th}}(\omega)]\,\omega_0 s - \omega_0^2\right\} \chi e^{st} = 0, \tag{4.13}$$

such that $\delta_{\mathrm{th}}(\omega)$ is defined consistently with δ_{rad} and δ_{visc}.

The work of Doinikov et al.[46] and Ooi et al.[47] was conducted using the thermal damping coefficient given by Clay and Medwin,[72] and therefore the same expression for δ_{th} will be used here:

$$\delta_{\mathrm{th}}(\omega) = 3(\gamma - 1)\left[\frac{z(\sinh z + \sin z) - 2(\cosh z - \cos z)}{z^2(\cosh z - \cos z) + 3(\gamma - 1)z(\sinh z - \sin z)}\right], \tag{4.14}$$

where

$$z = R_0\sqrt{\frac{2\omega\rho_g C_p}{\kappa_g}},$$

κ_g is the thermal conductivity of the gas inside the bubble, ρ_g is the density of the gas, and C_p is the specific heat of the gas. In the multi-bubble case, the individual bubble values (R_0, R, ω) require subscripts.

The inclusion of viscosity and thermal damping in the equations of motion only affects the matrix **S** in Eqs. (4.4), (4.5), (4.7), and (4.8). The change due to viscosity is included by adding

$$\frac{4\eta s}{\rho_0}\mathrm{diag}(1/R_{0i}^2) \tag{4.15}$$

to **S**, and the effects of thermal damping are included by adding

$$s\ \mathrm{diag}[\omega_{0i}\delta_{i,\mathrm{th}}(\mathrm{Im}\{s\})] \tag{4.16}$$

to **S**. The characteristic equation is still $\det(\mathbf{S}+\mathbf{C}) = 0$, but with the matrix **S** modified for viscosity and thermal effects. In the remainder of this section an eigenvalue analysis of the characteristic equations with viscous and thermal damping is used to examine the behavior of multiple bubbles in a line and in a spherical cluster.

4.2.1 Line array of bubbles

Previous work by Doinikov et al.[46] and Ooi et al.[47] on compressibility effects in a system of coupled bubbles considered the natural modes of a linear chain of equally sized bubbles with uniform spacing in a compressible liquid. An equivalent system will be considered here. Bubbles of equal size with equilibrium radius R_0 are placed in a line with distance D_0 between bubbles. Because the bubbles are all of equal size, the subscript i of the equilibrium radius R_0 and natural frequency ω_0 is suppressed. An example geometry for a system of five bubbles in this configuration is shown in Fig. 4.7.

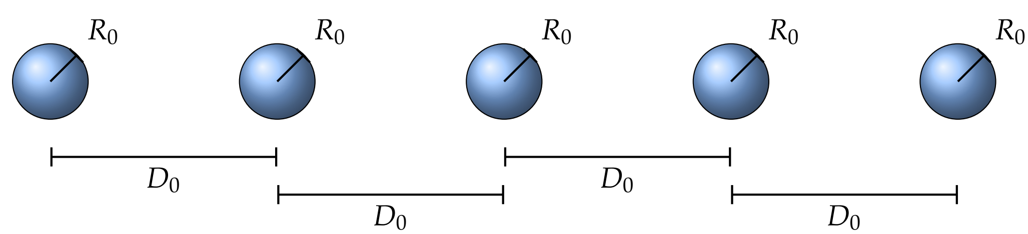

Figure 4.7: Line array of five equally sized bubbles with equilibrium radius R_0 and successive spacing D_0.

Previous analyses[46,47] and experiments[47,54] were conducted on a system of equally sized bubbles with an equilibrium radius of R_0 = 3.5 mm and a spacing of D_0 = 32.1 mm between bubbles in the array such that $D \approx 9.1R_0$. To enable comparison of results, the work in this section will consider a system of bubbles with the same equilibrium radius, R_0 = 3.5 mm. Doinikov et al.[46] and Ooi et al.[47] presented results for the variation in damping coefficients for N modes in a system of N bubbles with N ranging from 2 to 11. The inclusion of delays due to liquid compressibility transforms the characteristic equation (Eq. (4.2)) into a transcendental equation with an infinite number of roots.[73] This is starkly different from the standard case for a system of (instantaneously) coupled oscillators in which the characteristic equation has twice as many roots (complex conjugate pairs) as the number of oscillators in the system. For a system of delay differential equations (DDE) system it may be impossible to completely characterize the eigenvalues due to the transcendental nature of the characteristic equation. The minimum damping coefficient is of key importance because if any mode has negative damping, the solution of the equations of motion for the response of the system to arbitrary excitation will generally be unstable. Therefore, only the minimum damping coefficient of *any* mode in the system is considered here. In contrast, in the previous analysis[46,47] in which the damping of a selected number of modes was considered, they were not necessarily the modes with the lowest damping.

The minimum damping coefficient is calculated for systems containing N = 2, 5, 10, and 20 bubbles with the bubble spacing D_0 ranging from $2R_0$ to $1000R_0$ (7 mm to 3.5 m). All three methods for including compressibility effects (C1-L, C2-L, and C3-L) are employed, with the matrices in the characteristic equation being given in Eqs. (4.5), (4.7), and (4.8). The matrix $\mathbf{S}$ is augmented by Eqs. (4.15) and (4.16) to include the effects of viscosity and thermal damping in the calculations.

The results of these calculations are shown in Fig. 4.8.

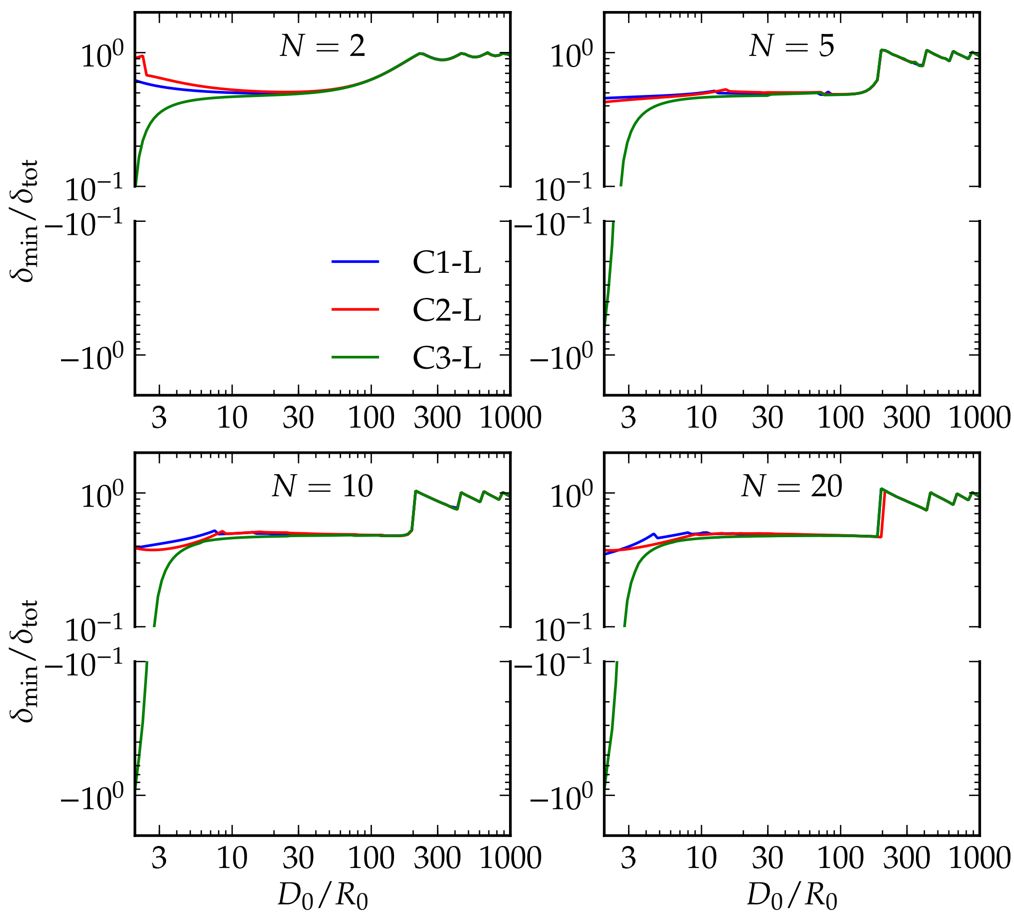

Figure 4.8: Calculated minimum damping coefficient for a line array of equally sized bubbles (R_0 = 3.5 mm). Results for line arrays containing 2, 5, 10, and 20 bubbles are shown. The spacing between successive bubbles D_0 ranges from $2R_0$ to $1000R_0$. The damping coefficient is normalized by the total dimensionless radiation damping of a single bubble at resonance, δ_{tot} .

In Fig. 4.8 the vertical axis is the minimum damping coefficient $\delta_{\min}$ normalized by the total damping coefficient δ_{tot} for a single bubble at resonance,

$$\delta_{\text{tot}} = \delta_{\text{rad}} + \delta_{\text{visc}} + \delta_{\text{th}}(\omega_0). \tag{4.17}$$

The radiation damping coefficient is given by Eq. (3.37), the viscous damping coefficient is given by Eq. (4.12), and the thermal damping coefficient $\delta_{\text{th}}(\omega)$ is given by Eq. (4.14) evaluated at $\omega = \omega_0$. For a bubble with equilibrium radius $R_0 = 3.5$ mm, δ_{tot} is approximately 0.027 for an air bubble in water.

In Fig. 4.8, the horizontal axis is the spacing D_0 between bubbles in the line array normalized by the equilibrium radius R_0, and D_0 is also equal to the minimum distance between any bubble pair in the system. Each plot corresponds to a different number of bubbles in the array, with the arrays containing 2, 5, 10, and 20 bubbles. The C1-L, C2-L, and C3-L approximations are marked with blue, green, and red lines, respectively. All three approximations approach $\delta_{\text{min}}/\delta_{\text{tot}} = 1$ as the separation distance becomes large and the strength of the coupling between the bubbles is reduced. The sawtooth shape is due to the separation distance passing through multiples of the acoustic wavelength at the natural frequency of the mode.

The C1-L model remains stable (positive minimum damping coefficient) for the four different numbers of bubbles in the system and for the full range of bubble spacings. In contrast to the undamped case in Section 4.1, the minimum damping does not approach zero for closely spaced bubble systems as it did for the undamped systems in Sections 3.3 and 4.1. This is expected from the increase in damping due to the inclusion of liquid viscosity and thermal effects. As was discussed in Section 3.3, the damping of the anti-phase mode of the two-bubble system without viscous and thermal damping approaches zero as the bubble separation distance decreases. However, the inclusion of viscous and thermal damping prevents the minimum damping coefficient from approaching zero. The C2-L approximation converges to the C1-L model for values of D_0 greater than ~$4R_0$ for all four numbers of bubbles considered here. For the 2-bubble case (and the 3-bubble case, which is not shown) both the C1-L and C2-L approximations predict a slight increase in damping for more closely spaced bubbles. This is the opposite of the effect observed in clusters containing more than 4 bubbles, in which the damping decreases as D_0 decreases. It is also opposite the behavior of the minimum damping observed in the 2-bubble system shown in Fig. 3.5. The reason for this unexpected increase is unknown but it is consistent with the results presented in Fig. 6, part (b) of Ref. 40.

The C3-L approximation is stable for the 2-bubble case and requires values of $D_0 > 3R_0$ for stability in the 5-, 10-, and 20-bubble cases. The C3-L model converges to the results of the C1-L approximation for values of $D_0 > 10R_0$ for all four numbers of bubbles shown in Fig. 4.8. The C3-L approximation for the 5-bubble case converges to the C1-L model near $D_0 = 3R_0$, but this appears to be coincidental. As the number of bubbles increases, the C3-L system remains unstable at slightly higher values of D_0, but the curve remains essentially unchanged for systems containing more than 20 bubbles.

The work of Doinikov et al.[46] and Ooi et al.[47] considered some of the same configurations presented here with the same viscous and thermal damping included. Bubbles in each system were separated by $9.1R_0$, and systems consisting of 2 to 11 bubbles were considered. The C3-L approximation was used to include compressibility effects, and viscous and thermal damping were included with the same methods that are used here. Our results may be compared to the results of Doinikov et al. and Ooi et al. when $D_0 = 9.1R_0$ for the 2-, 5-, and 10-bubble systems. The values for comparison are obtained from Fig. 3 in Doinikov et al.[46] The minimum effective dimensional damping coefficients reported by Doinikov et al. are $47.6s^{-1}$ for the 2-bubble array, $47.3s^{-1}$ for the 5-bubble array, and $46.8s^{-1}$ for the 10-bubble array. The dimensional damping coefficient with viscous, thermal, and radiation damping for a single bubble is reported as $87.5\mathrm{s}^{-1}$, which is obtained from Fig. 1 in Doinikov et al.[46] The minimum damping of the 5- and 10-bubble arrays is thus approximately half that of a single bubble. In order to compare to the current results, it is necessary to compute the ratio of the minimum damping coefficient to the single-bubble damping coefficient. The ratio of damping coefficients is 0.544 for the 2-bubble case, 0.54 for the 5-bubble case, and 0.535 for the 10-bubble case.

For the calculations shown in Fig. 4.8, the ratio of minimum damping coefficient to the single-bubble damping coefficient is 0.49 for the 2-bubble case, 0.47 for the 5-bubble case, and 0.48 for the 10-bubble case. This corresponds to 11%, 15% and 11% differences, respectively, between the damping coefficients calculated here and those reported in Doinikov et al.[46] Presumably, the reason for these differences lies in the method used to obtain the eigenvalues of the system. In their analyses, Doinikov et al. and Ooi et al. used the roots of the characteristic equation of the model for bubbles in an incompressible liquid as the initial guess to numerically solve for the roots of the delayed characteristic equation. Numerical methods for finding roots can be extremely sensitive to the initial guess of the root value. Because the characteristic equation of a time-delayed system possesses an infinite set of roots, it is likely that one of those roots will lie near the roots of the related delay-free system. However, the closest root is not necessarily the root corresponding to the minimum damping. Therefore, to obtain the results presented here, multiple initial guesses were used to explore the region near each root and the minimum result is reported. Thus, while Doinikov et al. and Ooi et al. report reduced damping, it is not necessarily the minimum damping present in the system.

4.2.2 Bubble cluster

The same approach used in Section 4.1 is now used to study systems of bubbles placed randomly in a sphere, with the inclusion of viscous and thermal damping in the equations of motion. All bubbles in the systems considered here are of equal size, with an equilibrium radius of 3.5 mm. Bubbles of this size are chosen to facilitate comparison with the results of the previous section. The minimum damping coefficient is calculated from the characteristic equation (Eq. (4.2)) with the matrix $\mathbf{S}$ augmented to include the effects of viscous and thermal damping as given by Eqs. (4.15) and (4.16). The bubbles are placed randomly within a sphere with nominal cluster radius R_{cl}. Again, 100 realizations are considered for each cluster radius, with the cluster radius ranging from $10R_0$ to $500R_0$.

The same 20-bubble systems used in Section 4.1 are used here and the results are presented in the same format. Figure 4.9 shows the quartiles for the distribution of the minimum damping coefficients calculated for the viscous and thermal damped systems using the C1-L approximation (part (a)), the C2-L approximation (part (b)), and the C3-L approximation (part (c)) to include the effects of liquid compressibility.

The horizontal axis is the bubble cluster radius R_{cl} normalized by the equilibrium radius R_0 of the bubbles in the system. The vertical axis is the minimum damping coefficient δ_{min} normalized by the total damping of a single bubble δ_{tot} given by Eq. (4.17). For a bubble with equilibrium radius $R_0 = 3.5$ mm, δ_{tot} is approximately 0.027. The damping coefficients for clusters of bubbles are similar to the coefficients for lines of bubbles reported in the previous section. Figures 4.1 and 4.9 show results for the same systems, the only difference being the inclusion of viscous and thermal damping in Fig. 4.9. Similarly, Figs. 4.4 and 4.10 show the minimum damping coefficients for the same systems as functions of D_{min} and D_{mean}, with viscous and thermal damping included in Fig. 4.10. The overall damping in the systems is increased by the inclusion of viscous and thermal damping. The behavior of the mode with the minimum damping coefficient is dominated by the viscous and thermal damping. The C1-L and C2-L approximations have converged even for the smallest configurations, and in neither case does the minimum damping approach zero. It is apparent that the fluid compressibility reduces the damping. For the C1-L approximation shown in part (a) of Fig. 4.9 the minimum damping is in the range of 30–50% of the single bubble damping. The C2-L approximation produces similar results.

Only the C3-L approximation produces unstable systems, but the instabilities disappear for much smaller clusters than in the undamped case considered in Section 4.1. Without damping, the C3-L system was unstable for cluster radii

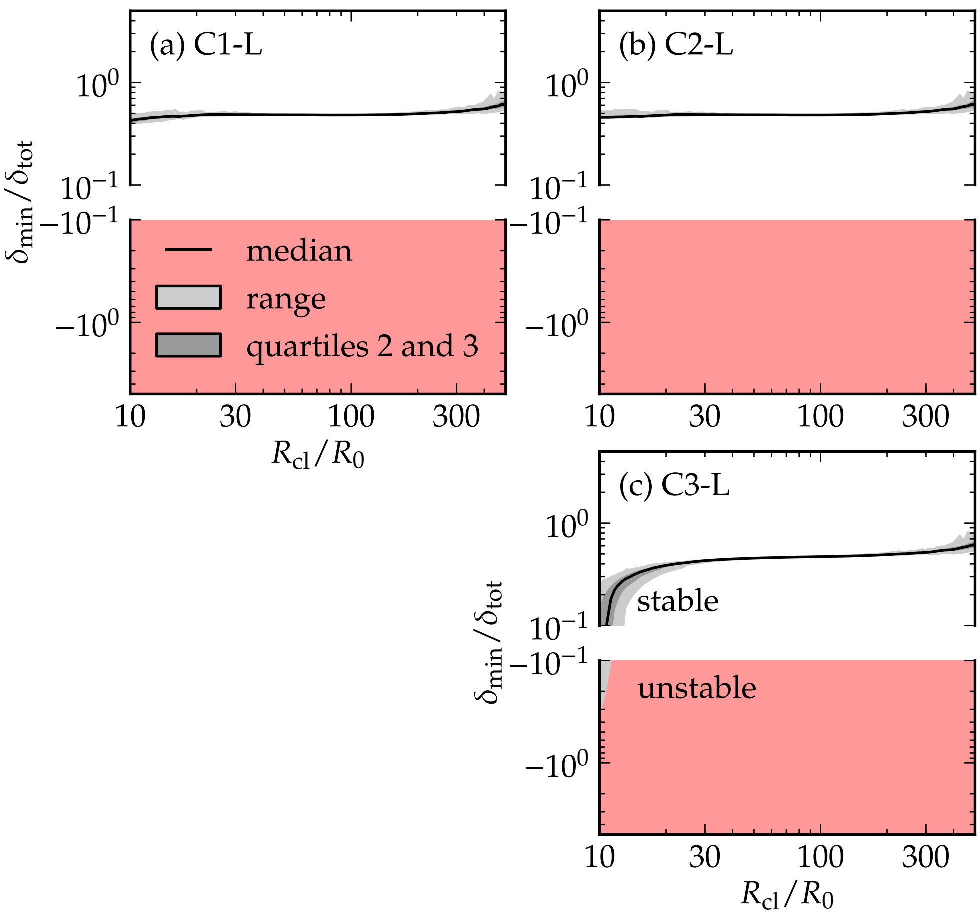

Figure 4.9: Quartiles of the distribution of minimum damping coefficients calculated for clusters containing 20 bubbles as a function of the cluster radius R_{cl}. Viscous and thermal damping effects are included. Stable regions of the parameter space are indicated by a white background, unstable regions are indicated by a colored background.

greater than $100R_0$. With the effects of damping, the system is stable by $R_{\text{cl}} = 12R_0$ and has converged to the C1-L model by $R_{\text{cl}} = 20R_0$.

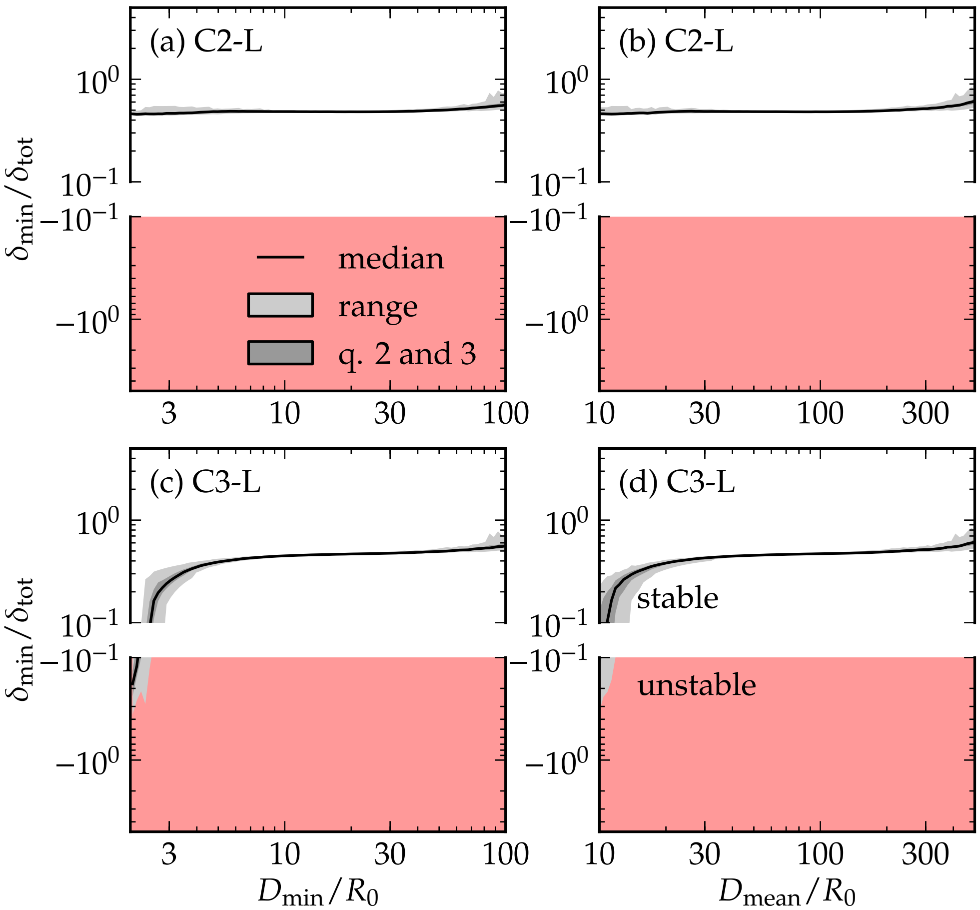

Figure 4.10: Quartiles of the distribution of minimum damping coefficients for a 20 bubble cluster with viscous and thermal damping effects as a function of the minimum bubble separation distance $D_{\min}$ (left column) and mean bubble separation distance D_{mean} (right column). The bubbles have an equilibrium radius of 3.5 mm. The top row was produced by the C2-L model (Eq. (4.7)) and the bottom row was produced by the C3-L model (Eq. (4.8)). Stable regions of the parameter space are indicated by a white background, unstable regions are indicated by a colored background.

It was observed in Section 4.1 that the stability of the system appears to be correlated with the minimum bubble spacing in the system. Figure 4.10 shows plots of the spread of δ_{min} as a function of the minimum separation distance (left column) and the mean separation distance (right column). The top and bottom rows correspond to the C2-L and C3-L approximations for compressibility, respectively. As noted earlier, the C2-L approximation is uniformly stable with the increased damping. The C1-L and C2-L models are stable. The C3-L model is unstable for some geometries with minimum separation distance $D_{\text{min}} < 3R_0$, but the stability is greatly improved by the increased damping. The C3-L model does not converge to the C1-L model until $D_{\text{min}} \approx 6R_0$. As was observed in Fig. 4.9, the transition from unstable to stable in damped systems occurs for much lower values of the characteristic lengths when compared to the undamped system. It is interesting to note that the increased damping due to viscous and thermal effects is sufficient to stabilize many of the systems where the single-bubble radiation damping alone did not produce a stable system.

Because the bubbles in the systems considered in this section are rather large (3.5 mm), the damping is relatively low. The damping coefficients at resonance for a single bubble given by Eqs. (3.16), (4.12), and (4.14) are shown in Fig. 4.11 as functions of bubble radius. Shown are the viscous, thermal, and radiation damping coefficients along with the total damping coefficient. The figure shows that the damping increases significantly for smaller bubbles. Therefore, systems containing smaller bubbles will be more stable than the systems examined here. This has been verified with simulations similar to those presented here, but the results are not presented graphically at this time.

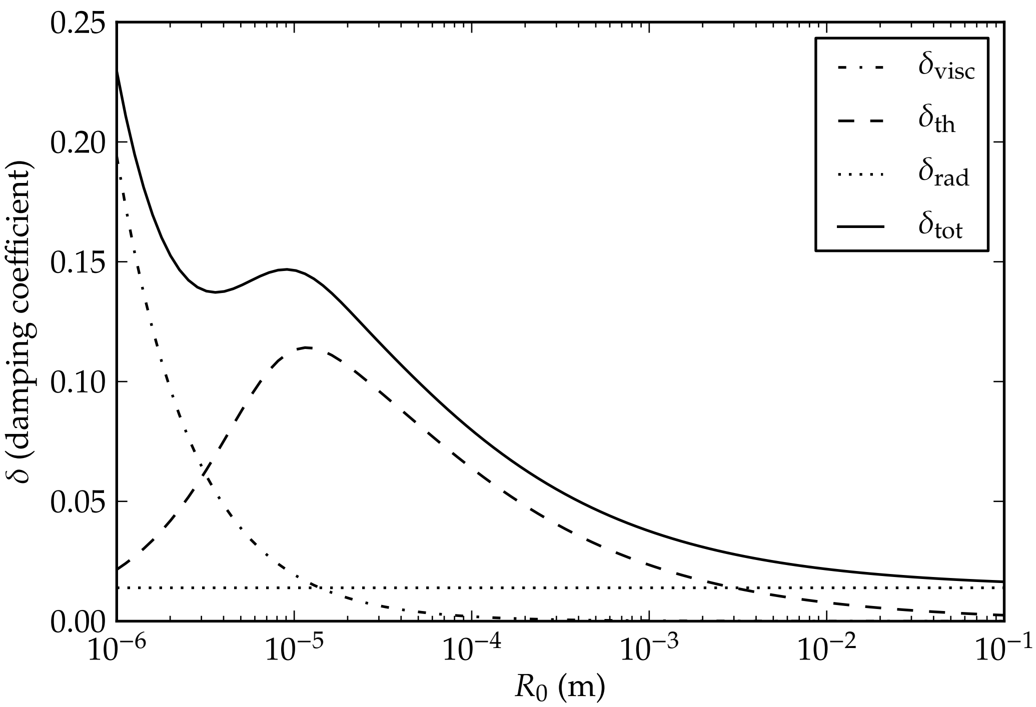

Figure 4.11: Dimensionless damping coefficients for a single bubble as functions of bubble radius. Shown are the viscous, thermal, and radiation damping coefficients along with the total damping coefficient.

The results in this section apply only to the stability of the system and not to the general dynamics. Although the stability of the systems obtained by all three method for including compressibility effects is essentially the same for clusters with $D_{min} > 12R_0$, this does not mean that the dynamics of the systems will be similarly equivalent. A more thorough analysis of the eigenvalues of the system is required to determine the overall convergence of the three levels of approximation.

4.3 Forced response of a bubble system

Here, the transient response of a 20 bubble system to pulsed external forcing as predicted by the fully nonlinear equations of motion with liquid viscosity is considered. The pulses used to excite the bubble system here are very short and therefore the response of the system is similar to free response, the only difference being the variation in times at which the pulse arrives at a given bubble. The pressure produced by a pair of acoustically driven bubbles near a rigid plane is also considered.

4.3.1 Bubble cluster

For the first case, the chosen geometry is a cluster of 20 bubbles with an equilibrium radius of 10 μm randomly placed within an oblate ellipsoidal region. The bubble size here is greatly reduced in comparison to the bubbles considered in the previous section. The bubble size in the previous section was chosen specifically to coincide with previous work by Doinikov et al.[46] The smaller bubble size chosen in the current section more closely reflects the bubble sizes observed in lithotripsy and other biomedical treatments that motivated the work in this dissertation. Also, the damping experienced by bubbles increases as the bubble size decreases.[55] Two of the semi-principal axes are equal with a length of $10R_0$ while the third semi-principal axis has a length of $50R_0$. The total length of the ellipse is $100R_0$ (0.1 mm) and the width is $20R_0$ (0.02 mm). The bubbles are placed so that the minimum spacing between any pair of bubbles is greater than $10R_0$. The forcing is produced by a pressure pulse consisting of two cycles of a sine wave with a frequency of 173

MHz. Thus the pressure wave is 1.7 cm long, 1700 times the equilibrium bubble radius, or 17 times as long as the whole bubble cluster. The pulse is planar and propagates parallel to the longest semi-principal axis of the system.

Due to the lack of an appropriate model for the thermal damping of multi-bubble systems in nonlinear motion, thermal damping effects are neglected here. However, it should be noted that the damping coefficient of viscosity and radiation damping combined is 0.029 for a single bubble at this size. The total single-bubble damping coefficient δ_{tot} in the previous section was 0.027 (see Fig. 4.11), and thus the damping of the relevant linearized systems is comparable. The minimum damping coefficient δ_{min} calculated for this geometry by the method given in the previous section with the C3 approximation is 0.01, and therefore the system is expected to remain stable.

A solution to the Hamiltonian equations of motion for the bubbles in an compressible liquid with the C2 approximation for compressibility, Eqs. (2.62) and (2.79), and the C3 approximation for compressibility, Eqs. (2.24) and (2.78b), are obtained by numerical integration using the delay differential equation numerical integration package RADAR5[74,75] (see Appendix B).

The average radial displacement R_{disp} given by Eq. (3.5), normalized by the equilibrium bubble radius, is shown in Fig. 4.12. The normalized average radial displacement has values near $0.5R_0$, which indicates that the nonlinear equations of motion are required. The predictions of two different models are shown, the C2 approximation for liquid compressibility effects (blue curve) and the C3 approximation (green curve). The response predicted by the two models is dramatically

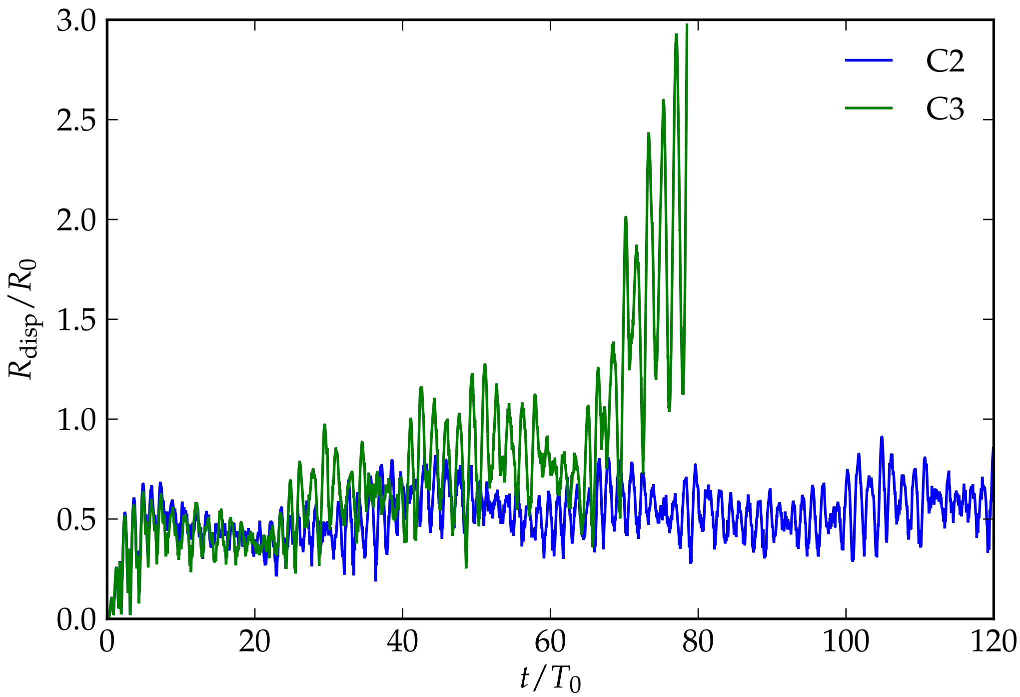

Figure 4.12: Normalized average radial displacement for a cluster of 20 bubbles randomly placed in an ellipsoid, subjected to a 0.04 MPa single-cycle pulse at 173 kHz. Two different models are shown, the C2 approximation for compressibility effects (blue) and the C3 approximation (green). All cases include liquid viscosity but not thermal effects.

different. The prediction of the C2 model remains stable, but is still oscillating at the end of the simulation. The model for a compressible liquid with single-bubble radiation damping becomes unstable, and the simulation is halted near $t/T_0 = 80$ due to a bubble collision. The simulation of the C2 model cannot currently be continued due to restrictions on simulation length imposed by the super-computing facility utilized to make these computations. The computation must be parallelized in order to continue, but this work has not yet been completed.

There are two important results from this simulation. First, although the equivalent linearized system is stable, the nonlinear system is not. One hypothesis for this fact is that the effects of liquid compressibility become more important as the amplitude of the radial motion in the system increases. This increase may act to destabilize the system of equations obtained by the C3 approximation for compressibility effects even when the linearized system is stable. Second, although the C2 approximation for compressibility effects remains stable, the amplitude of the radial motion does not decrease as expected. The fact that the amplitude of the motion remains relatively large suggests that the dynamical system for this geometry may possess a limit cycle or bifurcation in the phase space.[76] It is not known if this reduction in damping for large amplitude motion is due to the artificial restriction of fixed bubbles, i.e., no translation, or if it represents a precursor to an instability due to series truncation errors. Ideally the model with the C1 approximation for compressibility effects would be studied, but a numerical version of this model has not yet been implemented.

4.3.2 Two bubbles near a wall

In an attempt to simulate systems relevant to shock-wave lithotripsy and other biomedical treatments in which bubbles undergo violent collapse in response to short pulses of high amplitude, a system of two bubbles near a rigid boundary is now considered. The geometry is shown in Fig. 4.13, where two bubbles are separated by a distance D_1 and positioned so that their common axis is normal to the wall. The bubble nearest the wall is a distance D_2 away from the wall. The system is modeled by the method of images; the rigid wall is removed and an image bubble is placed opposite each bubble. The image method is exact for rigid planar surfaces in the absence of viscosity. An image source is also included, and thus the reflection of the incident plane wave from the wall is modeled. The geometry with the images is shown in Fig. 4.14. Also shown in the figure are the two locations at which the pressure produced by the bubble system will be computed, p_L to the left of the bubbles and p_W at the wall (or in the center of the cluster including the image bubbles). Thus, the problem of two-bubbles near a rigid wall requires a simulation of four bubbles.

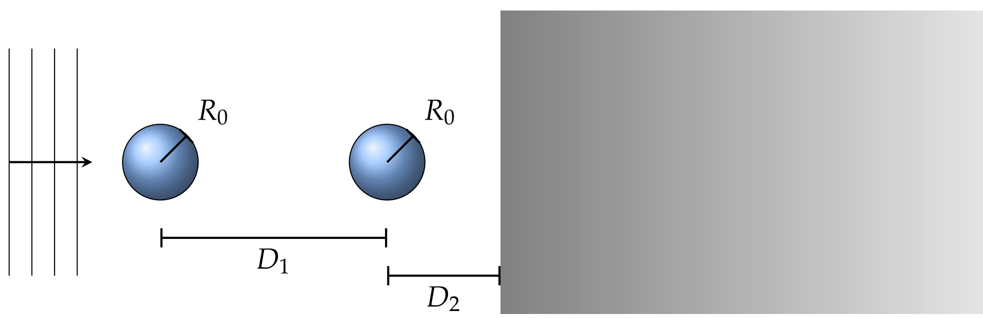

Figure 4.13: Geometry of two bubbles near a rigid wall.

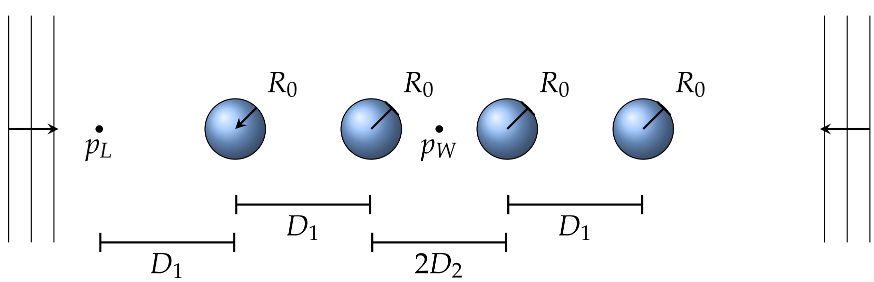

Figure 4.14: Geometry of equivalent four-bubble system with image source. Locations of the pressures compared in Fig. 4.15 are marked by p_W and p_C.

In the systems considered here, the bubbles are equally sized with an equilibrium radius of $R_0 = 10\ \mu$m and are placed so that the separation distance between each bubble is equal to D_1. Physically this means that the distance from the nearest bubble to the wall is half the distance separating the bubble furthest from the wall from the bubble nearest the wall ($D_1 = 2D_2$). The excitation is provided by an acoustic plane wave consisting of a single cycle of a sine wave which is 5.8 μs in duration (8.6 mm long), which is equal to a single cycle of a 172 kHz sine wave. The simulations are carried out for a range of pressure source amplitudes ranging from 0.01 MPa to 1.0 MPa, and a range of the separation distances D_1 from $20R_0$ to $100R_0$. The ratio of bubble separation distance D_1 to pulse length ranges from 0.02 to 0.12. With this waveform, a 1 MPa pulse can generate radial displacement in excess of $15R_0$. The effects of liquid viscosity are included in the simulations but thermal effects are neglected. Bubble translation is also neglected.

Two different models are used to simulate the system and the predicted pressures are compared. One is the C4 model for bubbles in an incompressible liquid (no delays) with single-bubble radiation damping and viscous damping. This model has been used previously to simulate high-amplitude motion of coupled bubbles.[22] This model is marked C4 here, with the suffix N to indicate that delays are neglected. The other is the C2 model for compressibility effects with viscous damping (including time delays in bubble interaction). The Hamiltonian form of each model is integrated numerically with the numerical DDE package RADAR5.

In order to compare the predictions of the two models, the percent difference between the maximum predicted pressures is calculated. This is the same method used to compare predicted pressures in Section 3.4. The percent difference is given by

$$\frac{p_{\max}^{(C2)} - p_{\max}^{(C4)}}{p_{\max}^{(C4)}} \times 100\%, \tag{4.18}$$

where $p_{\max}^{(C4)}$ is the maximum pressure predicted by the C4 model (C3 without delays) and $p_{\max}^{(C2)}$ is the maximum pressure predicted by the C2 model for compressibility effects. The results of these calculations for the full range of source pressure amplitudes and bubble separation distances is shown in Fig. 4.15. The vertical axis is the source pressure amplitude in MPa and the horizontal axis is the distance D_1 normalized by the equilibrium radius R_0. The white portion in the upper left corner of each plot represents the region of the parameter space in which the bubbles grow large enough to collide and the simulation is halted.

The results in Fig. 4.15 clearly demonstrate the importance of including the effects of liquid compressibility when simulating bubble systems. The system with C2 compressibility effects predicts pressures that range from less than half to more than twice the pressure predicted by the C4 model for bubbles in an incompressible liquid with single-bubble radiation damping. As was discussed in Section 3.4, this variation in pressure can be attributed to the variation in arrival times due to propagation delays and the increased coupling strength in the C2 model. However, the differences in the predictions are much larger for the system of two bubbles near a rigid wall considered here. If the pressure produced by the collapse of the first bubble to experience the incident pulse arrives during the rebound of the (second) bubble nearest the wall, then the rebound can be significantly damped and the pressure radiated by the system will be reduced. Because the rebound event occurs

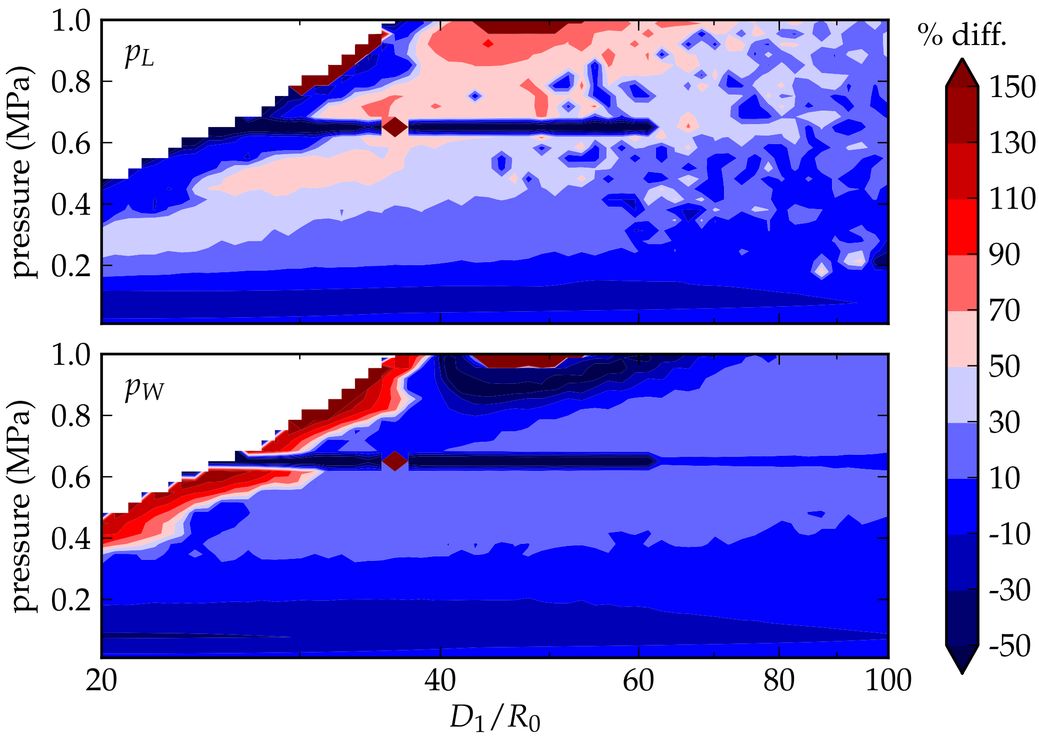

Figure 4.15: Comparison of pressure produced by two bubbles near a rigid wall as predicted by the C4 model for single-bubble radiation damping without delays and the C2 model for a compressible medium. The percent difference between the two maximum pressure predictions at two locations is shown. The top plot shows the percent difference a distance D_1 behind the bubble farthest from the wall. The bottom plot shows the percent difference at the wall.

very rapidly, the regions of the parameter space in which the re-radiated pressure will be damped are narrow (dark blue in the plot). If the pressure produced by the collapse of the first bubble arrives during the collapse of the second bubble, the collapse will be accelerated and the radiated pressure can be dramatically increased (gray up to dark red in the plot). If the pulse from the first bubble arrives during the growth phase or after rebound then the outcome is uncertain. The pressure may be affected but the effect is not as strong.

4.4 Summary

In this chapter the C1, C2, and C3 approximations for liquid compressibility in a multi-bubble system were analyzed. The C1 approximation incorporates liquid compressibility in the bubble model by delaying the radiated self-acting pressure produced by a bubble by the time required to propagate from the center the bubble to the bubble wall. The C2 approximation is the result of a Taylor expansion of the delayed self-action term in the C1 approximation, and an iterative substitution is used to reduce third-order derivatives, and terms up to $O(R^2/D^2)$ and $O(1/c_0)$ are retained. The C3 approximation is similar to the C2 approximation but terms of $O(R/D)$ that are also of $O(1/c_0)$ are neglected. Thus the C3 approximation uses the single-bubble radiation damping expression.

An eigenvalue analysis of the linearized equations of motion was employed to study the stability of systems of bubbles placed randomly in a spherical cluster. The stability was determined by numerically calculating the minimum damping of any mode in the system. The C1-L approximation for compressibility was shown to produce uniformly stable systems. The C2-L and C3-L approximations produce systems that become unstable for clusters with closely spaced bubbles. Several characteristic lengths for the cluster were considered and it was shown that the minimum separation distance between bubbles in the cluster correlated most strongly with system stability. In undamped systems with only compressibility effects, the C2-L approximation is consistently stable for minimum separation distances greater than $10R_0$. This is consistent with the accuracy of the iterative expansion used to obtain the C2 approximation. On the other hand, the C3-L approximation is stable only for systems with minimum separation distances greater than $50R_0$.

An eigenvalue analysis was also used to study the behavior of systems with viscous and thermal damping. Systems consisting of a line of equally spaced, equally sized bubbles were analyzed. Although the inclusion of viscous and thermal damping mitigates the instability of systems with the C3-L approximation, the C2-L approximation still produces more stable systems that agree with the results of the C1-L approximation. The results from analysis of bubble arrays were compared to the work of Doinikov et al.[46] and Ooi et al.[47] Differences between the current work and previous work are attributed to the fact that the previous work reported a reduced damping coefficient, but not necessarily the minimum damping coefficient. This discrepancy results from the transcendental nature of the characteristic equation of a system with delays in bubble interaction. Systems consisting of clusters of equally sized bubbles were analyzed with the inclusion of viscous and thermal effects. It was found that cluster systems exhibit behavior similar to line arrays, with similar stability properties and trends. These results suggest that it is necessary to use either the C1 or C2 approximations to simulate multi-bubble dynamics. The C2 approximation should only be used if the minimum separation distance is greater than $\sim 10R_0$.

Simulations of bubble motion produced by the models with the C2 and C3 approximations were compared for a system of 20 bubbles placed randomly in an ellipse responding to an external pulse. The C3 model became unstable. The C2 model remained stable, but exhibited no observable damping. It is not known if this lack of damping is a result of truncation error in the series expansion used to obtain the C2 approximation or if this is a physical property of the system. Resolution of this question requires simulations using the C1 approximation, which has not been implemented for numerical integration.

Finally, a model for bubbles in a incompressible liquid with single-bubble radiation damping (C4), and a model based on the C2 approximation, were used to predict the pressure produced by a pair of bubbles near a rigid wall in response to external forcing for a range of source pressure amplitudes and bubble spacings. The inclusion of compressibility effects by the C2 approximation can either increase or decrease the predicted pressure relative to the predictions of the C4 model. The pressure was reduced by as much as half in some cases and increased by as much as a factor of 2 in other cases. Thus the results were similar to those for the forced two-bubble system considered in Section 3.4 but more dramatic. The results of this chapter illustrate the importance of correctly including compressibility effects in simulations of multi-bubble systems.

Chapter 5

Approximations of Time Delays and Delay Differential Equations for Bubble Systems in a Compressible Liquid

Numerical integration of delay differential equations (DDEs) is computationally intensive. Hence, the number of bubbles that can be included in a simulation is limited. Two approximate methods to facilitate numerical solution of the delayed equations of motion in order to increase the number of bubbles that may be simulated are presented here. The first method produces approximate expressions for the implicitly defined delays given in Section 2.2.3. The second method converts the delayed equations of motion given in Eq. (2.62) from a system of DDEs to a system of approximately equivalent ordinary differential equations (ODEs). In both cases the method used to obtain the approximations is similar to the method by which the C2 approximation is obtained from the C1 approximation, that is, delayed variables are expanded in a Taylor series for small delays.

5.1 Approximations for implicitly defined delays

The expressions for the delays given in Eqs. (2.36)–(2.38) represent implicit definitions of the interaction delays. In order to solve the equations of motion numerically, these implicit expressions must also be solved to find the appropriate delays. Appendix B describes a method by which certain numerical solvers may be used to include implicit delay expressions, but for small delays a first-order Taylor expansion is sufficient.[53,77]

Our approach is identical to the method used in Section 2.3 to convert the delayed self-action of a bubble into a delay-free, approximate expression involving derivatives of the original expression. Only the center-to-center delay given by Eq. (2.39) will be considered here.

Two-bubble interactions

For the two-bubble interaction terms, the implicit definition of the delay is given by Eq. (2.39),

$$\tau_{ij} = \frac{1}{c_0}\left(\left|[\mathbf{X}_j]_{\tau_{ij}} - \mathbf{X}_i\right|\right). \tag{5.1}$$

For small values of τ_{ij} the delayed variables can be expanded in a Taylor series as follows:

$$\begin{aligned}[\mathbf{X}_j]_{\tau_{ij}} &= \mathbf{X}_j(t - \tau_{ij}) \\ &\approx \mathbf{X}_j - \tau_{ij}\dot{\mathbf{X}}_j.\end{aligned} \tag{5.2}$$

These approximations are substituted into the equation for the delay to obtain

$$\tau_{ij} = \frac{1}{c_0}\left[|\mathbf{X}_j - \mathbf{X}_i| - \tau_{ij}\left(\dot{\mathbf{X}}_j \cdot \mathbf{n}_{ij}\right)\right], \tag{5.3}$$

which can be solved to find an approximate explicit expression for τ_{ij},

$$\tau_{ij} = \frac{\left|\mathbf{X}_j - \mathbf{X}_i\right|}{c_0 + \dot{\mathbf{X}}_j \cdot \mathbf{n}_{ij}}. \tag{5.4}$$

Eq. (5.4) is only valid for small values of τ_{ij} and when $(\dot{\mathbf{X}}_j \cdot \mathbf{n}_{ij})/c_0$ is small. Comparison of Eq. (5.4) and Eq. (2.38) reveals that Eq. (2.38) may be a suitable approximation for Eq. (5.4) in systems with low translational velocities.

Three-bubble interactions

For three-bubble interactions the delay is given implicitly by Eq. (2.61),

$$\tau_{ijk} = \frac{1}{c_0}\left\{\left|[\mathbf{X}_j]_{\tau_{ij}} - \mathbf{X}_i\right| + \left|[\mathbf{X}_k]_{\tau_{ijk}} - [\mathbf{X}_j]_{\tau_{ij}}\right|\right\}, \tag{5.5}$$

where $\tau_{ijk} = \tau_{ij} + \tau_{jk}$. The approximate versions of the delayed quantities obtained by Taylor expansion are

$$\begin{aligned}[\mathbf{X}_j]_{\tau_{ij}} &= \mathbf{X}_j(t - \tau_{ij}) \\ &\approx \mathbf{X}_j - \tau_{ij}\dot{\mathbf{X}}_j, \qquad (5.6\text{a}) \\ [\mathbf{X}_k]_{\tau_{ijk}} &= \mathbf{X}_j(t - \tau_{ijk}) \\ &\approx \mathbf{X}_k - \tau_{ijk}\dot{\mathbf{X}}_k. \qquad (5.6\text{b})\end{aligned}$$

These approximations can be substituted into Eq. (5.5) to obtain an approximate expression for the three-bubble delay,

$$\tau_{ijk} = \frac{1}{c_0}\left[\left|\mathbf{X}_j - \mathbf{X}_i\right| - 2\tau_{ij}\dot{\mathbf{X}}_j \cdot \mathbf{n}_{ij} + \left|\mathbf{X}_k - \mathbf{X}_j\right| - \tau_{ijk}\dot{\mathbf{X}}_k \cdot \mathbf{n}_{jk}\right], \tag{5.7}$$

where τ_{ij} is given by Eq. (5.4). This equation may now be solved to obtain an approximate explicit expression for τ_{ijk}:

$$\tau_{ijk} = \frac{|\mathbf{X}_j - \mathbf{X}_i| + |\mathbf{X}_k - \mathbf{X}_j| - 2\tau_{ij}\left(\dot{\mathbf{X}}_j \cdot \mathbf{n}_{ij}\right)}{c_0 + \dot{\mathbf{X}}_k \cdot \mathbf{n}_{jk}}. \tag{5.8}$$

Eq. (5.8) is the approximate, explicit expression for the three-bubble interaction delay for center-to-center delays that is used in place of Eq. (5.7).

The approximate Eqs. (5.4) and (5.8) are not suitable for use in the Hamiltonian equations of motion due to the time derivatives of generalized coordinates that appear on their right-hand sides. It is necessary to eliminate these derivatives before integrating the system numerically. One possible approach is to use the analytical expressions for $\dot{\mathbf{X}}_i$ given in Eq. (2.24) given for an incompressible medium to provide an approximate answer; another approach that provides superior results is presented in the following section.

5.2 Approximation of delay differential equations by Taylor expansion

For systems with small delays it is often possible to convert a system of DDEs to a system of ODEs. The mathematical motivation for this method is provided by Chicone.[77] The method follows the same approach as in Sections 2.3 and 5.1. A Taylor expansion of a delayed function for small values of the delays is used to remove the delays from the system of equations. The delayed coordinates and momenta for two-bubble interactions are expanded as

$$[R_j]_{\tau_{ij}} \approx R_j - \tau_{ij}\dot{R}_j, \tag{5.9a}$$

$$[G_j]_{\tau_{ij}} \approx G_j - \tau_{ij}\dot{G}_j, \tag{5.9b}$$

$$[\mathbf{X}_j]_{\tau_{ij}} \approx \mathbf{X}_j - \tau_{ij}\dot{\mathbf{X}}_j, \tag{5.9c}$$

$$[\mathbf{M}_j]_{\tau_{ij}} \approx \mathbf{M}_j - \tau_{ij}\dot{\mathbf{M}}_j. \tag{5.9d}$$

The approximate expressions for delayed variables in the three-bubble interactions are

$$[R_k]_{\tau_{ijk}} \approx R_k - \tau_{ijk}\dot{R}_k, \tag{5.10a}$$

$$[G_k]_{\tau_{ijk}} \approx G_k - \tau_{ijk}\dot{G}_k, \tag{5.10b}$$

$$[\mathbf{X}_k]_{\tau_{ijk}} \approx \mathbf{X}_k - \tau_{ijk}\dot{\mathbf{X}}_k, \tag{5.10c}$$

$$[\mathbf{M}_k]_{\tau_{ijk}} \approx \mathbf{M}_k - \tau_{ijk}\dot{\mathbf{M}}_k. \tag{5.10d}$$

Substitution of these approximations into Eq. (2.62) results in a system of equations in which derivatives of the coordinates appear on both sides of the equation. The result of this substitution for the radial equation of motion without translation is

$$\dot{R}_i = \frac{1}{4\pi\rho_0}\left[\frac{G_i}{R_i^3} - \sum_{j\neq i}\frac{(G_j - \tau_{ij}\dot{G}_j)}{R_i(R_j - \tau_{ij}\dot{R}_j)D_{ij}} + \sum_{k\neq i,j}\frac{(R_k - \tau_{ijk}\dot{R}_k)(G_j - \tau_{ij}\dot{G}_j)}{R_i(R_j - \tau_{ij}\dot{R}_j)D_{ik}D_{jk}}\right]. \tag{5.11}$$

The results for the other equations are similar. These equations are non-separable, and therefore they cannot be written in a form that is amenable to numerical integration with standard tools.

In order to numerically solve the equations of motion containing approximate delays it is necessary to write them in a form that is well posed for numerical integration. Success in obtaining approximate forms by iterative substitution in previous chapters (Sections 2.3, 3.3, and 4.1) motivates the use of an iterative approach here. The two relevant ordering parameters for the problem at hand are the ratio of bubble radius to separation distance R/D for bubble coupling, and the inverse of the small-signal acoustic sound speed $1/c_0$ for effects of liquid compressibility.

The equations presented in this work contain bubble interaction terms accurate up to $O(R^2/D^2)$ and compressibility effects accurate to $O(1/c_0)$. It is thus sufficient to seek approximations valid to the same order.

It is possible to iteratively substitute the right-hand sides of the approximate equations of motion for the derivatives while retaining terms of the desired order in R/D and $1/c_0$. This process is extremely tedious, and while it can be carried out by means of a computer algebra system it must be repeated for every modification to the model which results in an explosion of terms. A more efficient approach can be used to generate solutions accurate to the same order.

To motivate this approach, consider that in order to be integrated numerically by standard methods, a system of first-order differential equations with state vector $\mathbf{y}$ must be written in the following notation:

$$\dot{\mathbf{y}} = F(t, \mathbf{y}), \tag{5.12}$$

where F is a function of a vector that returns a vector of the same dimension as $\mathbf{y}$. The equations of motion for a system of bubbles in an incompressible medium (Eq. (2.24)) can be written in this form. A system of first-order, regular, delay differential equations requires delayed values of the state vector as input, and thus must be written in the form

$$\dot{\mathbf{y}} = F^{(d)}[t, \mathbf{y}, \mathbf{y}(\boldsymbol{\alpha})], \tag{5.13}$$

where $\mathbf{y}(\boldsymbol{\alpha})$ represents the state vector evaluated at the times in the vector $\boldsymbol{\alpha} = [t - \tau_{12}, t - \tau_{13}, \cdots]^{\mathrm{T}}$ to provide the required delayed values. The delayed Hamiltonian equations of motion for a system of bubbles in a compressible medium, Eq. (2.62), can be written in the same form.

Rather than pursuing a system of equations with the form of Eq. (5.12) by analytical iteration, an alternate approach is to write the approximation of Eq. (5.13) as a system of equations with an approximate function that requires the state vector and its derivative as inputs,

$$\dot{\mathbf{y}} = F^{(a)}(t, \mathbf{y}, \dot{\mathbf{y}}). \tag{5.14}$$

If the derivative of the state vector $\dot{\mathbf{y}}$ can be approximated to the same order as the approximation used in $F^{(a)}$, then this result can be used as an input to the approximate function $F^{(a)}$ on the right-hand side of Eq. (5.14). It is possible to generate a state vector that satisfies this requirement by means of an iterative computation, rather than by an iterative algebraic substitution. Let $\dot{\mathbf{y}}^{(0)} = F(t, \mathbf{y})$ and let $\dot{\mathbf{y}}^{(n)}$ represent the nth application of the map $F^{(a)}(t, \mathbf{y}, \cdot)$ to $\dot{\mathbf{y}}^{(0)}$, that is,

$$\dot{\mathbf{y}}^{(1)} = F^{(a)}(t, \mathbf{y}, \dot{\mathbf{y}}^{(0)}), \tag{5.15}$$

$$\begin{aligned} \dot{\mathbf{y}}^{(2)} &= F^{(a)}(t, \mathbf{y}, \dot{\mathbf{y}}^{(1)}) \\ &= F^{(a)}\left[t, \mathbf{y}, F^{(a)}(t, \mathbf{y}, \dot{\mathbf{y}}^{(0)})\right]. \end{aligned} \tag{5.16}$$

If the function $F^{(a)}$ is valid to mth order in some parameter χ, then $\dot{\mathbf{y}}^{(m)}$ represents an approximation to $\dot{\mathbf{y}}$ valid to the same order in χ.

Now consider the approximation of the delay differential equations of motion for a system of bubbles. In the approximate form of the equations of motion for the delayed bubble system, the function $F^{(a)}$ is found by substituting the approximations for the delayed variables given in Eqs. (5.9) and (5.10) into Eq. (2.62). The result is valid to $O(R^2/D^2)$ and $O(1/c_0)$, and thus two iterations to calculate the approximate state vector are required to obtain

$$\dot{\mathbf{y}} = F^{(a)}(t, \mathbf{y}, \dot{\mathbf{y}}^{(2)}), \tag{5.17}$$

which may be used to calculate the required derivative of the state vector for numerical integration. The result is valid to the same order as the approximate function $F^{(a)}$.

The iterative approximation in Eq. (5.17) is well suited to use for numerical integration of the equations of motion and permits the use of the existing expressions without modification. The iterative method described here is also useful in evaluating the delay expressions given in Section 5.1. The time derivatives required for the right-hand side of the delay expressions may be obtained by iterative calculation using the approximate form of the Hamiltonian equations of motion. In general, the results produced by this calculation are valid to the same order as the original approximation.

A special case that must be considered is if one of the variables becomes small while simultaneously undergoing a high rate of change, because the approximation to the delayed version of the variable may approach zero or change sign. As an example, consider the approximate equation for the delayed bubble radius:

$$\begin{aligned} [R_j]_{\tau_{ij}} &= R_j(t - \tau_{ij}) \\ &\approx R_j - \tau_{ij}\dot{R}_j. \end{aligned} \tag{5.18}$$

In high-amplitude motion, the radius of a bubble becomes very small during collapse and rebound. Near the same time, the bubble wall velocity and acceleration become large. As a result, the approximations for the delayed bubble radii may approach zero or change sign. Because the delayed bubble radius appears in the denominator of terms in the equations of motion, an arbitrarily small value that may change sign for the delayed bubble radius will cause numerical integration to become unstable or to halt. This effect limits the amplitudes at which the algorithm described in this section may be used. If very large amplitude motion is expected, then the iterative substitution and expansion must be carried out to obtain equations of motion in which the denominators of terms do not approach zero. This expansion has not yet been performed.

5.3 Comparison of approximations

Here, the accuracy of the approximations presented in Sections 5.1 and 5.2 are compared to the corresponding models without approximations. Comparisons of results for the multi-bubble systems are made by integrating the equations numerically and using the metrics given in Section 3.2 to analyze the results.

The first approximation tested is that for the implicit expression of the delays in bubble-bubble interactions, Eqs. (5.4) and (5.8). This approximation was derived in Section 5.1. The geometry chosen for this approximation is a cluster of six bubbles with the same equilibrium radius of $R_0 = 20\,\mu$m placed randomly within a sphere having a radius of $15R_0$. The bubbles are excited by a two-cycle 35.5 kPa sinusoidal pulse at 173 kHz which is the resonance frequency of the bubbles. The wall-to-center delay given by Eq. (2.36) is used in this comparison. Although it was determined on physical grounds in Section 2.2.3 that this delay is not the best one for bubble interactions, it is used here because it provides a system with an implicitly defined delay. Thus the results presented here are not physically significant, but rather represent a proof of concept for the method of approximation.

The wall-to-center delay (Eq. (2.36)) is used rather than the correct center-to-center (Eq. (2.39)) delay because the definition of the center-to-center delay is implicit only in the case of translating bubbles. Including the effects of translation complicates the comparison of the two different system, thus translation is neglected here. Instead, by using the wall-to-center delay it is possible to neglect bubble translation and still test the approximation for an implicitly defined delay. The effects of liquid viscosity are included but thermal effects are neglected. The bubble system is stable with $\delta_{\mathrm{min}}/\delta_{\mathrm{tot}} = 0.18$, where δ_{tot} is the damping factor of a single bubble.

In Fig. 5.1, the model with the approximation of the delay calculated from the implicit relations is compared to the model with the exact delay for the same system. The pulse generates bubble oscillations with maxima of nearly 40% of the equilibrium radius, and thus the nonlinear equations of motion are necessary to model the response of the system. Figure 5.1(a) shows the average radial displacement of the bubbles in the system. The time along the horizontal axis is normalized by the natural period of a single bubble, T_0. The result of the calculation with the approximate delay (dashed line) agrees extremely well with the result of the calculation with the implicitly defined delay (solid line). In part (a) it is nearly

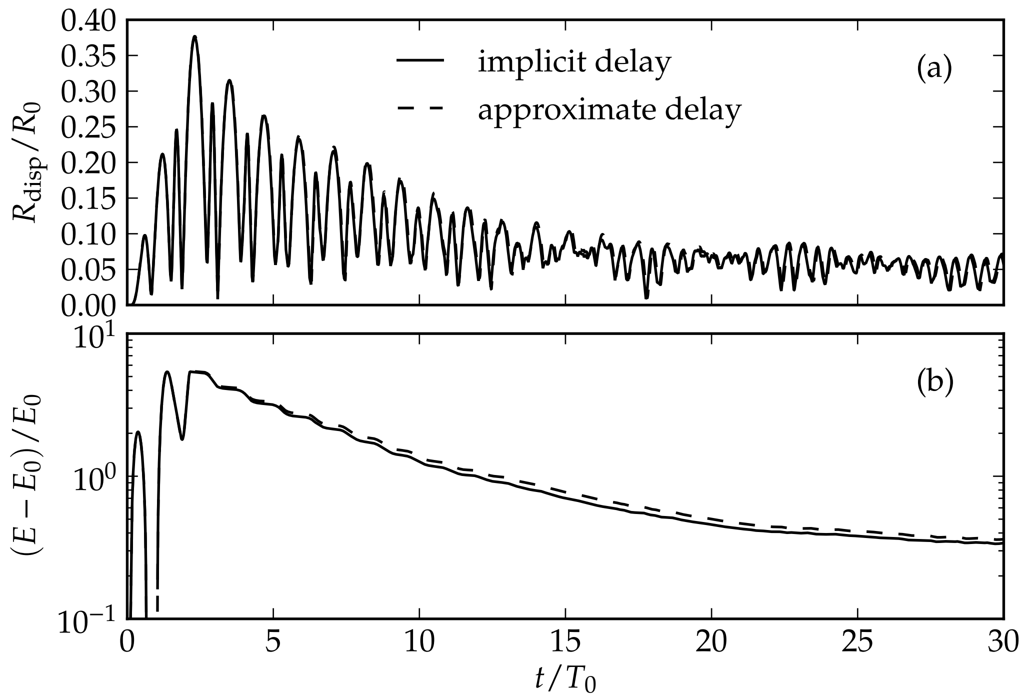

Figure 5.1: Comparison of approximate and implicit methods for calculation of bubble interaction delays. The average radial displacement normalized by the equilibrium bubble radius (a) and the total normalized energy (b) are shown for a system of six bubbles with equilibrium radii of 20 μm. The bubbles are subjected to two cycles of a 35.5 kPa sinusoidal pulse at their resonance frequency (173 kHz).

impossible to distinguish the two. Part (b) shows the normalized energy in the system calculated using Eq. (3.9), with the equilibrium energy defined in Eq. (3.10). The energy in the system with the approximate delay deviates only slightly from the energy in the system with the implicit delay. It thus follows the same trends and exhibits excellent agreement with the result produced by using the implicitly defined delays. The results suggest that the approximation for the implicitly defined delay given in Section 5.1 is adequate for general use.

In order to examine the efficacy of the approximation of the delayed variables with the results of a Taylor expansion for small delays, a system of 15 bubbles driven by an acoustic field is considered. The 15 bubbles all have an equilibrium radius of $R_0 = 10\,\mu$m and are randomly placed in a sphere with a radius of $R_{\mathrm{cl}} = 50\,R_0$. The minimum separation distance between bubbles is approximately $20R_0$ and the maximum separation distance is approximately $85R_0$. The bubbles are driven by a sinusoidal pulse with an amplitude of 15.2 kPa. The pulse consists of two cycles at 330 kHz.

The response of the bubble system is predicted using three different models, the Hamiltonian model for a system of bubbles in a compressible medium with the C2 approximation for compressibility effects given in Eqs. (2.62) and (2.82), the approximate version of the same model based on the method given in Section 5.2, and finally, the C4 model. The C4 model is for a system of bubbles in an incompressible medium where the bubbles experience single-bubble radiation damping and is obtained by combining Eqs. (2.24) and (2.78b). Viscous damping is included, and both the C2 and C4 models are stable with $\delta_{\mathrm{min}}/\delta_{\mathrm{tot}} = 0.19$. The equations for all four levels of approximation are given together in Appendix C.

The results of numerical integration of the three different models are compared in Fig. 5.2. The prediction of the approximate ODE model developed in Section 5.2 (green curve) shows good agreement with the prediction of the DDE model (blue curve), especially in comparison to the prediction of the equations of motion for bubbles in a nearly incompressible medium (red curve). The model with the approximate forms of the delayed variables experiences slightly higher

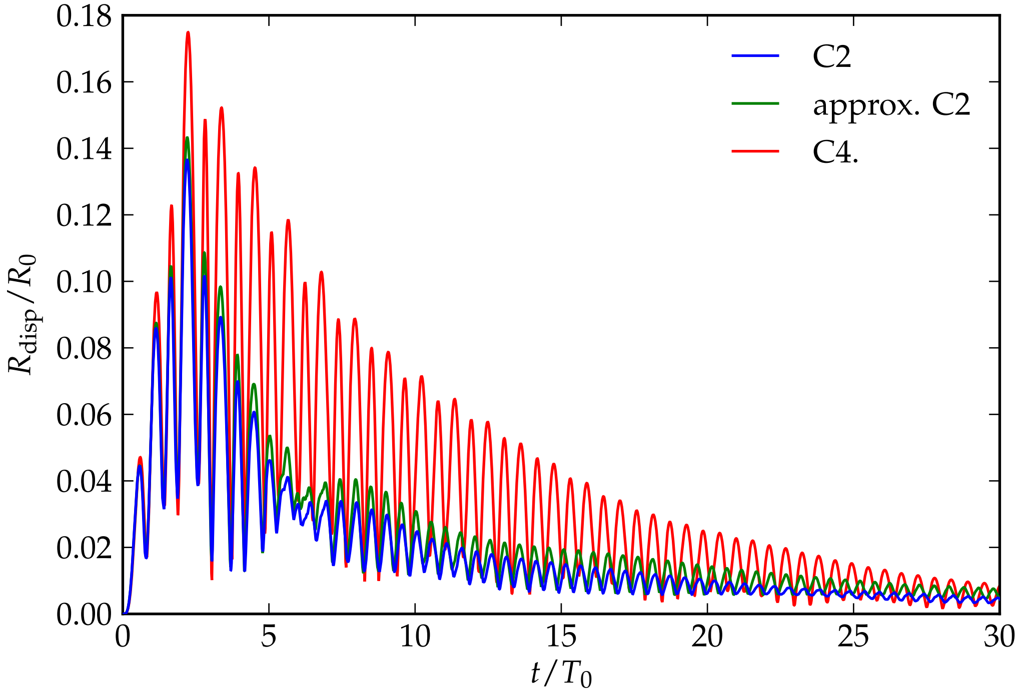

Figure 5.2: Comparison of delay differential equation model with C2 compressibility effects (C2), corresponding approximate ODE model with C2 approximations (approx. C2, and a model for an single-bubble radiation damping without delays in bubble interaction (C4). The average radial displacement is shown for a system of 15 bubbles with equilibrium radii of 10 μm subjected to two cycles of a 15.2 kPa sinusoidal pulse at 330 kHz.

amplitude motion than the DDE model, but the general amplitude and trends are similar.

The models with the C2 compressibility and either delays (blue curve) or approximated delays (green curve) appear to exhibit three distinct phases of damping. The time along the horizontal axis is normalized by the natural period of a single bubble T_0. After the incident acoustic wave has passed ($t/T_0 \approx 2$), the system enters free response. Initially, both C2 models damp much more quickly than the model for a nearly incompressible medium (red curve). This corresponds to the in-phase mode of the system, which damps much more quickly than would an equivalent single bubble. The region of increased damping ends at $t/T_0 \approx 6$. For $6 \lesssim t/T_0 \lesssim 12$ the damping of the system is reduced, becoming less than the damping of the delay-free system with the single-bubble compressibility effects shown in red. When $t/T_0 \gtrsim 12$, the system enters the third region, when the apparent damping is reduced even further. Presumably the last two damping regions correspond to the modes in which compressibility effects reduce the damping. In contrast, the system with single bubble radiation damping and no delays (red curve) experiences apparently constant damping over the time shown. Thus, in spite of the slight difference in amplitudes, the approximate C2 model captures the dominant effects present in the fully delayed model.

It should be noted that the simulation shown in Fig. 5.2 is near the greatest amplitude of radial motion that may be simulated using the approximate algorithm from Section 5.2. Higher amplitude simulations require the development of analytic expressions by means of an iterative algebraic substitution rather than the iterative computation presented here.

5.4 Summary

An approximate method to replace the implicit state-dependent delay expressions for the propagation delay in a bubble system with explicit expressions was presented. A related method to convert the system of DDEs into an approximate system of ODEs was also presented. Good agreement between these methods and the delayed system with implicitly defined delays was demonstrated for cases with low amplitude radial oscillations. Both of these approximation methods require that the system possess sufficiently small delays. The method to generate a system of ODEs that approximates the system of DDEs requires that the bubble wall velocities be sufficiently small. This requirement severely limits the use of the method in applications with large driving pressures and high bubble wall velocities. It is possible that an iterative algebraic substitution could produce a system of equations that does not suffer from this restriction, but this work has not been undertaken here.

Chapter 6

Summary and Future Work

The work presented in this dissertation was undertaken to develop and implement an accurate model to predict the high-amplitude radial motion of clusters of bubbles in a compressible liquid. Liquid compressibility introduces two dominant effects that must be included in a model. The first effect is commonly referred to as radiation damping. This is the damping of radial bubble motion due to energy lost to acoustic radiation into the liquid surrounding a bubble. The second effect is the delay in bubble interaction due to the time required for a pressure wave to travel from one bubble to the other. It is common to include the radiation damping experienced by a single bubble but neglect the interaction delays. The majority of previous work has focused on bubbles in an incompressible or an incompressible liquid with single-bubble radiation damping. The effects of liquid compressibility are expected to be most noticeable in extensive clusters, and in systems undergoing high-amplitude radial motion, but the work presented here suggests that treating even small bubble systems with a model for a truly incompressible liquid or an incompressible liquid but with single-bubble radiation damping taken into account is insufficient. Thus corrections for the effects of liquid compressibility must be included.

Three different levels of approximations for the effects of liquid compressibility were presented here. The first method, based on the work of Ilinskii and Zabolotskaya,[24] incorporated compressibility effects by delaying the radiated self-acting pressure produced by a bubble by the time required to propagate from the center of the bubble to the bubble wall. This method was labeled C1 to distinguish it from the other methods. The C1 method relies on the assumption that the bubble radius is much smaller than the acoustic wavelength in the surrounding medium, a standard and valid assumption for cavitation.

The second method is also based on the work of Ilinskii and Zabolotskaya.[24] The delayed self-acting pressure of the C1 approximation is expanded to first order in a Taylor series to eliminate the delay. The resulting equations of motion are iteratively substituted into themselves to eliminate the third-order derivatives produced by the Taylor expansion, and terms up to $O(R^2/D^2)$ and $O(1/c_0)$ are retained. This method is labeled C2. The C2 approximation requires the same assumption as the C1 approximation, that the bubble radius be much smaller than the acoustic wavelength in the surrounding medium.

The third method uses the same iterative approach employed in the C2 approximation to eliminate third-order derivatives, but terms of $O(1/c_0)$ that are also $O(R/D)$ are neglected. This is equivalent to assuming that the interaction of the bubbles does not affect the radiation damping and hence the single-bubble radiation damping expression can be used. This is the approach that has been used in previous work,[38–40,44,46,47,51] as was discussed in Sections 2.3.2 and 3.3.

The work presented here represents the first full implementation of the nonlinear delay differential equations of motion for a system with multiple bubbles using an integrator for delay differential equations. The numerical model was based on the equations of motion developed using a Hamiltonian formalism by Ilinskii et al,[23] which were extended to include the effects of compressibility using the C2 approximation. The number of bubbles that can be simulated is limited by the fact that the numerical integration of DDEs is a computationally intensive process, and the number of interactions that must be calculated scales as N^3. This restricts the number of bubbles that may simulated using the full time-delayed model to $\sim$30 bubbles.

Chapter 2 described the Hamiltonian model for a coupled bubble system and presented modifications to this model to include the effects of liquid compressibility. The primary modification was the inclusion of propagation delay in the bubble self-action and in bubble-bubble interactions. This modification converted the equations of motion from a system of ordinary differential equations to a system of delay differential equations. All previous work on delay differential equations for bubble systems has employed Lagrangian models, and the benefits of using a Hamiltonian formalism for delay differential equations were considered. Four different delay types that have been used previously were presented, and physical justification for choosing the delay associated with propagation between bubble centers was given. The three-bubble interaction terms present in the Hamiltonian model were analyzed and the necessary delay expressions were found. Instead of following the common assumption that bubble interactions do not affect radiation damping, expressions for the radiation damping in a system of interacting bubbles were derived to first order in $1/c_0$ and second order in R/D through an iterative substitution of the Hamiltonian equations of motion. These corrections are labeled C2 in this work. The approximation of using the single-bubble radiation damping in a system coupled bubbles, motivated by the assumption that bubble interactions do no affect radiation damping, was labeled C3. It has also previously been assumed that, because the speed of sound in water is high, and the time delays for closely spaced bubbles are small, the time delays in bubble interaction can be neglected.[78,79] the approximation in which time delays are neglected, and the single-bubble radiation damping is employed, are labeled C4. The equations of motion produced by the four levels of approximation (C1, C2, C3, and C4; see Table 2.1) are collected in Appendix C.

In Chapter 3, the motion of a single bubble in a compressible medium predicted by the C2 and C3 approximations of Hamiltonian equations of motion developed in Section 2.3.1 was compared to the predictions of a Keller-Miksis model.[26,29] The C2 and C3 models for single bubble systems are identical, but differences between the two arise in systems containing multiple bubbles. The predictions of the Keller-Miksis equation agree with the results of the Hamiltonian equations to within numerical precision. The standard linear equations of motion for a system of coupled bubbles were modified to include the effect of liquid compressibility. The effects of viscous and thermal damping were neglected. The new equations were used to generate linear expressions analogous to the corrections for bubble coupling in a compressible liquid presented in Section 2.3.2. The three levels of approximation were labeled C1, C2, and C3. The linearized versions of these approximations were marked with an L, i.e., C1-L, C2-L, C3-L. The C3(-L) model has been used in previous work on coupled bubbles in a compressible medium.[38–40,44,46,47] The eigenvalue analysis of the C3-L model revealed that the model is unstable for pairs of bubbles separated by less than $\sim 50R_0$. The results of numerical integration of the time-delay, C2 Hamiltonian model for low-amplitude motion were compared to the C1-L model and good agreement was obtained, the primary difference being the slight increase in the damping of closely spaced bubbles predicted by the numerical implementation of the Hamiltonian model. The predictions of numerical integration of the Hamiltonian equations of motion with the C2 approximation were compared to the predictions of the Hamiltonian equations of motion with the delay-free C3 approximation The delay-free C3 model is labeled C4. Finally, simulations of a forced two-bubble system with both the C2 model and the C3 model without delays revealed that the inclusion of compressibility effects significantly changes the radiated field produced by the bubble system.

Chapter 4 extended the analysis presented in Chapter 3 to systems containing more than 2 bubbles. An eigenvalue analysis of the stability of the linearized versions of the equations of motion generated by the three methods for including compressibility effects in multi-bubble systems was conducted by calculating the minimum damping coefficient in the system. A large number of randomly generated spherical bubble systems was considered. The stability of the bubble systems was shown to be most correlated with the minimum separation distance between bubbles in the cluster. A statistical analysis of the results showed that without damping, the C1 approximation for compressibility effects produces stable systems, and the C2 approximation produces systems that are unstable for systems in which bubbles have a minimum spacing less than ~$10R_0$. In contrast, in some cases the C3 approximation produces systems that are unstable despite having a minimum spacing greater than $40R_0$.

The stability of systems with viscous and thermal damping was also considered for systems consisting of a line array of bubbles, and bubbles randomly placed in a sphere. It was shown that the addition of thermal and viscous damping improved the stability of both the C2 and the C3 systems, as expected, with C3 systems remaining stable for most systems with a minimum separation distance greater than ~$6R_0$. The minimum damping is almost completely dominated by the viscous and thermal damping, although the inclusion of compressibility effects dramatically reduces the damping. The results of the eigenvalue analysis of damped systems was compared to previous work[46,47,54] with similar results, the slight differences being attributed to the differences in methods used to calculate the eigenvalues. Although the analysis of minimum damping coefficients does not reveal significant differences between the three approximations for including compressibility effects, this does not necessarily imply that there is no difference in the dynamics of systems considered. An expanded analysis of the eigenvalues of the transcendental characteristic equations is required to ascertain the total effect of liquid compressibility on system dynamics. This analysis has not yet been conducted.

The response of bubble systems to an external pressure source was also considered in Chapter 4. Numerical integration was used to compare the response of the same bubble geometry calculated using the C2 and C3 approximations. The randomly generated system of bubbles of equal size ($R_0 = 20\,\mu$m) was driven by a single cycle of a sine wave at 173 kHz with an amplitude of 35.5 kPa. Viscous effects where included but not thermal effects. The system with C3 compressibility effects was unstable, while the system with C2 compressibility remained stable. Although the C2 system remains stable, it does not exhibit significant damping. It is not known if this is a physical feature of the system or an artifact of the series expansion used to obtain the C2 approximation from the C1 method for including liquid compressibility. Resolution of this uncertainty requires a numerical implementation of the nonlinear C1 model which has not been completed. Finally, the pressure produced by two bubbles near a rigid wall with external forcing was predicted using the method of images. The maximum pressure was predicted at the wall and behind the bubbles. The pressures predicted by a model with C2 compressibility approximations and a model with C3 compressibility approximations without delay (nearly incompressible) were compared for a range of bubble separation distances and source pressures. Similar to the results of Section 4.3, the delays and additional coupling terms associated with the C2 approximations significantly altered the pressure produced by the system. The pressure was either increased or decreased depending on the separation distance and collapse time of the bubbles in the system. The percent difference in the predicted pressures ranges from 50% to over 200%.

Chapter 5 presented a method to obtain explicit, approximate expressions for the implicitly defined delays given in Chapter 2. Numerical integration of the equations of motion with approximate delays was compared to integration of the implicit delayed equations of motion, and there is good agreement between the two. The chapter also developed a method to convert the delay differential equations of motion for a bubble system into a set of approximate ordinary differential equations. Rather than using an iterative algebraic substitution to obtain equations of motion valid to the desired order, an iterative computation was used to generate values for the approximations of the delayed variables. Comparison of the DDE system with the approximate ODE system showed good agreement. The process used to generate the approximate ODEs requires that the bubble wall velocities be reasonably small. Both approximations are limited by a requirement that the delays within the system be small. Unfortunately, the necessary assumptions underlying the approximation for converting the equations of motion from DDEs to ODEs limits the utility in the high-amplitude bubble motion typical of therapeutic ultrasound applications.

Additionally, four appendices have been included. Appendix A presents the method by which implicitly defined delays may be included in numerical integration of DDEs, as well as presenting the motivation for choosing the numerical tools used in this work. Appendix B discusses scaling constants and other considerations for nondimensionalization of the model equations of motion. The expressions to extract the necessary terms from sums to generate the conservation relations for the kinetic energy in a system of coupled bubbles are also given. The equations of motion produced by the four approximations for the effects of liquid compressibility are collected in Appendix C. In Appendix D, the method for modeling bubble coalescence proposed by Ilinskii et al.[50] is modified to conserve energy and mass in the system, and rewritten in terms of the Hamiltonian coordinates and momenta.

Future work will benefit from an implementation of the C1 model equations of motion, which fully account for compressibility effects. A more detailed analysis of the C2 approximations is also required. It is necessary to consider the relative importance of the terms in order to determine if the long expressions given in Section 2.3.2 may be truncated. In order to accurately consider translation effects in high-amplitude motion it is necessary to extend the C2 corrections for liquid compressibility to second order in $1/c_0$. It may be possible to apply a method similar to the C1 approximation to the equations of motion for a translating bubble. This is analogous to the Liénard-Wiechert potentials for a moving charge.[80]

It is necessary to find additional experimental results that can be used to corroborate the importance of compressibility effects implied by the results of this work. Some studies that could possibly be simulated with the model developed here are the work of Bremond et al.[78], and Leroy et al.[41]

Simulation of large systems of bubbles in high-amplitude motion will require the development of suitable ODE approximations to the DDE model presented here. In order to convert the delay differential equations of motion to approximate ODEs an analytic expansion of the approximate time delays by computer algebra system should be performed. Numerical integration of the resulting equations of motion should be compared to the results of the delay differential equations of motion for high amplitude oscillations. It may be possible to use the approximate ODEs to develop a model in which a large cluster is divided into subclusters, with the approximate ODEs being used to model bubble dynamics in each subcluster and the interaction between subclusters being delayed appropriately. This approach may be useful for including the effects of liquid compressibility in large clusters of bubbles.

Appendix A

Nondimensionalization Parameters and Manipulation of Sums

A.1 Nondimensionalization parameters

The nondimensionalization begins by choosing a reference, or scaling, length L_0. Typically the scaling length is chosen to be the characteristic equilibrium radius of bubbles in the system being modeled. Leighton[55] presents the natural frequency of the linearized equation for a single bubble as

$$\omega_0 = \frac{1}{R_0}\sqrt{3\gamma\frac{P_0}{\rho_0} + (3\gamma - 1)\frac{2\sigma}{\rho_0 R_0} - (3\gamma - 1)P_v - \frac{4\eta^2}{\rho_0^2 R_0^2}}. \tag{A.1}$$

If the chosen scaling length corresponds to a characteristic bubble radius then it is appropriate to set the scaling time to the duration of the natural period of a single bubble with the characteristic equilibrium radius. The natural frequency is used to define the scaling time by setting $R_0 = L_0$ in the equation above and defining $T_0 = 2\pi/\omega_0$. Thus, the nondimensional time $\tilde{t}$ is given by $\tilde{t} = t/T_0$. With these definitions, the generalized coordinates of the bubble model (upper-case) and derived quantities may be related to their nondimensional counterparts (lower-case) as follows:

$$
\begin{aligned}
v_s &= \frac{L_0}{T_0} \\
&= \frac{1}{2\pi}\sqrt{3\gamma\frac{P_0}{\rho_0} + (3\gamma-1)\frac{2\sigma}{\rho_0 L_0} - (3\gamma-1)P_v - \frac{4\eta^2}{\rho_0^2 L^2}} \qquad \text{(A.2a)}
\end{aligned}
$$

$$R_{0i} = L_0 r_{0i}, \qquad \text{(A.2b)}$$

$$R_i = L_0 r_{0i} r_i, \qquad \text{(A.2c)}$$

$$G_i = 4\pi\rho L_0^3 v_s r_{0i}^4 g_i, \qquad \text{(A.2d)}$$

$$\mathbf{X}_i = L_0 \mathbf{x}_i, \qquad \text{(A.2e)}$$

$$\mathbf{M}_i = \frac{2\pi}{3} L_0^3 v_s r_{oi}^3 \mathbf{m}_i, \qquad \text{(A.2f)}$$

$$D_{ij} = L_0 d_{ij}. \qquad \text{(A.2g)}$$

A.2 Extracting indexed terms from sums

In order to obtain the correct expressions for the kinetic energy conservation relation for bubble collision presented in Appendix D it is necessary to isolate all terms which contain coordinates of the colliding bubbles. This is accomplished by means of "filter" expressions generated from Kronecker delta functions, δ_{ij}. To extract the term in which the index $i = \alpha$ from a single sum, simply multiply the summation by $\delta_{i\alpha}$ and evaluate the result:

$$\sum_{i=1}^{N} a_i \delta_{i\alpha} = a_\alpha. \qquad \text{(A.3)}$$

Finding appropriate filter expressions for multi-index sums is more complicated, especially when there are conditions on the sums. A procedure to generate the necessary discrete filters is outlined here.

Consider that $(1-\delta_{i\alpha})$ is only zero when $i = \alpha$. Multiplying a sum by $(1-\delta_{i\alpha})$, subtracting from the original sum and evaluating will remove all terms for which $i \neq \alpha$. For the single index case, this is obvious because the multiplying factor $1 - (1 - \delta_{i\alpha})$ simplifies to $\delta_{i\alpha}$, but in the multi-index case the result is not as clear.

A.2.1 Double sums

In order to isolate the terms with index α or β from a double sum subject to the indicial constraints $i \neq j$ and $\alpha \neq \beta$, consider that the expression

$$1 - (1 - \delta_{i\alpha})(1 - \delta_{i\beta})(1 - \delta_{j\alpha})(1 - \delta_{j\beta}) \tag{A.4}$$

is zero only when i or j is not equal to α or β. Expand the product and apply the conditions to the individual terms. The result is

$$1 - (1 - \delta_{i\alpha})(1 - \delta_{i\beta})(1 - \delta_{j\alpha})(1 - \delta_{j\beta}) = \delta_{i\alpha} + \delta_{i\beta} + \delta_{j\alpha} + \delta_{j\beta} - \delta_{i\alpha}\delta_{j\beta} - \delta_{i\beta}\delta_{j\alpha}. \tag{A.5}$$

To extract the terms with index α or β from a double sum, multiply the sum by

$$\delta_{i\alpha} + \delta_{i\beta} + \delta_{j\alpha} + \delta_{j\beta} - \delta_{i\alpha}\delta_{j\beta} - \delta_{i\beta}\delta_{j\alpha} \tag{A.6}$$

and evaluate the delta functions. This expression is essentially a discrete filter for the desired terms.

A.2.2 Triple index sums

A similar process can be applied to a triple sum over i, j, and k with the constraints $k \neq i, j$, $\alpha \neq \beta$. The filter expression is given by

$$
\begin{aligned}
1-(1-\delta_{i\alpha})(1-\delta_{i\beta})(1-\delta_{j\alpha})(1-\delta_{j\beta})(1-\delta_{k\alpha})(1-\delta_{k\beta}) = {} & \delta_{i\alpha}+\delta_{i\beta}+\delta_{j\alpha}+\delta_{j\beta}+\delta_{k\alpha} \\
& +\delta_{k\beta}-\delta_{i\alpha}\delta_{j\alpha}-\delta_{i\beta}\delta_{j\beta} \\
& -\delta_{i\alpha}\delta_{j\beta}-\delta_{i\beta}\delta_{j\alpha}-\delta_{i\alpha}\delta_{k\beta} \\
& -\delta_{i\beta}\delta_{k\alpha}-\delta_{j\alpha}\delta_{k\beta}-\delta_{j\beta}\delta_{k\alpha} \\
& +\delta_{i\alpha}\delta_{j\alpha}\delta_{k\beta}+\delta_{i\beta}\delta_{j\beta}\delta_{k\alpha}.
\end{aligned}
\tag{A.7}
$$

The discrete filter expressions given in this section can be used to obtain the expressions for the total kinetic energy of two bubbles in multi-bubble system given in Section D.7.

Appendix B

Delay Differential Equations

Delay differential equations (DDEs) form a rich and active area of mathematics research. Despite similarities to ordinary differential equations, the underlying theory of delay differential equations is less well developed. For certain classes of DDEs, including state-dependent neutral DDEs, general existence proofs for solutions do not yet exist. For further information on current topics in research on delay differential equations, the reader is referred to Lakshaman and Senthilkumar.[64]

Numerical integration of delay differential equations is challenging due to the need for a continuous history of the state vector. Error control is needed over the entire history, not just at discrete points. Without error control over the history, the magnitude of the error in the solution is unknown. Additional information on numerical integration of delay differential equations can be found in Bellen and Zennaro.[81]

B.1 Numerical tools for delay differential equations

Two different numerical solvers are used in this work, RADAR5 and DDE_SOLVER. Both are Fortran 90 programs developed for stiff delay differential equations with state-dependent delays, but they employ different methods and each provides unique features.

RADAR5[74,75] uses a collocation method based on a Radau IIA method to provide continuous interpolated output of the solution.[81] The solver accepts input with a singular mass matrix on the right-hand side of the differential equation and thus permits the use of the method given in the next section to solve singular equations to find the implicitly defined delays. RADAR5 can be used to solve neutral DDEs. However, it does not provide root-finding capabilities and thus cannot be used in problems involving colliding bubbles. Additionally, the interface is somewhat archaic.

DDE_SOLVER[82] was designed to provide a simpler DDE solver with a modern interface. It provides root-finding capabilities, and therefore it is useful in solving colliding bubble problems. However, DDE_SOLVER cannot solve singular equations and thus it cannot be used to calculate the implicitly defined delays. Instead, the approximate expressions for the delays given in Section 5.1 must be used.

B.2 State-dependent delay differential equations

B.2.1 Solving for implicitly defined delays

If a DDE solver capable of solving neutral DDEs, such as RADAR5, is used, the implicitly defined delays may be obtained simultaneously with the solution by augmenting the system with a set of singular equations for the delays.[53,81]

It is common to write systems of DDEs in the form

$$\mathbf{M}\dot{\mathbf{y}} = f\left\{t, \mathbf{y}(t), \mathbf{y}[\alpha_1(t)], \ldots, \mathbf{y}\left[\alpha_N(t)\right]\right\}, \tag{B.1}$$

where $\boldsymbol{\alpha}(t)$ is the vector of delayed times, and $\mathbf{M}$ is a (possibly singular) matrix. If the numerical solver allows problems where $\mathbf{M}$ is singular, then it is possible to represent both neutral DDEs and singular equations. As an example, consider the Hamiltonian formulation for a system of two coupled bubbles without translation. The equations of motion for this system may be written in the notation of Eq. (B.1) as

$$\begin{bmatrix} 1 & 0 & 0 & 0 \\ 0 & 1 & 0 & 0 \\ 0 & 0 & 1 & 0 \\ 0 & 0 & 0 & 1 \end{bmatrix} \begin{bmatrix} \dot{R}_1 \\ \dot{R}_2 \\ \dot{G}_1 \\ \dot{G}_2 \end{bmatrix} = \begin{bmatrix} \frac{1}{4\pi\rho_0}\left(\frac{G_1}{R_1^3} - \frac{[G_2]_{\tau_{12}}}{R_1[R_2D_{12}]_{\tau_{12}}}\right) \\ \frac{1}{4\pi\rho_0}\left(\frac{G_2}{R_2^3} - \frac{[G_1]_{\tau_{21}}}{R_2[R_1D_{21}]_{\tau_{21}}}\right) \\ \frac{1}{4\pi\rho_0}\left(\frac{3}{2}\frac{G_1^2}{R_1^4} - \frac{G_1[G_2]_{\tau_{12}}}{R_1^2[R_2D_{12}]_{\tau_{12}}}\right) + 4\pi R_1^2(P_1 - P_0 - p_{e1}) \\ \frac{1}{4\pi\rho_0}\left(\frac{3}{2}\frac{G_2^2}{R_2^4} - \frac{G_2[G_1]_{\tau_{21}}}{R_2^2[R_1D_{21}]_{\tau_{21}}}\right) + 4\pi R_2^2(P_2 - P_0 - p_{e2}) \end{bmatrix}. \tag{B.2}$$

The delays τ_{12} and τ_{21} are defined implicitly by

$$\tau_{ij} = \frac{\Delta_{ij}(\tau_{ij})}{c_0}, \tag{B.3}$$

where the distance Δ_{ij} depends on which of Eqs. (2.36)–(2.38) is chosen (Eq. (2.39) was chosen on physical grounds presented in Section 2.2.3). Possible values for Δ_{ij} include

$$\Delta_{ij}(\tau_{ij}) = |\mathbf{X}_j - \mathbf{X}_i|, \tag{B.4a}$$

$$\Delta_{ij}(\tau_{ij}) = |[\mathbf{X}_j]_{\tau_{ij}} - \mathbf{X}_i|, \tag{B.4b}$$

$$\Delta_{ij}(\tau_{ij}) = |[\mathbf{X}_j]_{\tau_{ij}} - \mathbf{X}_i| - R_i - [R_j]_{\tau_{ij}}, \tag{B.4c}$$

$$\Delta_{ij}(\tau_{ij}) = |[\mathbf{X}_j]_{\tau_{ij}} - \mathbf{X}_i| - [R_j]_{\tau_{ij}}. \tag{B.4d}$$

The system given in Eq. (B.2) is augmented by the delay relations to obtain

$$\begin{bmatrix}1&0&0&0&0&0\\0&1&0&0&0&0\\0&0&1&0&0&0\\0&0&0&1&0&0\\0&0&0&0&0&0\\0&0&0&0&0&0\end{bmatrix}\begin{bmatrix}\dot{R}_1\\\dot{R}_2\\\dot{G}_1\\\dot{G}_2\\0\\0\end{bmatrix}=\begin{bmatrix}\frac{1}{4\pi\rho_0}\left(\frac{G_1}{R_1^3}-\frac{[G_2]_{\tau_{12}}}{R_1[R_2D_{12}]_{\tau_{12}}}\right)\\\frac{1}{4\pi\rho_0}\left(\frac{G_2}{R_2^3}-\frac{[G_1]_{\tau_{21}}}{R_2[R_1D_{21}]_{\tau_{21}}}\right)\\\frac{1}{4\pi\rho_0}\left(\frac{3}{2}\frac{G_1^2}{R_1^4}-\frac{G_1[G_2]_{\tau_{12}}}{R_1^2[R_2D_{12}]_{\tau_{12}}}\right)+4\pi R_1^2(P_1-P_0-p_{e1})\\\frac{1}{4\pi\rho_0}\left(\frac{3}{2}\frac{G_2^2}{R_2^4}-\frac{G_2[G_1]_{\tau_{21}}}{R_2^2[R_1D_{21}]_{\tau_{21}}}\right)+4\pi R_2^2(P_2-P_0-p_{e2})\\\tau_{12}-\frac{\Delta_{12}(\tau_{12})}{c_0}\\\tau_{21}-\frac{\Delta_{21}(\tau_{21})}{c_0}\end{bmatrix}, \quad \text{(B.5)}$$

which may be solved with an appropriate numerical solver.

This method may be adapted to multi-bubble systems. However, the number equations associated with the delays is large. For a system of N bubbles with first-order coupling in R/D there are $N(N-1)$ delays. For a system with second-order coupling there are $N^2(N-1)$ delays. Modeling second-order coupling in a system of 10 bubbles will thus require solution of 900 auxiliary equations for the implicit delays. When applicable, the method given in Section 5.1 is preferred.

Appendix C

Collection of Compressibility Approximations

For reference, the equations of motion corresponding to the four labels assigned to the different levels of approximation for liquid compressibility effects are collected here. Translation, along with viscous and thermal damping, are neglected for simplicity.

The convention for delayed variables introduced in Chapter 2 is used here, whereby $g(t-\tau) = [g]_\tau$. The C1 approximation with delayed self-action pressure and delay in bubble interaction is given in Lagrangian coordinates:

$$\text{C1:} \quad \frac{1}{R_i}\left[R_i^2\ddot{R}_i + 2R_i\left(\dot{R}_i\right)^2\right]_{\frac{R_i}{c_0}} - \frac{1}{2}\left(\dot{R}_i\right)^2 = \frac{P_i - P_0 - p_{ei}}{\rho_0} \tag{C.1}$$

$$-\sum_{i\neq j}\left[\frac{R_j}{D_{ij}}\left(R_j\ddot{R}_j + 2\dot{R}_j\right)\right]_{\tau_{ij}}. \tag{C.2}$$

The remaining nonlinear equations of motion are given in Hamiltonian coordinates. The C2 approximation, in which the delayed self-action terms are expanded in a Taylor series and the higher-order derivatives are eliminated by iterative substitution while retaining terms up to $O(1/c_0) \times O(R^2/D^2)$, is

$$\text{C2:}\quad \dot{R}_i = \frac{1}{4\pi\rho_0}\left(\frac{G_i}{R_i^3} - \sum_{j\neq i}\frac{[G_j]_{\tau_{ij}}}{R_i[R_jD_{ij}]_{\tau_{ij}}} + \sum_{j\neq i,k}\frac{[R_j]_{\tau_{ij}}[G_k]_{\tau_{ijk}}}{R_i[D_{ij}]_{\tau_{ij}}[R_kD_{jk}]_{\tau_{ijk}}}\right), \tag{C.3}$$

$$\dot{G}_i = \frac{1}{4\pi\rho_0}\left(\frac{3}{2}\frac{G_i^2}{R_i^4} - \sum_{j\neq i}\frac{G_i[G_j]_{\tau_{ij}}}{R_i^2[R_jD_{ij}]_{\tau_{ij}}} + \sum_{j\neq i,k}\frac{[R_j]_{\tau_{ij}}G_i[G_k]_{\tau_{ijk}}}{R_i^2[D_{ij}]_{\tau_{ij}}[R_kD_{jk}]_{\tau_{ijk}}}\right. \tag{C.4}$$

$$\left. - \frac{1}{2}\sum_{i\neq j,k}\frac{G_i[G_k]_{\tau_{ik}}}{[R_jD_{ij}]_{\tau_{ij}}[R_kD_{ik}]_{\tau_{ik}}}\right) \tag{C.5}$$

$$+ 4\pi R_i^2\,(P_i - P_0 - p_{ei}) + C_i^{(c,0)} + C_i^{(c,1)} + C_i^{(c,2)}. \tag{C.6}$$

The terms $C_i^{(c,n)}$ are defined in Eqs. (2.80)–(2.82). The C3 approximation, in which the delayed self-action terms are expanded in a Taylor series and the higher-order derivatives are eliminated by iterative substitution while neglecting terms of $O(1/c_0) \times O(R/D)$, leaving the single-bubble radiation damping, is

$$\text{C3:}\quad \dot{R}_i = \frac{1}{4\pi\rho_0}\left(\frac{G_i}{R_i^3} - \sum_{j\neq i}\frac{[G_j]_{\tau_{ij}}}{R_i[R_jD_{ij}]_{\tau_{ij}}} + \sum_{j\neq i,k}\frac{[R_j]_{\tau_{ij}}[G_k]_{\tau_{ijk}}}{R_i[D_{ij}]_{\tau_{ij}}[R_kD_{jk}]_{\tau_{ijk}}}\right), \tag{C.7}$$

$$\dot{G}_i = \frac{1}{4\pi\rho_0}\left(\frac{3}{2}\frac{G_i^2}{R_i^4} - \sum_{j\neq i}\frac{G_i[G_j]_{\tau_{ij}}}{R_i^2[R_jD_{ij}]_{\tau_{ij}}} + \sum_{j\neq i,k}\frac{[R_j]_{\tau_{ij}}G_i[G_k]_{\tau_{ijk}}}{R_i^2[D_{ij}]_{\tau_{ij}}[R_kD_{jk}]_{\tau_{ijk}}}\right. \tag{C.8}$$

$$\left. - \frac{1}{2}\sum_{i\neq j,k}\frac{G_i[G_k]_{\tau_{ik}}}{[R_jD_{ij}]_{\tau_{ij}}[R_kD_{ik}]_{\tau_{ik}}}\right) \tag{C.9}$$

$$+ 4\pi R_i^2\,(P_i - P_0 - p_{ei}) + C_i^{(c,0)}. \tag{C.10}$$

The C4 approximation is obtained from the C3 approximation by neglecting all delays in bubble interaction:

$$\text{C4:}\quad \dot{R}_i = \frac{1}{4\pi\rho_0}\left(\frac{G_i}{R_i^3} - \sum_{j\neq i}\frac{G_j}{R_iR_jD_{ij}} + \sum_{j\neq i,k}\frac{R_jG_k}{R_iD_{ij}R_kD_{jk}}\right), \tag{C.11}$$

$$\dot{G}_i = \frac{1}{4\pi\rho_0}\left(\frac{3}{2}\frac{G_i^2}{R_i^4} - \sum_{j\neq i}\frac{G_iG_j}{R_i^2R_jD_{ij}} + \sum_{j\neq i,k}\frac{R_jG_iG_k}{R_i^2D_{ij}R_kD_{jk}} - \frac{1}{2}\sum_{i\neq j,k}\frac{G_iG_k}{R_jD_{ij}R_kD_{ik}}\right) \tag{C.12}$$

$$+ 4\pi R_i^2\left(P_i - P_0 - p_{ei}\right) + C_i^{(c,0)}. \tag{C.13}$$

The linearized equations of motion are obtained from the Lagrangian formulations with $R_i(t) = R_{0i} + \xi_i(t)$ ($|\xi_i| \ll R_{0i}$). The equations corresponding to the four labels, C1-L, C2-L, C3-L, and C4-L, are

$$\text{C1-L:}\quad \ddot{\xi}_i(t - R_{0i}/c_0) + \omega_{0i}^2\xi_i(t) + \sum_{i\neq j}\frac{R_{0j}^2}{D_{ij}R_{0i}}\ddot{\xi}_j(t-\tau_{ij}) = -\frac{p_{ei}(t)}{R_{0i}\rho_0}, \tag{C.14}$$

$$\begin{aligned}\text{C2-L:}\quad & \ddot{\xi}_i(t) + \omega_{0i}\delta_{\mathrm{rad}}\dot{\xi}_i(t) + \omega_{0i}^2\xi_i(t) + \sum_{i\neq j}\frac{R_{0j}^2}{D_{ij}R_{0i}}\ddot{\xi}_j(t-\tau_{ij}) \\ & - \sum_{i\neq j}\frac{\omega_{0j}^2R_{0j}^2}{c_0D_{ij}}\dot{\xi}_j(t-\tau_{ij}) + \sum_{j\neq i,k}\frac{\omega_{0k}^2R_{0j}R_{0k}^2}{c_0D_{ij}D_{jk}}\dot{\xi}_k(t-\tau_{ij}-\tau_{jk}) \\ & = -\frac{p_{ei}(t)}{R_{0i}\rho_0} - \frac{1}{\rho_0c_0}\frac{\partial p_{ei}}{\partial t}(t) - \sum_{i\neq j}\frac{R_{0i}R_{0j}}{\rho_0c_0D_{ij}}\frac{\partial p_{ej}}{\partial t}(t-\tau_{ij}) \\ & + \sum_{j\neq i,k}\frac{R_{0j}R_{0k}^2}{\rho_0c_0D_{ij}D_{jk}}\frac{\partial p_{ek}}{\partial t}(t-\tau_{ij}-\tau_{jk}),\end{aligned} \tag{C.15}$$

$$\text{C3-L:}\quad \ddot{\xi}_i(t) + \omega_{0i}\delta_{i,\mathrm{rad}}\dot{\xi}_i(t) + \omega_{0i}^2\xi_i(t) + \sum_{i\neq j}\frac{R_{0j}^2}{D_{ij}R_{0i}}\ddot{\xi}_j(t-\tau_{ij}) = -\frac{p_{ei}(t)}{R_{0i}\rho_0}, \tag{C.16}$$

$$\text{C4-L:} \quad \ddot{\xi}_i(t) + \omega_{0i}\delta_{i,\mathrm{rad}}\dot{\xi}_i(t) + \omega_{0i}^2\xi_i(t) + \sum_{i\neq j}\frac{R_{0j}^2}{D_{ij}R_{0i}}\ddot{\xi}_j(t) = -\frac{p_{ei}(t)}{R_{0i}\rho_0}, \tag{C.17}$$

where δ_{rad} is the single-bubble radiation damping coefficient given by Eq. (3.37).

Appendix D

Bubble Coalescence

A model in which bubbles may collide requires a method to account for the physical process of bubble coalescence. The coalescence of bubbles is a complicated process that cannot be fully described by a spherical bubble model. During coalescence the bubbles undergo large surface deformations and can no longer be approximated as spherical. However, the actual coalescence occurs very quickly in comparison to the characteristic time scale of the bubble system,[71] and hence conservation relations are used to relate the state of the bubbles before and after the collision occurs.

D.1 Conservation relations

The utilization of conservation relations to provide a connection between the pre- and post-coalescence states of a bubble system as an approach to this problem was first considered by Ilinskii et al.[50] The conserved quantities and corresponding equations used were

$$\text{center of mass:} \quad \mathbf{X}_a V_a + \mathbf{X}_b V_b = \mathbf{X}_c V_c, \tag{D.1a}$$

$$\text{momentum:} \quad \dot{\mathbf{X}}_a V_a + \dot{\mathbf{X}}_b V_b = \dot{\mathbf{X}}_c V_c, \tag{D.1b}$$

$$\text{volume:} \quad V_a + V_b = V_c, \tag{D.1c}$$

$$\text{kinetic energy:} \quad \dot{V}_a + \dot{V}_b = \dot{V}_c, \tag{D.1d}$$

$$\text{potential energy:} \quad P_a V_a + P_b V_b = P_c V_c, \tag{D.1e}$$

where the indices a and b indicate the coalescence of bubbles a and b into bubble c. Together these five equations determine the state of the new bubble: R_c, $\dot{R}_c$, P_c, $\mathbf{X}_c$, and $\dot{\mathbf{X}}_c$. Equations (D.1a), (D.1b), and (D.1e) were chosen to maintain the center of mass, conserve translational momentum, and conserve the potential energy of the bubbles, respectively. These equations are local to the colliding bubbles. In contrast, Eqs. (D.1c) and (D.1d) were chosen to maintain continuity of the radial mass flow and conserve kinetic energy far from the bubbles, and they do not conserve energy within the bubble system nor the mass of the gas within the bubbles. For systems containing large numbers of bubbles, it is necessary to ensure that the energy and the mass in the system is conserved. Indeed, numerical problems encountered in simulations of multiple interacting and coalescing bubbles were a consequence of system energy not being conserved. To achieve the conservation requirement, a new set of conservation relations has been developed. Additionally, the old relations were defined for the second-order Lagrangian equations of motion used in Ref. 50.

The choice of Hamiltonian equations of motion here dictates that the new relations be expressed in terms of the generalized coordinates and momenta.

D.2 New conservation relations

The new relations are derived from local requirements that mass, momentum, and energy be conserved during bubble coalescence. Although this method does not ensure continuity in the flow far from the bubbles, it does provide continuity in the collective state of the bubble system that is required for numerical integration. When coalescence occurs, the center of mass, translational momentum, mass of the gas inside the bubbles, total kinetic energy in the bubble system, and potential energy in the coalescing bubbles are all conserved. It is informative to discuss how these conservation relations are implemented for the chosen Hamiltonian coordinates.

D.3 Center of mass

The conservation relation for center of mass is unchanged. However, Eq. (D.1a) requires the radius of the new bubble to determine the center of mass. An alternate expression for the center of mass of two spheres is

$$\mathbf{X}_c = \frac{R_a^3 \mathbf{X}_a + R_b^3 \mathbf{X}_b}{R_a^3 + R_b^3}. \tag{D.2}$$

Therefore, the center of mass can be calculated without knowledge of R_c.

D.4 Translational momentum

Conservation of translational momentum is expressed naturally in the generalized coordinates of the Hamiltonian because the translational momentum is the generalized momentum $\mathbf{M}_i$. Momentum conservation is guaranteed simply by requiring that

$$\mathbf{M}_a + \mathbf{M}_b = \mathbf{M}_c. \tag{D.3}$$

This requirement differs from the old momentum conservation relation by accounting for the total momentum in the system, rather than accounting for only the momentum that would be experienced by a single bubble. This difference can be significant in large systems and in systems undergoing high-amplitude motion.

D.5 Internal mass

The old conservation relations required that the volume of the coalescing bubbles be conserved, whereas in the new relation it is required that the mass inside the bubbles be conserved. The mass of the gas inside the ith bubble is

$$m_i = \rho_i V_i. \tag{D.4}$$

In order to ensure that the mass of the gas inside the bubble is conserved it is required that

$$\rho_a V_a + \rho_b V_b = \rho_c V_c, \tag{D.5}$$

where ρ_a, ρ_b, and ρ_c are the densities of the gas inside bubbles a, b, and c, respectively. In the absence of gas diffusion through the bubble surface and if the assumption of uniform pressure within the bubble holds, the density of the gas inside the bubbles may be found from the equation of state,

$$\rho = \rho_0 \left(\frac{\hat{P}}{P_0} \right)^{1/\gamma}, \tag{D.6}$$

where $\hat{P}$ is the pressure inside the bubble, which for the ith bubble is

$$\hat{P}_i = \left(P_0 + \frac{2\sigma}{R_{0i}} \right) \left(\frac{R_{0i}}{R_i} \right)^{3\gamma}. \tag{D.7}$$

The mass conservation equation is thus

$$R_{0a}^3 \left(P_0 + \frac{2\sigma}{R_{0a}} \right)^{1/\gamma} + R_{0b}^3 \left(P_0 + \frac{2\sigma}{R_{0b}} \right)^{1/\gamma} = R_{0c}^3 \left(P_0 + \frac{2\sigma}{R_{0c}} \right)^{1/\gamma}. \tag{D.8}$$

The mass equation is only a function of the equilibrium radius, but unless $\sigma = 0$ (no surface tension) it must be solved numerically.

D.6 Internal and potential energy

The potential energy $\mathcal{V}$ in the bubble system is the sum of the internal energy stored in the compression state of the gas and the energy stored by surface tension in the curvature of the bubble wall. In contrast, the old potential energy relation only accounts for the internal energy in the gas. Note the difference between the font $\mathcal{V}$ used to represent the potential energy and V used to represent the bubble volume. The combined internal and potential energy stored in a single bubble is

$$\mathcal{V}_i = \frac{\hat{P}_i V_i}{\gamma - 1} + 4\pi\sigma R_i^2 + (P_0 + p_{ei}) V_i. \tag{D.9}$$

The first term represents the internal energy of the gas inside the bubble, and $\hat{P}_i$ is the pressure inside the bubble given by Eq. (D.7). The second term is the energy stored in the bubble wall by surface tension. The third term represents the potential energy due to displacement of fluid mass and due to the primary Bjerknes force exerted by the external source p_e on the bubble (buoyancy forces are neglected). Potential energy conservation requires that

$$\mathcal{V}_a + \mathcal{V}_b = \mathcal{V}_c. \tag{D.10}$$

This equation may be solved numerically for R_c.

D.7 Kinetic energy

In order to derive an equation relating the kinetic energy in the system before and after the collision, consider the total kinetic energy in the bubble system given by Eq. (2.21),

$$\begin{aligned}\mathcal{K} = \frac{1}{4\pi\rho}\Bigg[&\frac{1}{2}\sum_i \frac{G_i^2}{R_i^3} + 3\sum_i \frac{M_i^2}{R_i^3} - \frac{1}{2}\sum_{\substack{i,j\\ i\neq j}} \frac{G_i G_j}{R_i R_k D_{ij}} + 3\sum_{\substack{i,j\\ i\neq j}} \frac{G_i\left(\mathbf{M}_j \cdot \mathbf{n}_{ij}\right)}{R_i D_{ij}^2}\\ &+ \frac{1}{2}\sum_{\substack{i,j,k\\ k\neq i,j}} \frac{R_j G_i G_k}{R_i R_k D_{ij} D_{jk}}\Bigg] + \sum_i \mathbf{M}_i \cdot \mathbf{u}_{ei}.\end{aligned} \tag{D.11}$$

When the bubbles reside in a compressible medium it is necessary to include propagation delays in the calculation of the kinetic energy as shown in Eq. (2.64). For brevity, the delays are not included in the current derivation but can easily be included. To determine the kinetic energy associated with the coalescing bubbles, rewrite the kinetic energy of the system with the terms for the pre-collision bubbles, labeled a and b, and the post-collision bubble, labeled c, stated explicitly. A method to correctly extract the required terms from the kinetic energy expression is given in Section A.2. Terms that do not contain coordinates or momenta from the coalescing bubbles are subtracted from both sides and do not appear here:

$$\frac{1}{4\pi\rho_0}\left[\frac{1}{2}\frac{G_a^2}{R_a^3}+\frac{1}{2}\frac{G_b^2}{R_b^3}+3\frac{M_a^2}{R_a^3}+3\frac{M_b^2}{R_b^3}+\frac{G_a\,G_b}{R_a\,R_b\,D_{ab}}+\frac{1}{2}\frac{R_a\,G_b^2}{R_b^2\,D_{ab}^2}+\frac{1}{2}\frac{R_b\,G_a^2}{R_a^2\,D_{ab}^2}\right.$$
$$-3\frac{G_a\mathbf{M}_b\cdot\mathbf{n}_{ab}}{R_aD_{ab}^2}-3\frac{G_b\mathbf{M}_a\cdot\mathbf{n}_{ba}}{R_bD_{ab}^2}-\sum_{\substack{i\\ i\neq a}}\frac{R_a\,G_b\,G_i}{R_b\,R_i\,D_{ab}\,D_{ai}}-\sum_{\substack{i\\ i\neq b}}\frac{R_b\,G_a\,G_i}{R_a\,R_i\,D_{ab}\,D_{bi}}$$
$$-\frac{1}{2}\sum_{\substack{i\\ i\neq a}}\frac{R_i\,G_a^2}{R_a^2\,D_{ai}^2}-\frac{1}{2}\sum_{\substack{i\\ i\neq b}}\frac{R_i\,G_b^2}{R_b^2\,D_{bi}^2}-\sum_{\substack{i\\ i\neq a,b}}\frac{R_i\,G_a\,G_b}{R_a\,R_b\,D_{ai}\,D_{bi}}-\sum_{\substack{i\\ i\neq a}}\frac{G_a\,G_i}{R_a\,R_i\,D_{ai}}$$
$$-\sum_{\substack{i\\ i\neq b}}\frac{G_b\,G_i}{R_b\,R_i\,D_{bi}}+3\sum_{\substack{i\\ i\neq a}}\frac{G_a\,\mathbf{M}_i\cdot\mathbf{n}_{ai}}{R_aD_{ai}^2}+3\sum_{\substack{i\\ i\neq b}}\frac{G_b\,\mathbf{M}_i\cdot\mathbf{n}_{bi}}{R_bD_{bi}^2}+3\sum_{\substack{i\\ i\neq a}}\frac{G_i\,\mathbf{M}_a\cdot\mathbf{n}_{ia}}{R_i\,D_{ai}^2}$$
$$+3\sum_{\substack{i\\ i\neq b}}\frac{G_i\,\mathbf{M}_b\cdot\mathbf{n}_{ib}}{R_i\,D_{bi}^2}+\frac{1}{2}\sum_{\substack{i,j\\ i,j\neq a}}\frac{R_a\,G_i\,G_j}{R_i\,R_j\,D_{ai}\,D_{aj}}+\frac{1}{2}\sum_{\substack{i,j\\ i,j\neq b}}\frac{R_b\,G_i\,G_j}{R_i\,R_jD_{bi}\,D_{bj}}$$
$$\left.+\frac{1}{2}\sum_{\substack{i,j\\ i\neq a,j}}\frac{R_i\;G_a\,G_j}{R_a\,R_j\,D_{ai}\,D_{ij}}+\frac{1}{2}\sum_{\substack{i,j\\ i\neq b,j}}\frac{R_i\,G_b\,G_j}{R_b\,R_j\,D_{bi}\,D_{ij}}\right]+\mathbf{M}_a\cdot\mathbf{u}_{ea}+\mathbf{M}_b\cdot\mathbf{u}_{eb}$$
$$=\frac{1}{4\pi\rho_0}\left[\frac{1}{2}\frac{G_c^2}{R_c^3}+3\,\frac{M_c^2}{R_c^3}-\sum_{\substack{i\\ i\neq c}}\frac{G_c\,G_i}{R_c\,R_i\,D_{ci}}+3\,\sum_{\substack{i\\ i\neq c}}\frac{G_c\,\mathbf{M}_i\cdot\mathbf{n}_{ci}}{R_c\,D_{ci}^2}\right.$$
$$\left.+3\sum_{\substack{i\\ i\neq c}}\frac{G_i\,\mathbf{M}_c\cdot\mathbf{n}_{ic}}{R_i\,D_{ci}^2}+\frac{1}{2}\sum_{\substack{i,j\\ i,j\neq c}}\frac{R_c\,G_i\,G_j}{R_i\,R_j\,D_{ci}\,D_{cj}}+\frac{1}{2}\sum_{\substack{i,j\\ i\neq j\\ i,j\neq c}}\frac{R_iG_c\,G_j}{R_c\,R_j\,D_{ci}\,D_{ij}}\right]+\mathbf{M}_c\cdot\mathbf{u}_{ec}. \tag{D.12}$$

After solving the previously stated conservation equations, the only remaining unknown state variable for the new bubble is the radial momentum G_c. Equation (D.12) provides a relationship between the pre-collision state of the system and the post-collision radial momentum.

In order to simplify Eq. (D.12) and solve for G_c, define the quantities

$$A = \frac{1}{8\pi\rho_0}\frac{1}{R_c^3}, \tag{D.13a}$$

$$B = \frac{1}{4\rho_0\pi}\left[-\sum_{\substack{i\\ i\neq c}}\frac{G_i}{R_c\,R_i\,D_{ci}} + 3\sum_{\substack{i\\ i\neq c}}\frac{\mathbf{M}_i\cdot\mathbf{n}_{ci}}{R_c\,D_{ci}^2} + \frac{1}{2}\sum_{\substack{i,j\\ i\neq j,\, i,j\neq c}}\frac{R_i\,G_j}{R_c\,R_j\,D_{ci}\,D_{ij}}\right], \tag{D.13b}$$

$$C = \frac{1}{4\pi\rho_0}\left[3\,\frac{M_c^2}{R_c^3} + \frac{1}{2}\sum_{\substack{i,j\\ i,j\neq c}}\frac{R_c\,G_i\,G_j}{R_i\,R_j\,D_{ci}\,D_{cj}} + 3\sum_{\substack{i\\ i\neq c}}\frac{G_i\,\mathbf{M}_c\cdot\mathbf{n}_{ic}}{R_i\,D_{ci}^2}\right] + \mathbf{M}_c\cdot\mathbf{u}_{ec} - \mathcal{K}_{a+b}, \tag{D.13c}$$

where $\mathcal{K}_{a+b}$ is the kinetic energy associated with bubbles a and b, corresponding to the left-hand side of Eq. (D.12). With these definitions, Eq. (D.12) can be written as a quadratic,

$$AG_c^2 + BG_c + C = 0. \tag{D.14}$$

Here A is a monotonically decreasing, positive function of R_c. Because R_c is always positive, A is positive. $\mathcal{K}_{a+b}$ is the kinetic energy of the coalescing bubbles immediately before the collision, while the other terms on the right-hand side of Eq. (D.13c) represent only a portion of the kinetic energy after the collision. The kinetic energy must be the same before and after the collision, because $\mathcal{K}_{a+b}$ is subtracted from the other energy terms. Thus, C is always negative. Therefore the product AC is always negative and Eq. (D.14) has only real roots,

$$G_c = \frac{-B \pm \sqrt{B^2 - 4AC}}{2A}. \tag{D.15}$$

The root is chosen from the two options to match the sign of the sum $G_a + G_b$. This condition is chosen so that the flow surrounding the bubble does not abruptly reverse direction.

D.8 Comparison of results

In order to compare the new set of conservation relations derived here to the conservation relations of Ilinskii et al.,[50] a collision between two bubbles in free response is considered. The bubbles both have an equilibrium radius of $R_0 = 10\,\mu$m. One bubble is initially compressed to $0.03R_0$ while the other is initially expanded to $1.13R_0$. The bubbles are placed $6R_0$ apart and the system is centered at the origin, aligned with the x-axis. The effects of translation are included. Because the conservation relations of Ilinskii et al. do not account for surface tension, this effect is neglected here.

The motion of the bubbles is simulated using the Hamiltonian equations of motion, Eq. (2.24), until the collision occurs. When the collision between the two bubbles occurs, the simulation is halted and the new conservation relations derived here and the previous conservation relations, Eqs. (D.1), are used to calculate the equilibrium radius, current radius, radial velocity, position, and translational velocity of the new bubble. Where necessary, the corresponding momenta are also calculated. After the new coordinates and velocities are obtained, the kinetic energy

(Eq. (D.11)), internal energy (Eq. (D.9)), internal mass (Eq. (D.4)), translational momentum (Eq. (2.20)), and center of mass (Eq. (D.2)) of the two old bubbles and the new bubble are calculated and compared. The results of these calculations using the old conservation relations are presented in Table D.1. The table contains the percent difference of the conserved quantities in the pre- and post-collision systems. For some quantity Q, the percent difference between pre- and post-collision values is given by

$$\frac{Q^{(\mathrm{post})} - Q^{(\mathrm{pre})}}{Q^{(\mathrm{pre})}} \times 100\%.$$

With the new conservation relations, the relevant quantities are conserved to within numerical machine precision and thus are not shown in the table. Of the five quantities shown, the only one that is conserved by the old conservation relations is the center of mass. The other quantities increase appreciably, with the exception of the kinetic energy, which decreases slightly. This is not surprising because the old conservation relations were derived from far-field considerations in the host liquid, without requiring absolute local conservation of any quantity within the bubble system. The discrepancy between pre- and post-collision values calculated by the old conservation relations is even greater in large systems of bubbles. This is because the old conservation relations do not account for interaction energy and shared momentum of the bubbles. Thus, in systems of large bubbles the new conservation relations are preferred. This is especially true when integrating delay differential equations (DDEs) because the large discontinuities in the pre- and post-collision values can cause the integration to terminate, as DDEs are especially sensitive to discontinuities in the history.

	Difference between pre- and post-collision values
Kinetic energy	−4.2%
Internal energy	19%
Internal mass	50%
Translational momentum	9.3%
Center of mass	0.0%

Table D.1: Percent difference between pre- and post-collision values of the conserved quantities calculated with the conservation relations of Ilinskii et al.[50]

Bibliography

1 Yu. A. Pishchalnikov, O. A. Sapozhnikov, M. R. Bailey, J. C. Williams, R. O. Cleveland, T. Colonius, L. A. Crum, A. P. Evan, and J. A. McAteer, "Cavitation bubble cluster activity in the breakage of kidney stones by lithotripter shockwaves," *Journal of Endourology*, vol. 17, no. 7, pp. 435–446, Sep. 2003. [Online]. Available: `http://online.liebertpub.com/doi/abs/10.1089/089277903769013568`.

2 A. P. Evan, L. R. Willis, J. A. McAteer, M. R. Bailey, B. A. Connors, Y. Shao, J. E. Lingeman, J. C. Williams, N. S. Fineberg, and L. A. Crum, "Kidney damage and renal functional changes are minimized by waveform control that suppresses cavitation in shock wave lithotripsy," *The Journal of Urology*, vol. 168, no. 4, pp. 1556–1562, Oct. 2002. [Online]. Available: `http://www.jurology.com/article/S0022-5347(05)64520-X/abstract`.

3 B. R. Matlaga, J. A. McAteer, B. A. Connors, R. K. Handa, A. P. Evan, J. C. Williams, J. E. Lingeman, and L. R. Willis, "Potential for cavitation-mediated tissue damage in shockwave lithotripsy," *Journal of Endourology / Endourological Society*, vol. 22, no. 1, pp. 121–126, Jan. 2008, PMID: 18315482. [Online]. Available: `http://www.ncbi.nlm.nih.gov/pubmed/18315482`.

4 M. Bailey, V. Khokhlova, O. Sapozhnikov, S. Kargl, and L. Crum, "Physical mechanisms of the therapeutic effect of ultrasound (a review)," *Acoustical Physics*, vol. 49, pp. 369–388, 4 2003, 10.1134/1.1591291. [Online]. Available: `http://dx.doi.org/10.1134/1.1591291`.

5 J. McLaughlan, I. Rivens, T. Leighton, and G. ter Haar, "A study of bubble activity generated in ex vivo tissue by high intensity focused ultrasound," *Ultrasound in Medicine & Biology*, vol. 36, no. 8, pp. 1327–1344, 2010. [Online]. Available: `http://www.sciencedirect.com/science/article/pii/S0301562910002413`.

6 M. R. Bailey, L. N. Couret, O. A. Sapozhnikov, V. A. Khokhlova, G. ter Haar, S. Vaezy, X. Shi, R. Martin, and L. A. Crum, "Use of overpressure to assess the role of bubbles in focused ultrasound lesion shape in vitro," *Ultrasound in*

Medicine & Biology, vol. 27, no. 5, pp. 695–708, 2001. [Online]. Available: `http://www.sciencedirect.com/science/article/pii/S0301562901003428`.

7 Z. Xu, M. Raghavan, T. Hall, M.-A. Mycek, J. Fowlkes, and C. Cain, "Evolution of bubble clouds induced by pulsed cavitational ultrasound therapy - histotripsy," *Ultrasonics, Ferroelectrics and Frequency Control, IEEE Transactions on*, vol. 55, no. 5, pp. 1122–1132, May 2008.

8 Z. Xu, J. B. Fowlkes, E. D. Rothman, A. M. Levin, and C. A. Cain, "Controlled ultrasound tissue erosion: the role of dynamic interaction between insonation and microbubble activity," *The Journal of the Acoustical Society of America*, vol. 117, no. 1, pp. 424–435, Jan. 2005, PMID: 15704435 PMCID: PMC2677096. [Online]. Available: `http://www.ncbi.nlm.nih.gov/pmc/articles/PMC2677096/`.

9 Z. Xu, A. Ludomirsky, L. Y. Eun, T. L. Hall, B. C. Tran, J. B. Fowlkes, and C. A. Cain, "Controlled ultrasound tissue erosion," *IEEE transactions on ultrasonics, ferroelectrics, and frequency control*, vol. 51, no. 6, pp. 726–736, Jun. 2004, PMID: 15244286 PMCID: PMC2669757. [Online]. Available: `http://www.ncbi.nlm.nih.gov/pmc/articles/PMC2669757/`.

10 B. Niemczewski, "Observations of water cavitation intensity under practical ultrasonic cleaning conditions," *Ultrasonics Sonochemistry*, vol. 14, no. 1, pp. 13–18, 2007. [Online]. Available: `http://www.sciencedirect.com/science/article/pii/S1350417705001124`.

11 K. S. Suslick, "Sonochemistry," in *Comprehensive Coordination Chemistry II*, J. A. McCleverty and T. J. Meyer, Eds., Oxford: Pergamon, 2003, pp. 731–739. [Online]. Available: `http://www.sciencedirect.com/science/article/pii/B008043748601046X`.

12 T. G. Leighton, D. C. Finfer, P. R. White, G.-H. Chua, and J. K. Dix, "Clutter suppression and classification using twin inverted pulse sonar (twips)," *Proceedings of the Royal Society A: Mathematical, Physical and Engineering Science*, vol. 466, no. 2124, pp. 3453–3478, 2010. [Online]. Available: `http://rspa.royalsocietypublishing.org/content/466/2124/3453.abstract`.

13 B. Liang, X. S. Guo, J. Tu, D. Zhang, and J. C. Cheng, "An acoustic rectifier," *Nature Materials*, vol. 9, no. 12, pp. 989–992, 2010. [Online]. Available: `http://www.nature.com.ezproxy.lib.utexas.edu/nmat/journal/v9/n12/full/nmat2881.html`.

14 A. Shima, "Studies on bubble dynamics," *Shock Waves*, vol. 7, pp. 33–42, 1 1997, 10.1007/s001930050060. [Online]. Available: http://dx.doi.org/10.1007/s001930050060.

15 Lord Rayleigh, "On the pressure developed in a liquid during the collapse of a spherical cavity," *Philosophical Magazine Series 6*, vol. 34, no. 200, pp. 94–98, 1917. [Online]. Available: http://www.tandfonline.com/doi/abs/10.1080/14786440808635681.

16 N. Wang and P. Smereka, "Effective equations for sound and void wave propagation in bubbly fluids," English, *SIAM Journal on Applied Mathematics*, vol. 63, no. 6, pp. 1849–1888, 2003. [Online]. Available: http://www.jstor.org/stable/4096067.

17 D. Fuster and T. Colonius, "Modelling bubble clusters in compressible liquids," *Journal of Fluid Mechanics*, vol. 688, pp. 352–389, 2011. [Online]. Available: http://dx.doi.org/10.1017/S0022112011003806.

18 H. Grandjean, N. Jacques, and S. Zaleski, "Shock propagation in liquids containing bubbly clusters: a continuum approach," *Journal of Fluid Mechanics*, vol. 701, pp. 304–332, 2012. [Online]. Available: http://dx.doi.org/10.1017/S0022112012001590.

19 N. Hawker, M. Betney, and Y. Ventikos, "Single and multiple bubble shock-induced collapse: a computational study.," *The Journal of the Acoustical Society of America*, vol. 129, no. 4, pp. 2587–2587, 2011. [Online]. Available: http://link.aip.org/link/?JAS/129/2587/2.

20 T. Bui, E. Ong, B. Khoo, E. Klaseboer, and K. Hung, "A fast algorithm for modeling multiple bubbles dynamics," *Journal of Computational Physics*, vol. 216, no. 2, pp. 430–453, 2006. [Online]. Available: http://www.sciencedirect.com/science/article/pii/S0021999105005590.

21 E. Kurihara, T. A. Hay, Yu. A. Ilinskii, E. A. Zabolotskaya, and M. F. Hamilton, "Model for the dynamics of two interacting axisymmetric spherical bubbles undergoing small shape oscillations," *The Journal of the Acoustical Society of America*, vol. 130, no. 5, pp. 3357–3369, 2011. [Online]. Available: http://link.aip.org/link/?JAS/130/3357/1.

22 A. A. Doinikov, "Mathematical model for collective bubble dynamics in strong ultrasound fields," *The Journal of the Acoustical Society of America*, vol. 116, no. 2, pp. 821–827, 2004. [Online]. Available: http://link.aip.org/link/?JAS/116/821/1.

23 Yu. A. Ilinskii, M. F. Hamilton, and E. A. Zabolotskaya, "Bubble interaction dynamics in Lagrangian and Hamiltonian mechanics," *The Journal of the Acoustical Society of America*, vol. 121, no. 2, pp. 786–795, 2007. [Online]. Available: http://dx.doi.org/doi/10.1121/1.2404798.

24 Yu. A. Ilinskii and E. A. Zabolotskaya, "Cooperative radiation and scattering of acoustic waves by gas bubbles in liquids," *The Journal of the Acoustical Society of America*, vol. 92, no. 5, pp. 2837–2841, 1992. [Online]. Available: http://link.aip.org/link/?JAS/92/2837/1.

25 V. K. Kedrinskii, *Hydrodynamics of Explosions: Experiment and Models*, ser. High pressure shock compression of condensed matter. Springer, 2005. [Online]. Available: http://books.google.com/books?id=TBJKanXoXz4C.

26 J. B. Keller and I. I. Kolodner, "Damping of underwater explosion bubble oscillations," *Journal of Applied Physics*, vol. 27, no. 10, pp. 1152–1161, 1956. [Online]. Available: http://link.aip.org/link/?JAP/27/1152/1.

27 F. R. Gilmore, "The growth or collapse of a spherical bubble in a viscous compressible liquid," Hydrodynamics Laboratory, California Institute of Technology, Pasadena, CA, Tech. Rep. 26-4, Apr. 1952, p. 41.

28 V. A. Akulichev, "Structure of the solutions of equations describing the pulsations of cavitation voids," *Soviet Physics - Acoustics*, vol. 12, no. 4, pp. 455–458, 1966.

29 J. B. Keller and M. Miksis, "Bubble oscillations of large amplitude," *The Journal of the Acoustical Society of America*, vol. 68, no. 2, pp. 628–633, 1980. [Online]. Available: http://link.aip.org/link/?JAS/68/628/1.

30 Y. Tomita and A. Shima, "On the behavior of a spherical bubble and the impulse pressure in a viscous, compressible liquid," *Transactions of the Japan Society of Mechanical Engineers*, vol. 43, no. 367, pp. 1027–1035, 1977. [Online]. Available: http://ci.nii.ac.jp/naid/110002357477/.

31 D. Fuster, C. Dopazo, and G. Hauke, "Liquid compressibility effects during the collapse of a single cavitating bubble," *The Journal of the Acoustical Society of America*, vol. 129, no. 1, pp. 122–131, 2011. [Online]. Available: http://link.aip.org/link/?JAS/129/122/1.

32 A. Prosperetti and A. Lezzi, "Bubble dynamics in a compressible liquid. Part 1. First-order theory," *Journal of Fluid Mechanics*, vol. 168, pp. 457–478, 1986. [Online]. Available: http://dx.doi.org/10.1017/S0022112086000460.

33 A. Lezzi and A. Prosperetti, "Bubble dynamics in a compressible liquid. Part 2. Second-order theory," *Journal of Fluid Mechanics*, vol. 185, pp. 289–321, 1987. [Online]. Available: http://dx.doi.org/10.1017/S0022112087003185.

34 L. L. Foldy, "The multiple scattering of waves. I. general theory of isotropic scattering by randomly distributed scatterers," *Phys. Rev.*, vol. 67, pp. 107–119, 3-4 Feb. 1945. [Online]. Available: http://link.aps.org/doi/10.1103/PhysRev.67.107.

35 I. Tolstoy and A. Tolstoy, "Superresonant systems of scatterers. II," *The Journal of the Acoustical Society of America*, vol. 83, no. 6, pp. 2086–2096, 1988. [Online]. Available: http://link.aip.org/link/?JAS/83/2086/1.

36 I. Tolstoy, "Superresonant systems of scatterers. I," *The Journal of the Acoustical Society of America*, vol. 80, no. 1, pp. 282–294, 1986. [Online]. Available: http://link.aip.org/link/?JAS/80/282/1.

37 I. Tolstoy and A. Tolstoy, "Line and plane arrays of resonant monopole scatterers," *The Journal of the Acoustical Society of America*, vol. 87, no. 3, pp. 1038–1043, 1990. [Online]. Available: http://link.aip.org/link/?JAS/87/1038/1.

38 C. Feuillade, "Acoustically coupled gas bubbles in fluids: time-domain phenomena," *The Journal of the Acoustical Society of America*, vol. 109, no. 6, pp. 2606–2615, 2001. [Online]. Available: http://link.aip.org/link/?JAS/109/2606/1.

39 ——, "The attenuation and dispersion of sound in water containing multiply interacting air bubbles," *The Journal of the Acoustical Society of America*, vol. 99, no. 6, pp. 3412–3430, 1996. [Online]. Available: http://link.aip.org/link/?JAS/99/3412/1.

40 ——, “Scattering from collective modes of air bubbles in water and the physical mechanism of superresonances,” *The Journal of the Acoustical Society of America*, vol. 98, no. 2, pp. 1178–1190, 1995. [Online]. Available: `http://link.aip.org/link/?JAS/98/1178/1`.

41 V. Leroy, A. Strybulevych, M. G. Scanlon, and J. H. Page, “Transmission of ultrasound through a single layer of bubbles,” *Eur. Phys. J. E*, vol. 29, no. 1, pp. 123–130, 2009. [Online]. Available: `http://dx.doi.org/10.1140/epje/i2009-10457-y`.

42 N. C. Skaropoulos, H. D. Yagridou, and D. P. Chrissoulidis, “Interactive resonant scattering by a cluster of air bubbles in water,” *The Journal of the Acoustical Society of America*, vol. 113, no. 6, pp. 3001–3011, 2003. [Online]. Available: `http://link.aip.org/link/?JAS/113/3001/1`.

43 G. Kapodistrias and P. H. Dahl, “Effects of interaction between two bubble scatterers,” *The Journal of the Acoustical Society of America*, vol. 107, no. 6, pp. 3006–3017, 2000. [Online]. Available: `http://link.aip.org/link/?JAS/107/3006/1`.

44 R. Mettin, S. Luther, S. Kamphausen, and W. Lauterborn, “Dynamics of delay-coupled spherical bubbles,” *AIP Conference Proceedings*, vol. 524, no. 1, W. Lauterborn and T. Kurz, Eds., pp. 359–362, 2000. [Online]. Available: `http://link.aip.org/link/?APC/524/359/1`.

45 J. Cui, M. F. Hamilton, P. S. Wilson, and E. A. Zabolotskaya, “Bubble pulsations between parallel plates,” *The Journal of the Acoustical Society of America*, vol. 119, no. 4, pp. 2067–2072, 2006. [Online]. Available: `http://link.aip.org/link/?JAS/119/2067/1`.

46 A. A. Doinikov, R. Manasseh, and A. Ooi, “Time delays in coupled multibubble systems (L),” *The Journal of the Acoustical Society of America*, vol. 117, no. 1, pp. 47–50, 2005. [Online]. Available: `http://link.aip.org/link/?JAS/117/47/1`.

47 A. Ooi, A. Nikolovska, and R. Manasseh, “Analysis of time delay effects on a linear bubble chain system,” *The Journal of the Acoustical Society of America*, vol. 124, no. 2, pp. 815–826, 2008. [Online]. Available: `http://dx.doi.org/doi/10.1121/1.2945156`.

48 J. C. Atkisson, "Models for acoustically driven bubbles in channels," PhD thesis, The University of Texas at Austin, Austin, Texas, Aug. 2008.

49 S. Fujikawa and H. Takahira, "A theoretical study on the interaction between two spherical bubbles and radiated pressure waves in a liquid," *Acustica*, vol. 61, no. 3, pp. 188–199, 1986. [Online]. Available: http://www.ingentaconnect.com/content/dav/aaua/1986/00000061/00000003/art00007.

50 Yu. A. Ilinskii, M. F. Hamilton, E. A. Zabolotskaya, and G. D. Meegan, "Influence of compressibility on bubble interaction," *AIP Conference Proceedings*, vol. 838, no. 1, A. A. Atchley, V. W. Sparrow, and R. M. Keolian, Eds., pp. 303–310, 2006. [Online]. Available: http://link.aip.org/link/?APC/838/303/1.

51 M. F. Hamilton, Yu. A. Ilinskii, G. D. Meegan, and E. A. Zabolotskaya, "Interaction of bubbles in a cluster near a rigid surface," *Acoustics Research Letters Online*, vol. 6, no. 3, pp. 207–213, 2005. [Online]. Available: http://link.aip.org/link/?ARL/6/207/1.

52 C. R. Heckman, S. M. Sah, and R. H. Rand, "Dynamics of microbubble oscillators with delay coupling," *Communications in Nonlinear Science and Numerical Simulation*, vol. 15, no. 10, pp. 2735 –2743, 2010. [Online]. Available: http://www.sciencedirect.com/science/article/pii/S100757040900553X.

53 D. Sinden, E. Stride, and N. Saffari, "The effects of fluid compressibility on multibubble cavitation for high-intensity focused ultrasound.," *The Journal of the Acoustical Society of America*, vol. 129, no. 4, 2587–2587 (A), 2011. [Online]. Available: http://link.aip.org/link/?JAS/129/2587/3.

54 R. Manasseh, A. Nikolovska, A. Ooi, and S. Yoshida, "Anisotropy in the sound field generated by a bubble chain," *Journal of Sound and Vibration*, vol. 278, no. 4-5, pp. 807 –823, 2004. [Online]. Available: http://www.sciencedirect.com/science/article/pii/S0022460X03011751.

55 T. G. Leighton, *The Acoustic Bubble*. Waltham, MA: Academic Press, 1997. [Online]. Available: http://books.google.com/books?id=0RJif-xRyGMC.

56 H. Lamb, *Hydrodynamics*. Mineola, NY: Dover, 1945. [Online]. Available: http://books.google.com/books?id=O6NAAAAAIAAJ.

57 L. D. Landau and E. M. Lifshitz, *Mechanics*, ser. Course of Theoretical Physics. Oxford: Butterworth-Heinemann, 1976. [Online]. Available: http://books.google.com/books?id=e-xASAehg1sC.

58 H. Goldstein, *Classical Mechanics*, ser. Addison-Wesley Series in Physics. Boston: Addison-Wesley, 1980. [Online]. Available: http://books.google.com/books?id=9M8QAQAAIAAJ.

59 A. J. Reddy and A. J. Szeri, "Coupled dynamics of translation and collapse of acoustically driven microbubbles," *The Journal of the Acoustical Society of America*, vol. 112, no. 4, pp. 1346–1352, 2002. [Online]. Available: http://link.aip.org/link/?JAS/112/1346/1.

60 J. Magnaudet and D. Legendre, "The viscous drag force on a spherical bubble with a time-dependent radius," *Physics of Fluids*, vol. 10, no. 3, pp. 550–554, 1998. [Online]. Available: http://link.aip.org/link/?PHF/10/550/1.

61 A. D. Pierce, *Acoustics: An Introduction to Its Physical Principles and Applications*. Melville, NY: Acoustical Society of America, 1989. [Online]. Available: http://books.google.com/books?id=D8GqhULfKfAC.

62 D. T. Blackstock, *Fundamentals of Physical Acoustics*, ser. Wiley-Interscience. New York: Wiley, 2000. [Online]. Available: http://books.google.com/books?id=e_8sPIEd36YC.

63 A. A. Doinikov and S. T. Zavtrak, "Radiation forces between two bubbles in a compressible liquid," *The Journal of the Acoustical Society of America*, vol. 102, no. 3, pp. 1424–1431, 1997. [Online]. Available: http://link.aip.org/link/?JAS/102/1424/1.

64 M. Lakshmanan and D. V. Senthilkumar, *Dynamics of Nonlinear Time-Delay Systems*. Springer, 2010. [Online]. Available: http://books.google.com/books?id=nV5F0kMsqa4C.

65 C. Chicone, S. M. Kopeikin, B. Mashhoon, and D. G. Retzloff, "Delay equations and radiation damping," *Physics Letters A*, vol. 285, no. 1–2, pp. 17–26, 2001. [Online]. Available: http://www.sciencedirect.com/science/article/pii/S0375960101003279.

66 T. A. Hay, "A model of the interaction of bubbles and solid particles under acoustic excitation," PhD thesis, The University of Texas at Austin, Austin,

Texas, May 2008. [Online]. Available: www.lib.utexas.edu/etd/d/2008/hayt96603/hayt96603.pdf.

67 Maxima. (2011). Maxima, a computer algebra system. version 5.25.1, [Online]. Available: http://maxima.sourceforge.net/.

68 E. A. Zabolotskaya, "Interaction of gas bubbles in a sound field," *Soviet Physics - Acoustics*, vol. 30, pp. 365–368, 1984.

69 C. Devin, "Survey of thermal, radiation, and viscous damping of pulsating air bubbles in water," *The Journal of the Acoustical Society of America*, vol. 31, no. 12, pp. 1654–1667, 1959. [Online]. Available: http://dx.doi.org/doi/10.1121/1.1907675.

70 F. M. Asl and A. G. Ulsoy, "Analysis of a system of linear delay differential equations," *Journal of Dynamic Systems, Measurement, and Control*, vol. 125, no. 2, pp. 215–223, 2003. [Online]. Available: http://link.aip.org/link/?JDS/125/215/1.

71 R. Manasseh, G. Riboux, and F. Risso, "Sound generation on bubble coalescence following detachment," *International Journal of Multiphase Flow*, vol. 34, no. 10, pp. 938 –949, 2008. [Online]. Available: http://www.sciencedirect.com/science/article/pii/S030193220800061X.

72 C. S. Clay and H. Medwin, *Acoustical Oceanography: Principles and Applications*. Wiley, 1977. [Online]. Available: http://books.google.com/books?id=ZgFRAAAAMAAJ.

73 T. Erneux, *Applied Delay Differential Equations*. New York: Springer, 2009.

74 N. Guglielmi and E. Hairer, "Computing breaking points in implicit delay differential equations," *Advances in Computational Mathematics*, vol. 29, pp. 229–247, 3 2008, 10.1007/s10444-007-9044-5. [Online]. Available: http://dx.doi.org/10.1007/s10444-007-9044-5.

75 ——, "Implementing radau IIA methods for stiff delay differential equations," *Computing*, vol. 67, no. 1, pp. 1–12, 2001. [Online]. Available: http://www.springerlink.com.ezproxy.lib.utexas.edu/content/lkc7g8xqn65puqrg/abstract/.

76 J. V. José and E. J. Saletan, *Classical dynamics: a contemporary approach*. Cambridge University Press, 1998. [Online]. Available: http://books.google.com/books?id=Eql9dRQDgvQC.

77 C. Chicone, "Inertial and slow manifolds for delay equations with small delays," *Journal of Differential Equations*, vol. 190, no. 2, pp. 364–406, May 20, 2003. [Online]. Available: http://dx.doi.org/10.1016/S0022-0396(02)00148-1.

78 N. Bremond, M. Arora, C.-D. Ohl, and D. Lohse, "Controlled multibubble surface cavitation," *Physical Review Letters*, vol. 96, no. 22, p. 224 501, 2006. [Online]. Available: http://doc.utwente.nl/59080/.

79 W. Lauterborn and T. Kurz, "Physics of bubble oscillations," *Reports on Progress in Physics*, vol. 73, no. 10, p. 106 501, 2010. [Online]. Available: http://stacks.iop.org/0034-4885/73/i=10/a=106501.

80 J. D. Jackson, *Classical Electrodynamics*. Wiley, 1999. [Online]. Available: http://books.google.com/books?id=U3LBQgAACAAJ.

81 A. Bellen and M. Zennaro, *Numerical Methods for Delay Differential Equations*, ser. Numerical mathematics and scientific computation. Oxford: Clarendon Press, 2003. [Online]. Available: http://books.google.com/books?id=lcRMDdTNrosC.

82 S. Thompson and L. Shampine, "A friendly fortran DDE solver," *Applied Numerical Mathematics*, vol. 56, no. 3–4, pp. 503–516, Mar. 2006. [Online]. Available: http://www.sciencedirect.com/science/article/pii/S0168927405000966.